

JSCSEN 75(6)875–1018(2010)

Journal of the Serbian Chemical Society

Electronic
version

VOLUME 75

No 7

BELGRADE 2010

Available on line at



www.shd.org.rs/JSCS/

The full search of JSCS
is available through

DOAJ DIRECTORY OF
OPEN ACCESS
JOURNALS
www.doaj.org



CONTENTS

Organic Chemistry, Biochemistry and Biotechnology

- J. Wang, D. Lu, H. Zhao, B. Jiang, J. Wang, X. Ling, H. Chai and P. Ouyang*: Discrimination and classification of tobacco wastes by identification and quantification of polyphenols with LC–MS/MS 875
- M. Djurendić-Brenesel, N. Ajduković, K. Štajnic-Ristić, V. Pilija and I. Veselinović*: Δ^9 -Tetrahydrocannabinol content in cannabis samples seized in Novi Sad during 2008 ... 893
- R. Gevrenova*: Determination of natural colorants in plant extracts by high-performance liquid chromatography 903

Inorganic Chemistry

- K. Singh and D. Pal*: Synthetic, structural and biological studies of organosilicon(IV) complexes of Schiff bases derived from pyrrole-2-carboxaldehyde 917
- I. Khosravi and M. Yazdanbakhsh*: Preparation and characterization of novel oxo-centered basic *p*-chlorobenzoic bridging trinuclear complexes 929
- S. Chandra, M. Tyagi and S. Agarwal*: Synthesis and characterization of a tetraaza macrocyclic ligand and its cobalt(II), nickel(II) and copper(II) complexes 935

Theoretical Chemistry

- S. Jeremić, S. Radenković and I. Gutman*: Cyclic conjugation in benzo-annelated triphenylenes 943

Physical Chemistry

- A. Magda, R. Pode, C. Muntean, M. Medeleanu and A. Popa*: Synthesis and characterization of ammonium phosphate fertilizers with boron 951
- S. P. Jovanović, Z. M. Marković, D. N. Kleut, V. D. Trajković, B. S. Babić-Stojić, M. D. Dramićanin and B. M. Todorović Marković*: Singlet oxygen generation by higher fullerene-based colloids 965

Analytical Chemistry

- D. M. Milenović and Z. B. Todorović*: Development and application of a validated HPLC method for the analysis of dissolution samples of mexiletine hydrochloride capsules 975

Polymers

- Y. Liu, L. Wang, X. Tuo, S. Li and W. Yang*: A study on the microstructure of a nitrate ester plasticized polyether propellant dissolved in HCl and KOH solutions 987

Thermodynamics

- J. D. Jovanović and D. K. Grozdanić*: Reliable prediction of heat of vaporization of *n*-alkanes at 298.15 K (Note) 997

Environmental

- Dj. Petrović, M. Todorović, D. Manojlović and V. D. Krsmanović*: A simulation experiment as a method for the investigation of the mobility of heavy metals from inundated land 1005

Published by the Serbian Chemical Society
Karnegijeva 4/III, 11000 Belgrade, Serbia
Printed by the Faculty of Technology and Metallurgy
Karnegijeva 4, P.O. Box 35-03, 11120 Belgrade, Serbia



J. Serb. Chem. Soc. 75 (7) 875–891 (2010)
JSCS–4014

Discrimination and classification of tobacco wastes by identification and quantification of polyphenols with LC–MS/MS

JUN WANG^{1,2}, DINGQIANG LU^{1*}, HUI ZHAO¹, BEN JIANG¹, JIALI WANG¹,
XIUQUAN LING¹, HONG CHAI¹ and PINGKAI OUYANG¹

¹*School of Biotechnology and Pharmaceutical Engineering, Nanjing University of Technology, Nanjing 210009 and* ²*School of Biotechnology and Environmental Engineering, Jiangsu University of Science and Technology, Zhenjiang 212018, P. R. China*

(Received 9 November 2009, revised 25 February 2010)

Abstract: The chemical composition of polyphenols in tobacco waste was identified by HPLC–PDA–ESI/MS/MS and the contents of chlorogenic acids and rutin in 10 varieties of tobacco wastes were determined by HPLC–UV. The relationships between the contents of active polyphenols and the varieties of tobacco wastes were interpreted by hierarchical cluster analysis (HCA) and principal component analysis (PCA). The results showed that 15 polyphenols were identified in a methanolic extract of dried tobacco waste. The tobacco wastes were characterized by high levels of chlorogenic acids (3-CQA, 5-CQA, and 4-CQA) and rutin; their ranges in the 10 tobacco varieties were 0.116–0.196, 0.686–1.781, 0.094–0.192, and 0.413–0.998 %, respectively. According to multivariate statistics models, two active compound variables can be considered important for the discrimination of the varieties of tobacco wastes: chlorogenic acids and rutin. Consequently, samples of 10 tobacco varieties were characterized into three groups by HCA based on the PCA pattern. In conclusion, tobacco waste could be used as a new pharmaceutical material for the production of natural chlorogenic acids and rutin in the ethnopharmacological industry.

Keywords: tobacco (*Nicotiana tabacum* L.) waste; HPLC–PDA–ESI/MS/MS; chlorogenic acids; rutin; multivariate statistical analysis.

INTRODUCTION

Solid tobacco waste is classified as an agro-industrial waste. The total global tobacco (*Nicotiana tabacum* L.) waste production in the year 2005 was more than 1.25 million metric tons. In China, 460 million kg of tobacco waste per year are generated at various stages of the post-harvest processing of tobacco and during

* Corresponding author. E-mail: ludingqiang@njut.edu.cn
doi: 10.2298/JSC091109055W

the manufacture of tobacco products.¹ Tobacco waste has no immediate use and cigarette companies have to pay for its disposal. The majority of the waste is destroyed by burning. Indeed, the disposal of this waste is a serious problem because tobacco waste is toxic due to the presence of nicotine;² thus, governments worldwide must enforce legislation for the controlled disposal of tobacco waste in order to avoid harmful effects to the environment. As a type of high organic biomass, tobacco wastes have potential applications for soil amendment and the production of tailored organic fertilizer³ and desulfurization adsorbents.⁴

Currently, the chemical compositions of tobacco leaves and wastes have attracted a considerable amount of attention throughout the world,^{5–8} and tobacco waste is considered to be a good source of a large number of bioactive substances, such as chlorogenic acids and rutin.¹ Chlorogenic acid is a member of the caffeoylquinic acids (CQAs) family.⁹ The members of this family possess a wide range of biological properties, such as antibacterial, antioxidant, hepatocyte protective, antimutagenic, inhibitory of HIV-1 RT and active against the human herpes simplex virus, adenoviruses, SARS and AIV (H5N1).^{10–15} Similarly, rutin is a member of the phytochemical group of compounds the “protective” properties of which include antioxidant, antimicrobial, anticancer, and cardiovascular-protective activities.^{16,17} Therefore, considering that chlorogenic acid and rutin are highly valuable natural polyphenol compounds used as medical and industrial materials in China, the identification and quantification of these main polyphenols in tobacco waste is of great importance for its large scale application in the ethnopharmacological industry.

LC–MS was used previously to characterize cinnamoylamino acid conjugates, to discriminate between individual isomers of mono-acyl and di-acyl chlorogenic acids^{18–21} and to characterize flavonoids.²² In this study, ion trap HPLC–PDA–ESI/MS/MS and HPLC–UV methods were developed for the qualitative profile and quantitative determination, respectively, of polyphenols in tobacco waste. These methods were applied to the qualitative profiling of polyphenols in tobacco waste and the determination of the contents of chlorogenic acids and rutin in waste from 10 tobacco varieties.

The study revealed that the correct classification of the variety of the tobacco waste is a new problem in controlling the quality of tobacco waste. This is due to the fact that the unique combination of tobacco variety and cultivation zone results in different chemical compositions within the tobacco waste. Unfortunately, little attention has previously been paid to this question. Therefore, in an attempt to evaluate the relationships between the polyphenols within a given tobacco waste and the tobacco varieties in the waste source, multivariate analysis methods (MAM) are certainly necessary. MAM was successfully applied to determine the source of biomass from different geographical locations.^{23–26} Representative methods of MAM are hierarchical cluster analysis (HCA) and principal

component analysis (PCA). In this study, the HCA and PCA methods were developed to evaluate the tobacco waste resources to guide the high added value utilization of all varieties of tobacco wastes. The overall similarity of the active polyphenols contained in tobacco wastes among the varieties was calculated with the HCA method on the basis of the PCA pattern.

The objective of this work was the evaluation of tobacco waste as a potential ethnopharmacological resource for the production of chlorogenic acids and rutin, in order to develop a new bioprocess for the synthetic utilization of tobacco waste.²⁷ Processing tobacco wastes could solve the environmental problems derived from the disposal of large amounts of tobacco waste. Moreover, obtaining stabilized tobacco wastes as natural ethnopharmacological materials could be advantageous to the traditional Chinese medicine (TCM) industry in China. This would not only improve the uses available for tobacco wastes, but would also provide a new source of natural and functional polyphenols.

EXPERIMENTAL

Samples and reagents

The wastes of 10 tobacco samples were collected from different countries and regions of the world in 2007 and authenticated as the wastes of *Nicotiana tabacum* L. by Prof. Ding-qiang Lu (College of Life Science and Pharmaceutical Engineering, Nanjing University of Technology). All samples were dried at 60 °C using a herb disintegrator (Qinzhou Sanyang Package Equipment Co., Ltd.) and then sieved (60 mesh).

HPLC-grade methanol, acetic acid, and acetonitrile were purchased from TEDIA Co. (Fairfield, OH, USA). Chlorogenic acid (5-caffeoylquinic acid, 5-CQA), caffeic acid (CA), scopolin, and rutin were purchased from the National Institute for the Control of Pharmaceutical and Biological Products (NICBPB), Beijing, China. Neochlorogenic acid (3-caffeoylquinic acid, 3-CQA), cryptochlorogenic acid (4-caffeoylquinic acid, 4-CQA), and nicotine were purchased from Chengdu Biopurify Phytochemicals Ltd., Chengdu, China. Isoquercitrin, luteolin-7-rutinoside, and quinic acid (QA) were purchased from Sigma-Aldrich Inc. (St. Louis, MO, USA).

Sample preparation

Tobacco waste samples (0.15 kg) were extracted in 70 % v/v aqueous methanol (0.50 L), using ultrasonic waves for 30 min at a time, for a total of 2 h.²⁷ The bulk extracts were diluted with 70 % v/v aqueous methanol to form a solution of 1.0 mg/mL. Solutions of pure compounds were prepared at a concentration of 1.0 mg/mL in methanol. The sample solutions were filtered through a 0.45 µm filter and 10 µL of each was injected for analysis.

Equipment

HPLC-PDA-MS was performed on a Waters system (Millipore Corp., Milford, MA, USA). The LC equipment comprised a Waters 2695 Separations Module, an autosampler with a 50 µL loop and a Waters 2996 photodiode array detector with a light-pipe flow cell (recorded at 328, 320, 280, and 254 nm, and scanning from 200 to 400 nm). This was interfaced with a mass spectrometer fitted with Micromass[®] Quattro micro[™] API source and ESCi[™] Multi-Mode Ionization Plus ESI source.

HPLC–UV was performed using LB-5 pump (Beijing Satellite Manufactory, Beijing, China) with a UV detector (Shimadzu Seisakusho Ltd., Kyoto, Japan) and N-2000 workstation (Hangzhou Mingtong S & T Ltd., Hangzhou, China).

HPLC-PDA–ESI-MS/MS

The HPLC-PDA–ESI-MS/MS experiments were performed according to the literature.^{14,27} The HPLC separation was performed on an Alltima C₁₈ (250 mm×4.6 mm×5 μm) column (Alltech, Deerfield, IL, USA). The mobile phase contained solvents A and B, where A was water/acetonitrile/acetic acid (97.5:2:0.5 v/v/v) and B was acetonitrile/acetic acid (99.5:0.5 v/v). The gradient profile was as follows: 2 % B for 5 min; 2 to 5 % B in 5 min; 5 to 10 % B in 20 min; 10 to 35 % B in 3n 5 min; 35 to 100 % B in 15 min. Then the composition was re-established by going from 100 to 2 % B over 5 min and maintained at 2 % B for 5 min. The wavelength range of the PDA detection was from 200 to 400 nm. The flow rate was 1.0 mL min⁻¹ for HPLC and PDA detection, with the column kept at 40 °C. A splitter was connected between the PDA and MS detectors, which reduced the flow rate to 0.20 mL min⁻¹ for MS detection. The electrospray ESI-MS/MS was operated in the negative ion mode with scanning range of *m/z* 100–800. The capillary voltage was 3.0 kV, the cone voltage 30.0 kV and the ion source temperature was 120 °C. High purity nitrogen (99.9 %) at a flow rate of 500 L h⁻¹ and at 350 °C was used as a dry gas to evaporate the solvent. Nitrogen was also used as the nebulizer gas at 50 psi.

Determination of chlorogenic acids in tobacco wastes

The HPLC-UV experiments were performed according to the literature.^{14,27} The HPLC separation was performed on an Alltima C₁₈ (250 mm×4.6 mm×5 μm) column (Alltech, Deerfield, IL, USA). The mobile phase consisted of acetonitrile/ammonium acetate buffer (pH 4.5) (5:95 v/v). The flow-rate was 1.0 mL min⁻¹ and the UV detection was realized at 327 nm with the column kept at 30 °C.

Determination of rutin in tobacco wastes

The HPLC separation was performed on an Alltima C₁₈ (250 mm×4.6 mm×5 μm) column (Alltech, Deerfield, IL, USA). The mobile phase consisted of methanol/acetic acid solution (pH 4.5) (50:50 v/v). The flow-rate was 1.0 mL min⁻¹ HPLC and the UV detection was realized at 360 nm with the column kept at 30 °C.

Multivariate statistical analysis

Hierarchical cluster analysis and principal component analysis were employed to analyze the relationships between the contents of polyphenols (chlorogenic acids and rutin) and waste from the tobacco varieties. Multivariate methods were applied to the mean values of three replicates from each determination result. The initial variable values were standardized, the mean centered and autoscaled to variance prior to analysis to avoid any effects of the scale of the units with which they were measured.

Principal component analysis, PCA, was used to reduce the initial data from linear combinations of the original variables. PCA breaks down the matrix of the initial data, **X**, to express them as a least-square model.²⁸ PCA is a data compression method based on correlation amongst variables. The aim of PCA is to group correlated variables and replace them with new sets called principal components (PCs). PCs are completely uncorrelated and are built as simple linear combinations of the original variables. PCs contain most of the data set variability but in a much lower dimensional space. When redundancy is removed, only the first few principal components are required to describe the information contained in the ori-

ginal data set.^{24,29} The principal component loadings of the data were analyzed after application of Varimax normalized rotation of the PCs coordinate system. The score plots of the first PC may be used to investigate the interrelationships among the objects, as they allow the observation of clusters of objects. The interrelationships among the variables may also be studied through the respective loading plots.³⁰

Hierarchical cluster analysis, HCA, is a technique used for classifying objects that have been characterized by the values of a set of variables into different groups. The clusters are formed by grouping objects according to similarity, and the results are presented in the form of dendrograms, which allow the distances between objects to be visualized. The between-groups linkage or the unweighted pair group method with arithmetic mean (UPGMA) technique, which defines the distance between two clusters as the average of all the pairs of distances between elements of both clusters, was adopted.^{24,31,32} Similarities and dissimilarities were quantified by Square Euclidean distance measurements. The data analysis was realized using the SPSS v.13.0 statistical package (SPSS, 2005).

RESULTS AND DISCUSSION

Identification of the chemical constituents in tobacco wastes by HPLC-PAD-ESI/MS/MS

In the methanolic extracts of the dried tobacco wastes, compounds **1** (quinic acid), **2** (nicotine), **3** (3-CQA), **4** (scopolin), **5** (5-CQA), **6** (4-CQA), **7** (caffeic acid), **11** (rutin), **12** (isoquercitrin) and **13** (luteolin-7-rutinoside) were identified by comparing their retention times and UV and MS spectra with those of standard compounds. Moreover, the structures of all compounds in the methanolic extracts of dried tobacco wastes were determined by MS SCAN and MS MRM modes and by comparing the UV and MS spectrum data with those reported in literature.^{18,19,33-36} The 15 polyphenols identified from the methanolic extracts of the dried tobacco waste are given in Table I and the structures of the polyphenols identified from the tobacco wastes, with the IUPAC numbering system, are shown in Fig. 1.

TABLE I. Polyphenols identified in the methanolic extract of dried tobacco wastes

No.	τ_R min	Molecular weight	Parent ion MS m/z [M-H] ⁻	Daughter ion MS/MS m/z	λ_{max} / nm (UV)	Identification ^a
1	3.2	192	191.3	127.3	254	Quinic acid
2	6.7	162	161.3	103.7	259, 282	Nicotine
3	21.5	354	353.3	191.3, 179.3, 173.3, 135.3	240, 298 <i>sh</i> , 328	3- <i>O</i> -Caffeoyl- quinic acid (3-CQA)
4	31.4	192	191.3	179.3	254, 294 <i>sh</i> , 342	Scopolin
5	32.5	354	353.3	191.3, 179.3	240, 298 <i>sh</i> , 328	5- <i>O</i> -Caffeoyl- quinic acid (5-CQA)
6	33.2	354	353.3	191.3, 179.3, 173.3, 135.3	240, 298 <i>sh</i> , 328	4- <i>O</i> -Caffeoyl- quinic acid (4-CQA)

TABLE I. Continued

No.	τ_R min	Molecular weight	Parent ion MS m/z [M-H] ⁻	Daughter ion MS/MS m/z	λ_{max} / nm (UV)	Identification ^a
7	37.5	180	179.4	135.3	217, 240, 298 <i>sh</i> , 325	Caffeic acid
8	40.8	338	337.3	191.4, 173.3	240, 298 <i>sh</i> , 314	5- <i>O-p</i> -Coumaroylquinic acid (5- <i>p</i> CoQA)
9	42.9	368	367.7	191.4, 173.4	240, 298 <i>sh</i> , 324	4- <i>O</i> -Feruloylquinic acid (4-FQA)
10	43.5	338	337.3	191.4, 163.3	240, 298 <i>sh</i> , 314	3- <i>O-p</i> -Coumaroylquinic acid (3- <i>p</i> CoQA)
11	48.5	610	609.3	301.3, 271.3, 179.3, 151.3	256, 298 <i>sh</i> , 360	Rutin
12	50.5	464	463.3	271.3, 217.3, 179.3, 151.3	256, 298 <i>sh</i> , 362	Isoquercetin
13	51.7	594	593.4	285.3	255, 298 <i>sh</i> , 340	Luteolin-7-rutinoside
14	52.8	516	515.3	353.3, 335.3, 191.3, 179.3	240, 298 <i>sh</i> , 330	1,5-Di- <i>O</i> -caffeoylquinic acid (1,5-diCQA)
15	54.5	516	515.3	353.3, 191.3, 179.3, 135.3	240, 298 <i>sh</i> , 330	3,5-Di- <i>O</i> -caffeoylquinic acid (3,5-diCQA)

^aIUPAC numbering system for all CQAs

The HPLC profiles of the 70 % methanol extract of tobacco waste detected with negative ion mode ESI-MS TIC and UV at 320 nm are shown in Fig. 2.

Characterization of caffeoylquinic acids (MW 354)

Typically, as can be seen from Fig. 2, three peaks (**3**, **5**, and **6**) were found in the total ion chromatogram (TIC) detected by the negative ion ESI-MS scan mode and UV at 320 nm. The largest peak (**5**) was identified as chlorogenic acid (5-*O*-caffeoylquinic acid) by comparison with the standard compound. The chromatographic profiles of 70 % methanolic extracts of tobacco wastes detected by the negative ion ESI-MS multiple reaction monitoring (MRM) mode are shown in Fig. 3 as MS MRM ESI-TIC, MS MRM, m/z 353.3 \rightarrow 173.3 and MS, m/z 353.3 \rightarrow 191.3. Peak **6** was clearly identified as 4-*O*-caffeoylquinic acid by its MS MRM (m/z 353.3 \rightarrow 173.3) (Figs. 3A and 3B), because the MS² base peak of 4-CQA is m/z 173.3. Although the MS² base peak of 3-CQA and 5-CQA are both m/z 191.3, there was a difference in the secondary ion at m/z 179.5. Therefore, the smallest peak (**3**) was identified as 3-*O*-caffeoylquinic acid by its MS MRM (m/z 353.3 \rightarrow 191.3) (Figs. 3A and 3C) and by comparing the UV and MS spectra data with those reported in literature.^{18,19,33,34}

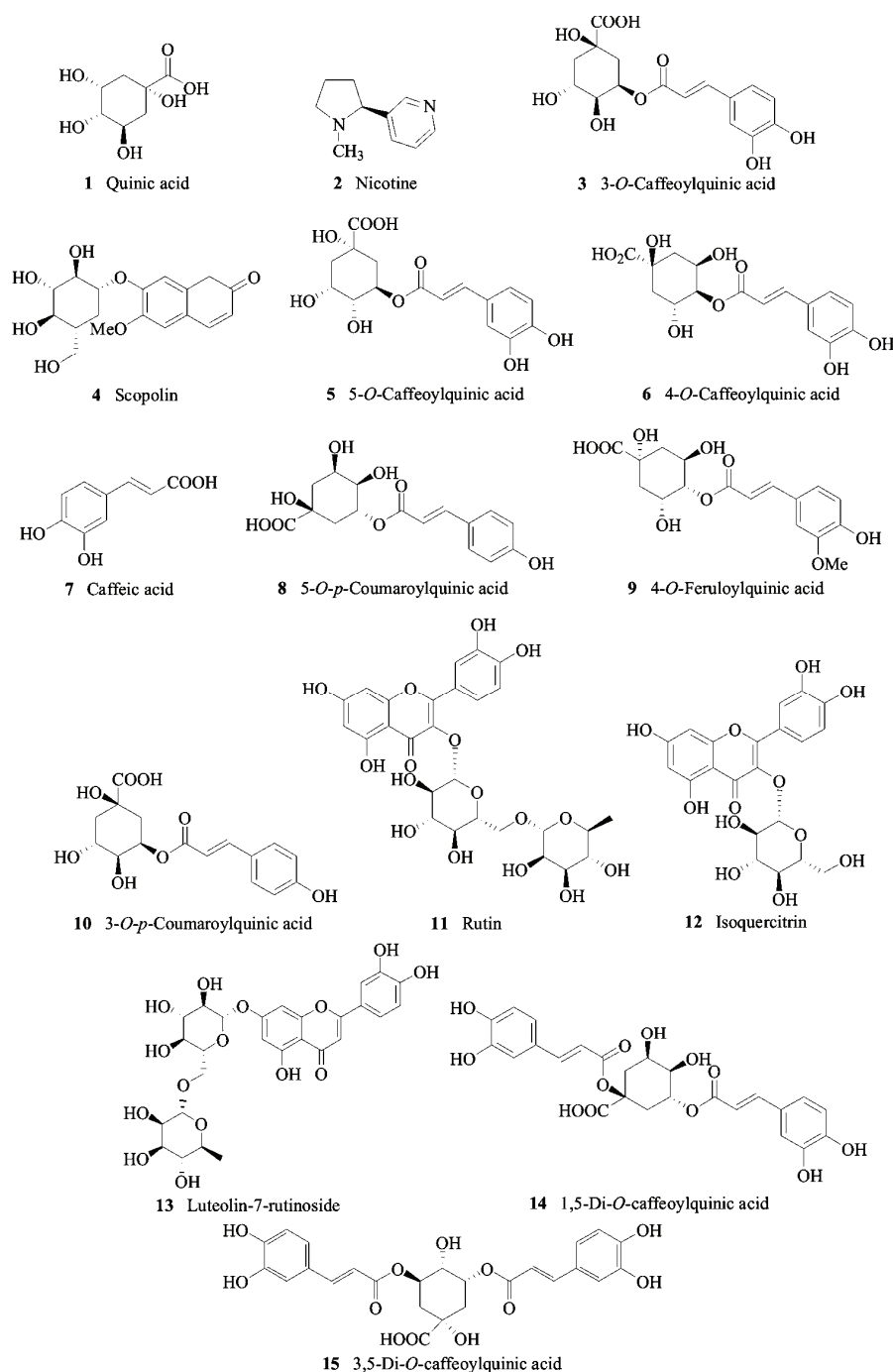


Fig. 1. Structure of the polyphenols identified in tobacco waste determined by HPLC-PDA-ESI/MS/MS.

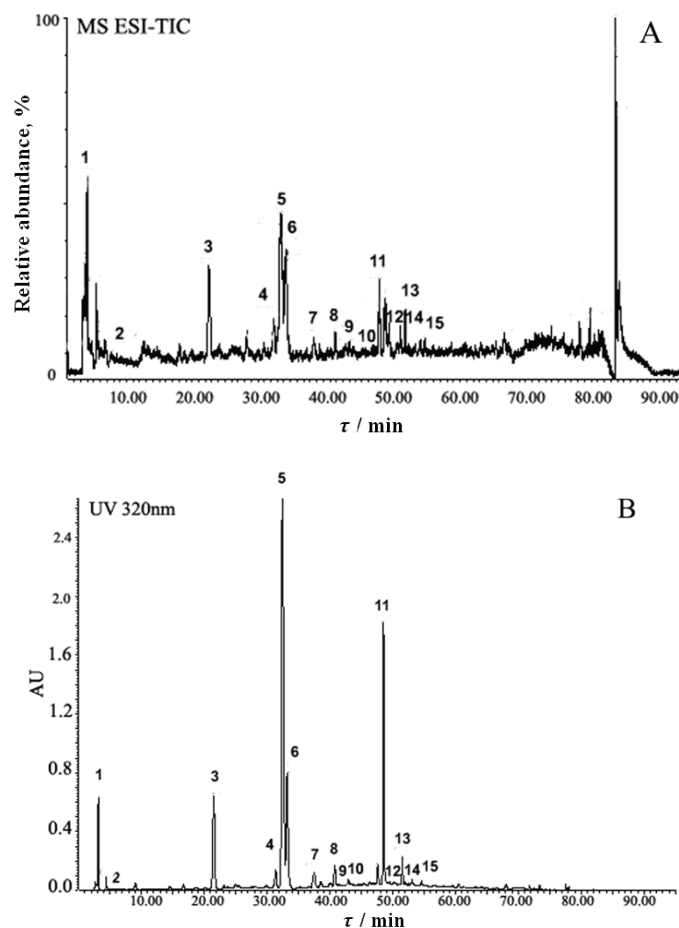


Fig. 2. Chromatographic profiles of a 70 % methanolic extract of tobacco wastes: MS SCAN ESI-TIC (A) and UV at 320 nm (B).

Characterization of p-coumaroylquinic acids (MW 338)

As can be seen from Fig. 2, two peaks (**8**, **10**) were found in the TIC detected by the negative ion ESI-MS scan mode and UV at 320 nm. The chromatographic profiles of 70 % methanolic extracts of the tobacco wastes are shown in Fig. 4 as MS MRM, m/z 337.3 \rightarrow 191.4, MS MRM, m/z 367.3 \rightarrow 173.3 and MS MRM m/z 515.3 \rightarrow 353.3. Based on the MS² base peak m/z 191.4, the larger peak (**8**) and the smaller peak (**10**) were easily identified as 5-*O-p*-coumaroylquinic acid (5-*p*CoQA) and 3-*O-p*-coumaroylquinic acid (3-*p*CoQA), respectively, by their MS MRM (m/z 337.3 \rightarrow 191.4, Fig. 4A) and by comparing the UV and MS² spectral data with those reported in the literature.^{18,19,34,35}

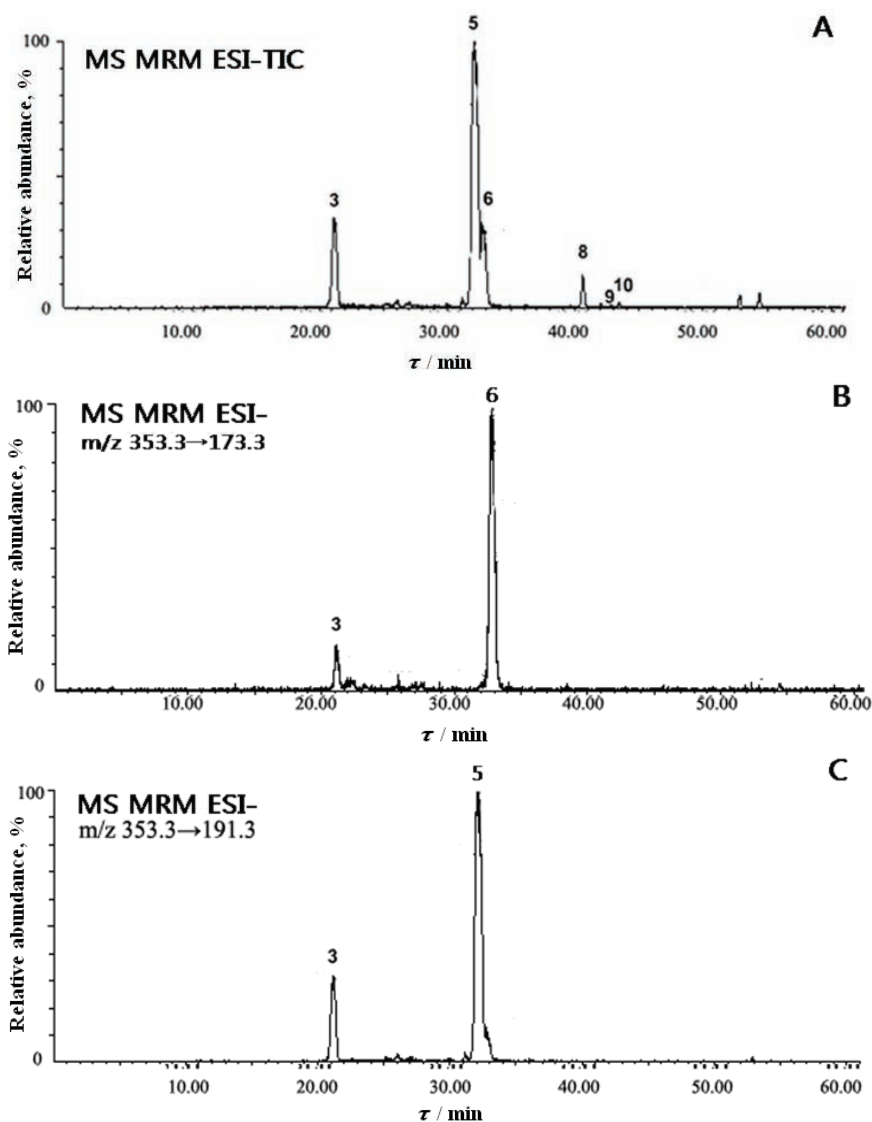


Fig. 3. Chromatographic profiles of a 70 % methanolic extract of tobacco wastes: A) MS MRM ESI-TIC; B) MS MRM, m/z 353.3 \rightarrow 173.3; C) MS MRM, m/z 353.3 \rightarrow 191.3.

Characterization of feruloylquinic acids (MW 368)

Based on the MS² base peak m/z 173.3, a peak (9) was found in the TIC, detected by negative ion ESI-MS and UV at 320 nm (Fig. 2), which was identified as 4-*O*-feruloylquinic acid (4-FQA) by its MS scan and MRM (m/z 367.3 \rightarrow 173.3) (Fig. 4B) spectral data and by comparing the UV and MS spectra data with those reported in the literature.^{18,37} However, as can be seen from Fig. 4B,

the MRM (m/z 367.3 \rightarrow 173.3) data also showed that a very small peak in the UV 320 nm chromatographic profiles (retention time: 42.02 min) had m/z 367.3 and m/z 173.3 ions and had the split pathway of m/z 367.3 \rightarrow 173.3, as well. Thus, it may be a derivative of 4-FQA.

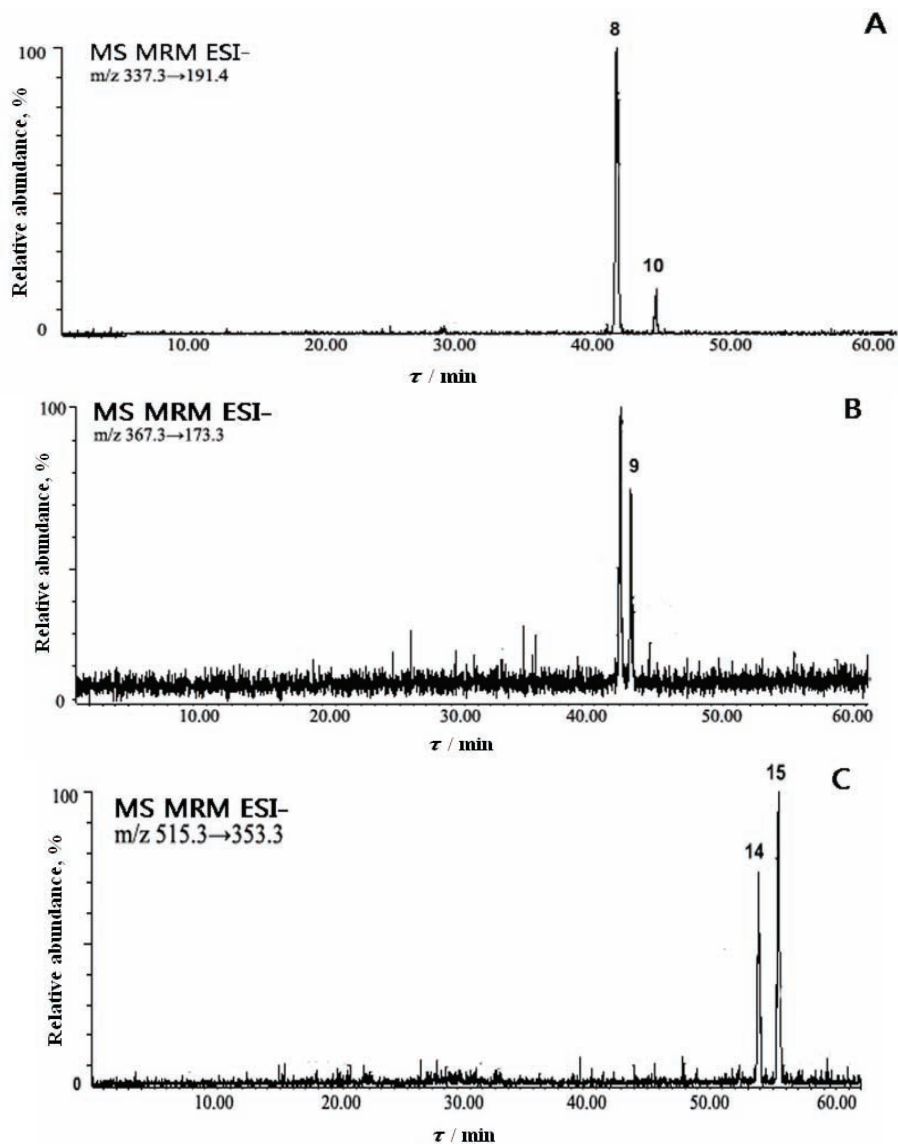


Fig. 4. Chromatographic profiles of a 70 % methanolic extract of tobacco wastes: A) MS MRM, m/z 337.3 \rightarrow 191.4; B) MS MRM, m/z 367.3 \rightarrow 173.3; C) MS MRM, m/z 515.3 \rightarrow 353.3.

Characterization of di-caffeoylquinic acids (MW 516)

Typically, two peaks (14 and 15) were found in the TIC detected by the negative ion ESI-MS scan mode and UV at 320 nm (Fig. 4C).

Comparing the UV and MS spectra data with those reported in literature,^{9,18} as can be seen from Fig. 4C, based on the MS² base peak m/z 353.3, peaks 14 and 15 were identified as 1,5-di-*O*-caffeoylquinic acid (1,5-diCQA) and 3,5-di-*O*-caffeoylquinic acid (3,5-diCQA) by their parent ion mode (m/z 515.3), daughter ion mode (m/z 353.3), and MS MRM (m/z 515.3 \rightarrow 353.3, m/z 353.3 \rightarrow 173.3 and m/z 353.3 \rightarrow 191.3).

Characterization of quinic acid, nicotine, scopolin, caffeic acid, rutin, isoquercitrin and luteolin-7-rutinoside

Seven peaks (1, 2, 4, 7, 11, 12 and 13) were found in the TIC detected by the negative ion ESI-MS SCAN mode and UV at 320 nm. Comparing the UV and MS spectra data with those reported in CA, peaks 1 (quinic acid), 2 (nicotine), 4 (scopolin), 7 (caffeic acid), 11 (rutin), 12 (isoquercitrin), and 13 (luteolin-7-rutinoside) were identified by comparing their retention times and UV and MS spectra with those of standard compounds.

Contents of chlorogenic acids and rutin in tobacco wastes by HPLC-UV

Calibration curves were obtained by plotting peak areas vs. six different concentrations of the standard solutions. The calibration curve equations were: neochlorogenic acid (3-CQA) $y = 6.196 \times 10^7 x - 4.453 \times 10^4$ ($r^2 = 0.9997$); chlorogenic acid (5-CQA) $y = 5.841 \times 10^7 x - 4.384 \times 10^4$ ($r^2 = 0.9996$); cryptochlorogenic acid (4-CQA) $y = 5.068 \times 10^7 x - 4.025 \times 10^4$ ($r^2 = 0.9996$)²⁷ and rutin $y = 3.001 \times 10^7 x - 1.100 \times 10^5$ ($r^2 = 0.9997$). The developed method was successfully applied to the simultaneous determination of 3-CQA, 5-CQA, 4-CQA, and rutin in 10 samples of tobacco waste that were obtained from various countries and regions in the world. The results of the determinations are given in Table II.

From the results presented in Table II, it was found that the contents of 3-CQA, 5-CQA, 4-CQA, chlorogenic acids, and rutin varied greatly among the different samples. In the majority of cases, the contents of 3-CQA, 5-CQA, 4-CQA and rutin in the 10 samples were within the ranges 0.116–0.196, 0.686–1.781, 0.094–0.192 and 0.413–0.998 %, respectively. Chlorogenic acids were the main components in the tobacco wastes, with total contents varying from 0.897 to 2.130 % in the 10 samples; an almost 2.4-fold variation. Similar variation could also be found for the contents of rutin in the tobacco wastes. The reasons for these variations in their contents might be the difference in the origin of the plant, the effect of environment, and/or other factors, such as the season at the time of collection, the drying process used, storage conditions, etc.

Evaluation of tobacco waste resource by HCA on the basis of PCA pattern

As variations in the contents of polyphenols may influence the quality and potency of tobacco wastes, it was necessary to develop an effective statistic analysis method to evaluate the quality of tobacco wastes. Thus, for the application of tobacco wastes as a potential ethnopharmacological resource in the production of chlorogenic acids and rutin, the overall similarity of chlorogenic acids and rutin contents among the varieties was calculated using the HCA method based on the PCA pattern.

TABLE II. Contents of neochlorogenic acid (3-CQA), chlorogenic acid (5-CQA), cryptochlorogenic acid (4-CQA), chlorogenic acids and rutin in 10 tobacco wastes ($n = 3$)

No.	Source	Content of active compounds, % ^a				
		3-CQA (x_1)	5-CQA (x_2)	4-CQA (x_3)	Chlorogenic acids ^b (x_4)	Rutin (x_5)
1	Jin'an Songyun 87BSL Kunming (B1L and B2L mixed) (2005)	0.150±0.015	0.870±0.048	0.111±0.014	1.132±0.075	0.998±0.065
2	Jin'an Songyun 87CSL Kunming (C1L and C2L mixed) (2005)	0.157±0.007	0.704±0.044	0.129±0.008	0.990±0.058	0.719±0.036
3	Zimbabwe B10A (2004)	0.116±0.007	0.686±0.052	0.094±0.011	0.897±0.069	0.655±0.057
4	Jin'an Songyun 87MZL Kunming (C4L, X2L and X3L mixed) (2005)	0.157±0.006	0.709±0.032	0.140±0.004	1.006±0.042	0.725±0.070
5	Nanrun Hongda B2F (2004)	0.182±0.003	1.483±0.033	0.158±0.003	1.823±0.038	0.848±0.069
6	Wei said Artemis K326 C1L (2002)	0.141±0.003	0.908±0.027	0.123±0.006	1.172±0.035	0.413±0.051
7	Nanrun Hongda X2F (2004)	0.196±0.009	1.114±0.068	0.192±0.014	1.502±0.090	0.537±0.052
8	Zimbabwe TL40 (2004)	0.154±0.002	0.950±0.033	0.157±0.008	1.261±0.042	0.614±0.077
9	Nanrun Hongda C2F (2004)	0.190±0.008	1.781±0.084	0.159±0.021	2.130±0.108	0.807±0.096
10	Jiangsu Tobacco Company Nanjing Branch (2007)	0.156±0.003	0.699±0.015	0.151±0.002	1.006±0.018	0.464±0.024

^aData are expressed as mean \pm SD of three experiments; ^bdata are the sum of contents of 3-CQA, 5-CQA and 4-CQA

The data was pre-processed using auto-scale and incremental linkage methods for data from tobacco wastes samples.²³ The goal of PCA is to group cor-

related variables and replace them with new sets called PCs. PCs contain most of the data set variability, but in a much lower dimensional space.²⁹ The first principal component, PC_1 , is defined as the direction of maximum variance of the entire data set. PC_2 is the direction that describes the maximum variance in the subspace orthogonal to PC_1 . The subsequent components are taken orthogonally and describe the maximum remaining variance.^{23–26} In the present study, the PCA score plots for the contents of chlorogenic acids and rutin in tobacco wastes using auto-scale pre-processing are shown in Fig. 5.

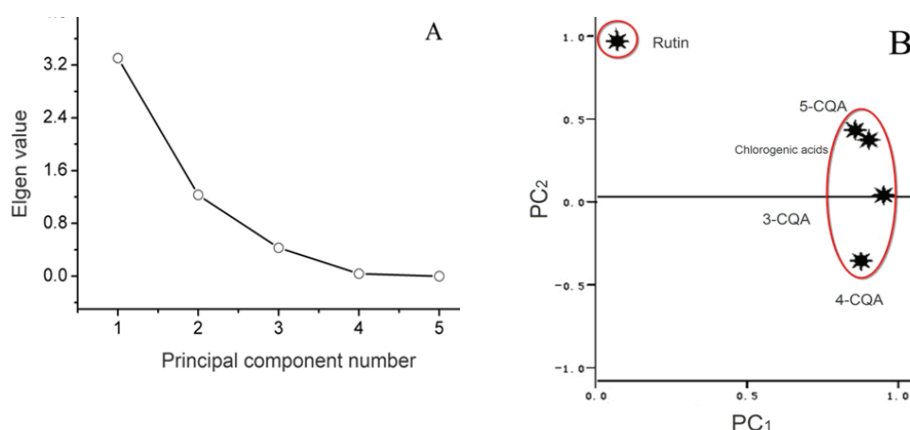


Fig. 5. PCA results for the contents of chlorogenic acids and rutin in different varieties of tobacco wastes. A) PCA score plots; B) the contribution of content parameters to PC_1 and PC_2 .

As can be seen from Fig. 5, for data of the contents of chlorogenic acids and rutin in tobacco wastes, two PCs describe 90.661 % of the data, and three PCs describe 99.264 % of the data. A clear differentiation between the tobacco waste samples from different locations was observed. PC_1 and PC_2 conserved 90.661 % of the total variance of the original data according to the following equations:

$$PC_1 = 0.935x_1 + 0.918x_2 + 0.786x_3 + 0.951x_4 + 0.250x_5 \quad (1)$$

$$PC_2 = -0.174x_1 + 0.230x_2 - 0.547x_3 + 0.163x_4 + 0.906x_5 \quad (2)$$

where x_1 – x_5 are the content of 3-CQA, 5-CQA, 4-CQA, chlorogenic acids and rutin given in Table II, respectively.

Equation (1) indicates the significant importance of the contributions of x_1 – x_4 to PC_1 , while Eq. (2) indicates that the contribution of x_5 to PC_2 is much greater than the other ones. According to the multivariate statistics models, two phenolic compound variables can be considered important for discriminating between varieties of tobacco wastes: chlorogenic acids and rutin. Therefore, data regarding the varieties of tobacco wastes can be analyzed by PC_1 and PC_2 , and the developed PCA method is suitable for reducing overlapping and unnecessary

data, in order to evaluate the relationships between the contents of polyphenols and the varieties of tobacco wastes.

The main objective of HCA is to display data in natural clusters, showing patterns in two-dimensional space.²² Similarities and dissimilarities between the contents of polyphenols and the varieties of tobacco wastes as the results of either direct cluster analysis or HCA based on the PCA pattern are shown in Figs. 6A and 6B, respectively.

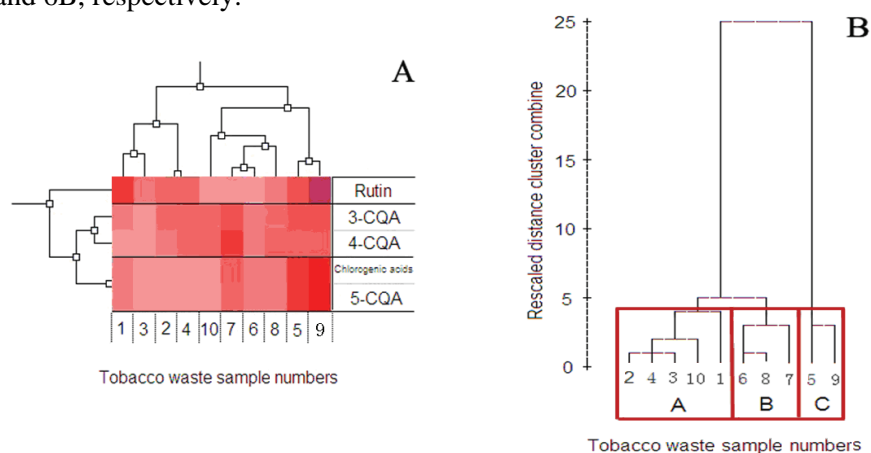


Fig. 6. Similarities and dissimilarities between the contents of the main polyphenols (chlorogenic acids and rutin) and different varieties of tobacco wastes, resulting from cluster analysis: A) direct cluster analysis; B) HCA based on the PCA pattern.

The dendrogram with tobacco wastes from different sources, shown in Fig. 6, is qualitative in nature and permits visualization of clusters and correlations amongst samples. Based on the contents of chlorogenic acids and rutin, see Fig. 6A, it is difficult to classify tobacco waste samples using the direct cluster analysis method. In HCA, the Euclidean distances among samples or variables are transformed into similarity indices. A small distance corresponds to a large index and means a large similarity.^{29–31} As can be seen from Fig. 6B, three distinct clusters represent the sources of the tobacco wastes samples; that is, group A contains sample 2, 4, 3, 10 and 1, group B contains sample 6, 8, and 7, and group C contains samples 5 and 9. Therefore, HCA analysis showed that it is possible to differentiate between phenolic contents and the sources of samples with different geographical origins, and of different varieties: the 10 varieties of tobacco wastes samples are clearly separated into three groups. In a general way, the developed HCA method based on the PCA pattern is suitable for grouping overlapping varieties of tobacco waste resources depending on the contents of polyphenols. The results obtained using the HCA method can provide valuable information to guide high added value usage of chlorogenic acids and rutin in varieties of tobacco wastes throughout the world.

CONCLUSIONS

In this paper, the identification of 15 polyphenols in tobacco wastes is reported. It was also demonstrated that tobacco wastes have a potential application as ethnopharmacological materials in the pharmacological industry, due to the unusual dominance of chlorogenic acids (chlorogenic acid, neochlorogenic acid and cryptochlorogenic acid) and rutin contained within the waste. Moreover, according to multivariate statistics models, using the HCA method based on the PCA pattern, the chlorogenic acid and rutin contents of tobacco waste can be considered important for discriminating between different varieties of tobacco wastes. Ten varieties of tobacco were characterized into three groups using this method. In conclusion, tobacco wastes containing natural chlorogenic acids and rutin could be advantageous for industrial applications and multivariate methods could be useful for the analysis and interpretation of a large number of tobacco waste resources in the world. In further studies, the heterogeneity of tobacco wastes must be regulated and problems concerning the collection, as well as conveyance of the biomass, must be resolved for the practical utilization of tobacco wastes.

Acknowledgements: This work was supported by National Basic Research Program of China (2009CB724700), National Natural Science Foundation of China (20876076), Ordinary University Science Research Project for Young Teacher of Jiangsu Province (08KJB530002), Start Project for Introduce Talent of Jiangsu University of Science and Technology (35211002), and Natural Science Foundation of Jiangsu Province (BK2009213).

ИЗВОД

РАЗЛИКОВАЊЕ И КЛАСИФИКАЦИЈА ДУВАНСКОГ ОТПАДА ОДРЕЂИВАЊЕМ ПОЛИФЕНОЛА МЕТОДОМ LC-MS/MS

JUN WANG^{1,2}, DINGQIANG LU¹, HUI ZHAO¹, BEN JIANG¹, JIALI WANG¹,
XIUQUAN LING¹, HONG CHAI¹ и PINGKAI OUYANG¹

¹College of Biotechnology and Pharmaceutical Engineering, Nanjing University of Technology, Nanjing 210009 и ²College of Biological and Environmental Engineering, Jiangsu University of Science and Technology, Zhenjiang 212018, P. R. China

Хемијски састав полифенола у дуванском отпаду је идентификован методом HPLC-PDA-ESI/MS/MS, садржај хлорогенских киселина и рутина у десет врста дуванског отпада је одређен методом HPLC-UV и однос између садржаја полифенола и врсте дуванског отпада је анализиран хијерархијском кластерском анализом (HCA) и анализом основних компоненти (PCA). Петнаест полифенола је идентификовано у метанолном екстракту сувог дуванског отпада. Измерене су велике концентрације хлорогенских киселина (3-CQA, 5-CQA и 4-CQA) и рутина, у опсегу 0,116–0,196, 0,686–1,781, 0,094–0,192 и 0,413–0,998 %. Према мултиваријантном статистичком моделу, две променљиве се могу сматрати важним у разликовању врсте дуванског отпада: хлорогенске киселине и рутин. Десет врста отпада је класификовано у три групе кластерском анализом на основу садржаја основних компоненти. Користећи ове податке, дувански отпад може наћи примену као фармацевтски материјал за изоловање природних хлорогенских киселина и рутина у етнофармаколошкој индустрији.

(Примљено 9. новембра 2009, ревидирано 25. фебруара 2010)

REFERENCES

1. X. Zhu, F. Zheng, Z. Cao, *Acta Tabacaria Sinica* **12** (2006) 58
2. P. P. Mumba, R. Phiri, *Int. J. Environ. Res.* **2** (2008) 225
3. S. Chaturvedi, D. K. Upreti, D. K. Tandon, A. Sharma, A. Dixit, *J. Environ. Biol.* **29** (2008) 759
4. M. Seredych, T. J. Badosz, *Environ. Sci. Technol.* **41** (2007) 3715
5. C. Crofcheck, M. Loiselle, J. Weekley, I. Maiti, S. Pattanaik, P. M. Bummer, M. Jayt, *Biotechnol. Prog.* **19** (2003) 680
6. S. K. Zhu, X. Lu, L. Dong, J. Xing, X. L. Su, H. W. Kong, G. W. Xu, C. Y. Wu, *J. Chromatogr. A* **1086** (2005) 107
7. H. F. Li, K. J. Zhong, X. Lu, C. M. Bai, J. G. Huang, H. L. Lu, C. F. Ma, S. K. Zhu, H. W. Kong, M. Y. Zhao, J. P. Xie, S. Niu, G. W. Xu, *Acta Chim. Sinica* **64** (2006) 1897
8. M. E. Hegazy, T. Hirata, A. Abdet-lateff, M. H. El-Razek, A. E. Mohamed, N. M. Hassan, P. W. Pare, A. A. Mahmoud, *Z. Naturforsch. A* **63** (2008) 403
9. M. N. Clifford, S. Knight, N. Kuhnert, *J. Agric. Food. Chem.* **53** (2005) 3821
10. W. J. Arion, W. K. Canfield, F. C. Ramos, P. W. Schindler, H. J. Burger, H. Hemmerle, G. Schubert, P. Below, A. W. Herling, *Arch. Biochem. Biophys.* **339** (1997) 315
11. S. S. Kim, C. K. Lee, S. S. Kang, H. A. Jung, J. S. Choi, *Arch. Pharmacol. Res.* **20** (1997) 148
12. B. Borkowski, G. Skuza, Z. Rogoz, *Herba Pol.* **45** (1999) 192
13. G. W. Plumb, M. T. Garcia-Conesa, P. A. Kroon, M. Rhodes, S. Ridley, G. Williamson, *J. Sci. Food Agric.* **79** (1999) 390
14. J. Wang, D. Q. Lu, H. Q. Qiao, X. Q. Ling, H. Zhao, P. K. Ouyang, *J. Biotechnol.* **136S** (2008) 369
15. C. M. Ma, M. Kully, J. K. Khan, M. Hattori, M. Daneshtalab, *Bioorg. Med. Chem.* **15** (2007) 6830
16. L. Gobbo-Neto, N. P. Lopes, *J. Agric. Food. Chem.* **56** (2008) 1193
17. H. W. Im, B. S. Suh, S. U. Lee, N. Kozukue, M. Ohnisi-Kameyama, C. E. Levin, M. Friedman, *J. Agric. Food. Chem.* **56** (2008) 3341
18. M. N. Clifford, K. L. Johnston, S. Knight, N. Kuhnert, *J. Agric. Food. Chem.* **51** (2003) 2900
19. M. N. Clifford, W. G. Wu, J. Kirkpatrick, N. Kuhnert, *J. Agric. Food. Chem.* **55** (2007) 929
20. C. M. Ma, M. Hattori, H. B. Chen, S. Q. Cai, M. Daneshtalab, *Phytochem. Anal.* **19** (2008) 294
21. D. Perrone, A. Farah, C. M. Donangelo, T. de Paulis, P. R. Martin, *Food Chem.* **106** (2008) 859
22. A. Petsalo, J. Jalonen, A. Tolonen, *J. Chromatogr. A* **1112** (2006) 224
23. M. de Andrade, D. Palmeira Souza, J. B. Paraiso Silva, A. P. Silveira Paim, *Quím. Nova* **31** (2008) 296
24. M. V. Gil, L. F. Calvo, D. Blanco, M. E. Sanchez, *Bioresour. Technol.* **99** (2008) 5763
25. Y. Ni, Y. Peng, S. Kokot, *Chromatographia* **67** (2008) 211
26. A. Gonzalvez, A. Llorens, M. L. Cervera, S. Armenta, M. de la Guardia, *Food Chem.* **112** (2009) 26
27. J. Wang, D. Q. Lu, X. Q. Ling, J. L. Wang, H. Q. Qiao, P. K. Ouyang, *Chromatographia* **69** (2009) 561
28. P. Geladi, M. Manley, T. Lestander, *J. Chemom.* **17** (2003) 503
29. S. M. Yidana, D. Ophori, B. Banoeng-Yakubo, *J. Environ. Manage.* **86** (2008) 80
30. L. C. de Melo, S. F. Braga, P. M. V. B. Barone, *J. Mol. Graphics Modell.* **25** (2007) 912
31. A. Dallos, H. S. Ngo, R. Kresz, K. Heberger, *J. Chromatogr. A* **1177** (2008) 175
32. M. G. Yalcin, S. Ilhan, *Bull. Environ. Contam. Toxicol.* **81** (2008) 57

33. M. N. Clifford, W. G. Wu, N. Kuhnert, *Food Chem.* **95** (2006) 574
34. M. N. Clifford, W. Zheng, N. Kuhnert, *Phytochem. Anal.* **17** (2006) 384
35. M. N. Clifford, S. Marks, S. Knight, N. Kuhnert, *J. Agric. Food. Chem.* **54** (2006) 4095
36. M. A. Smith, V. B. Weaver, D. M. Young, L. N. Ornston, *Appl. Environ. Microbiol.* **69** (2003) 524.



J. Serb. Chem. Soc. 75 (7) 893–902 (2010)
JSCS–4015

Δ^9 -Tetrahydrocannabinol content in cannabis samples seized in Novi Sad during 2008

MAJA DJURENDIĆ-BRENESEL*, NIKŠA AJDUKOVIĆ, KATARINA ŠTAJNIC-RISTIĆ,
VLADIMIR PILIJA and IGOR VESELINOVIĆ

*Institute of Forensic Medicine, Clinical Center Vojvodina, Hajduk Veljkova 7–9,
21000 Novi Sad, Serbia*

(Received 19 October, revised 15 December 2009)

Abstract: The three main cannabinoids Δ^9 -tetrahydrocannabinol (Δ^9 -THC), cannabidiol (CBD) and cannabinol (CBN) were identified and determined quantitatively using a GCD (GC-EI) instrument in 280 samples of illicit herbal cannabis, seized by the Police authorities in Novi Sad, during 2008. The samples were sent to the Institute of Forensic Medicine, Clinical Center Vojvodina, for forensic chemical analysis. The cannabinoid content of the samples enabled the classification of the cannabis into three chemical phenotypes and the differentiation into drug and textile-cannabis, using the Waller classification index. This differentiation has great forensic significance in the classification of certain cases as a criminal action. The experimental results showed that the Δ^9 -THC content in illicitly circulated cannabis slightly decreased from January to December 2008, as did the quality of the drug-cannabis. The reasons for the quality variations could lie in the geographical origin of the cannabis plants, the conditions of plants storage, various parts of the plants in samples and the time elapsed between harvesting and chemical analysis.

Keywords: cannabinoids; forensic samples; GCD analysis; phenotype; Waller index.

INTRODUCTION

Cannabis (*Cannabis sativa* L.) is a plant widely distributed throughout the world and its cultivation is prohibited in most countries, including Serbia. The fibre-type plants are legally cultivated in some regions under specific permission.

The three main cannabinoids found in *Cannabis sativa* L. are the psychoactive Δ^9 -tetrahydrocannabinol (Δ^9 -THC) and the non-psychoactive cannabidiol (CBD) and cannabinol (CBN). The highest cannabinoid content is found in the resin secreted by the flowering buds of the plants. Δ^9 -THC, which is the main psychoactive constituent, is found in similar amounts in male and female canna-

* Corresponding author. E-mail: maja.brenesel@gmail.com
doi: 10.2298/JSC091019070D

bis grown under the same conditions. It was shown that in the various parts of cannabis plant, the Δ^9 -THC content decreases in the following order: bracts, flowers, smaller stems, larger stems, roots and seeds.¹

Textile (fibre-type) cannabis is cultivated for a wide variety of hemp-based products, such as: edible seed oil, essential oils, flour, beverages (beer, lemonade and liqueur), cosmetics, lubricants, fuels and fibres for the paper and building industries.^{1,2} Resinous (drug-type) cannabis is illicitly cultivated for its psychoactive pharmacological action.³

Since cannabis is most commonly administered by smoking or ingesting, the THC predominantly acts on the central nervous (CNS) and cardiovascular systems. Common CNS effects include euphoria, a sense of well-being, relaxation, tachycardia, alteration in blood pressure and hallucinations at high doses.^{4,5}

For court testimonies and police authority purposes, seized cannabis samples, after chemical analysis, are classified into three chemical phenotypes: drug, intermediate and fibre-type, according to the Δ^9 -THC content and the Waller classification index, W , (Eq. (1)):^{6,7}

$$W = \frac{\% \Delta^9\text{-THC} + \% \text{CBN}}{\% \text{CBD}} \quad (1)$$

1. $\% \Delta^9\text{-THC} > 0.3$ and $W > 1$; the plant is classified as a drug-type (resinous cannabis) and could be abused as a psychoactive drug;

2. a) $\% \Delta^9\text{-THC} < 0.3$ and $W > 1$ or b) $\% \Delta^9\text{-THC} > 0.3$ and $W < 1$; the plant is classified as an intermediate-type and could be abused as a psychoactive drug;

3. $\% \Delta^9\text{-THC} < 0.3$ and $W < 1$; the plant is classified as a fibre-type (textile cannabis) and could not be abused.

It is necessary to emphasize that a low content of Δ^9 -THC ($\% \Delta^9\text{-THC} < 0.3$) in intermediate-type cannabis samples is not incompatible with their resinous character. As it is known that in these samples CBN, a degradation product of Δ^9 -THC, is present in a large amounts, the $\% \Delta^9\text{-THC} + \% \text{CBN}$ would approximate the Δ^9 -THC content. When the Waller classification index is low ($W < 1$) in intermediate-type cannabis samples, the CBD content is high, which indicates that the samples originated from relatively young potent plant.⁶

According to the law in European Union countries, the maximum permitted content of Δ^9 -THC in fibre-type cannabis varieties is 0.3%.^{8,9} Based on the Δ^9 -THC content and the Waller classification index, forensic cannabis samples are differentiated into drug cannabis, if they are drug or intermediate-type, and textile cannabis, if they are fibre-type. This differentiation has great forensic significance in the classification of certain cases as a criminal action.

EXPERIMENTAL

Sample preparation

Two hundred and eighty illicit herbal cannabis samples, seized by Police authorities in Novi Sad during 2008, were sent to the Institute of Forensic Medicine, Clinical Center Vojvodina, for forensic chemical analysis. The stems and seeds were manually separated from the dried plant material, leaving leaves, blossoms, small structural parts of the inflorescence and bracts. The resulting material was weighed and ground in a mortar. Each sample consisting of 50 mg ground powder was heated with 5 ml petroleum ether (boiling range 40–60 °C) at 60 °C for 20 min.^{10,11} After cooling, the petroleum ether extract was filtered and evaporated to dryness. The residue was reconstituted in 1.9 ml petroleum ether, 0.1 ml of epi-androsterone as the internal standard (IS) was added at a concentration 7 mg ml⁻¹ in ethanol,⁷ and a 1- μ l aliquot of the resulting solution was injected into the GCD instrument.

Gas chromatographic analysis

The cannabinoid content (% Δ^9 -THC, % CBD and % CBN) was determined chromatographically using a G 1800 A GCD instrument, equipped with an HP 6890 autosampler. GCD is an advanced gas chromatography (GC) system introduced by Hewlett Packard in 1994. The GCD consists of a chromatograph, electron ionization (EI) detection system for m/z up to 425 and a data acquisition system. The EI detection system generates retention time, abundance and mass spectral data that are comparable with those obtained with a GC–mass spectrometry (MS) instrument.

The conditions for the analysis were as follows: column HP-5MS (30 m \times 0.25 mm i. d., film thickness 0.25 μ m); injection port temperature: 250 °C; interface temperature: 280 °C; split mode: 1:11; oven temperature: initial, 50 °C; initial time: 0 min; heating rate: 25 °C min⁻¹, final temperature: 250 °C, final time: 10 min; helium flow rate: 1 ml min⁻¹.

Standard solutions

Stock standard solutions containing Δ^9 -THC, CBD and CBN at 1 mg ml⁻¹ concentration in methanol, purchased from Sigma–Aldrich, Germany, were diluted with petrol ether and calibration standards were prepared at the concentrations: 500, 250, 100 and 50 μ g ml⁻¹, containing epi-androsterone (IS) at a concentration 350 μ g ml⁻¹.

RESULTS AND DISCUSSION

The major constituents of the seized cannabis samples were identified and quantitatively determined using a GCD instrument. The retention times of Δ^9 -THC, CBD, CBN and epi-androsterone were 14.44, 12.99, 15.70 and 15.22 min, respectively. For quantitative analysis, the chosen characteristic mass fragments were monitored in the SCAN mode: m/z 314, 299 and 231 for Δ^9 -THC, m/z 231, 174 and 314 for CBD, m/z 295, 238 and 310 for CBN, and m/z 290, 246 and 107 for epi-androsterone.

The cannabinoid content of the cannabis samples led to the differentiation of the cannabis into drug, intermediate and fibre-type, then into drug and textile cannabis, according to the Waller classification index.

Typical total ion chromatograms (TIC) of drug, intermediate and fibre-type cannabis samples are presented in Figs. 1–3, respectively.

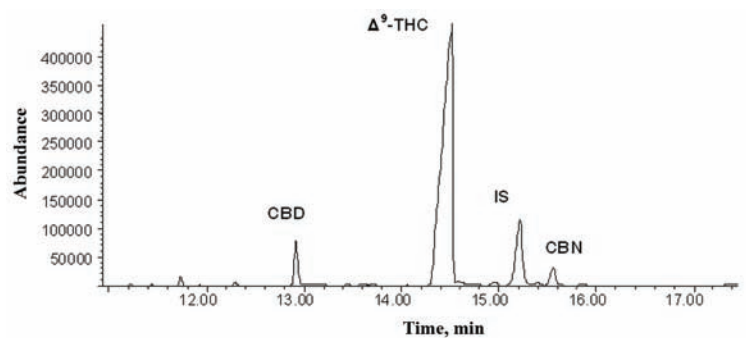


Fig. 1. TIC gas chromatogram of a drug-type cannabis sample.

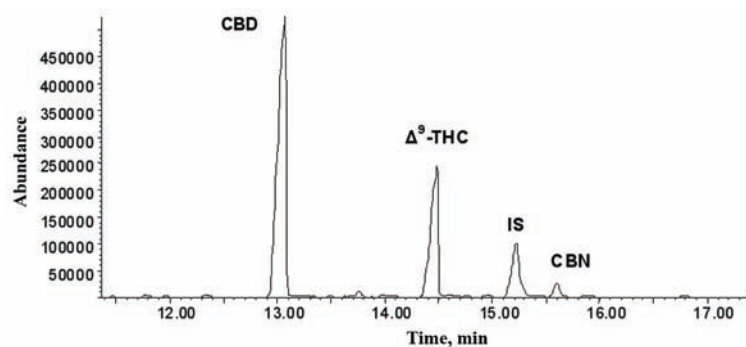


Fig. 2. TIC gas chromatogram of an intermediate-type cannabis sample.

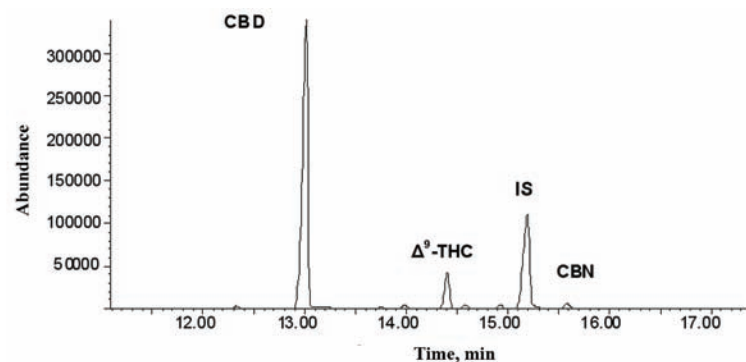


Fig. 3. TIC gas chromatogram of a fibre-type cannabis sample.

The percentage of Δ^9 -THC and the Waller classification index of the 280 cannabis samples seized during 2008 are presented in Table I.

The percent of drug, intermediate and fibre-type cannabis during 2008 is presented in Fig. 4 and the percent of cannabis samples classified as a drug or textile during 2008 is presented in Fig. 5.

TABLE I. % Δ⁹-THC and Waller classification index of 280 cannabis samples during 2008

Sample	Month	% THC	W index	Sample	Month	% THC	W index	Sample	Month	% THC	W index
1	January	3.001	3.69	95	June	0.158	1.48	189	October	2.126	6.38
2		2.143	1.75	96		3.670	10.15	190		0.059	0.03
3		3.433	7.11	97		0.910	8.56	191		0.037	0.02
4		4.633	5.23	98		3.520	7.32	192		0.507	8.36
5		4.262	4.25	99		0.366	7.63	193		1.124	4.62
6		0.570	8.03	100		1.207	13.03	194		0.643	1.06
7		0.765	7.56	101		1.317	13.59	195		1.413	4.32
8		0.466	9.05	102		2.844	43.80	196		1.814	5.8
9		0.844	6.23	103		0.127	0.17	197		1.579	4.65
10		0.577	11.13	104		0.652	15.66	198		0.035	1.61
11	February	0.346	6.35	105		2.586	2.78	199		0.226	1.06
12		1.378	4.28	106		2.372	9.30	200		0.328	1.94
13		0.013	0.02	107		0.452	0.86	201		0.028	0.35
14		1.642	1.42	108		3.640	50.43	202		0.359	0.49
15		1.804	2.35	109		0.257	6.20	203		1.223	1.27
16		1.602	2.08	110		0.816	7.04	204		1.568	5.03
17		4.000	1.27	111		2.007	16.78	205		0.086	0.19
18		3.789	1.27	112		3.094	2.81	206		0.612	0.45
19		1.159	17.42	113		2.306	2.62	207		0.599	3.10
20		1.323	1.02	114		1.596	2.88	208		0.479	6.73
21		2.443	2.04	115		0.988	4.89	209		1.788	2.68
22		4.359	1.96	116		0.563	3.53	210		3.781	3.35
23		2.146	17.90	117		1.432	14.97	211		0.801	3.04
24		1.160	18.50	118		1.978	23.16	212		1.949	0.84
25		0.469	60.02	119		1.048	6.51	213		0.163	0.05
26		0.823	5.23	120		0.102	26.59	214		0.784	0.63
27		0.052	0.07	121		0.156	20.94	215		0.910	0.43
28		1.231	7.24	122		1.931	19.02	216		0.152	0.36
29		1.036	6.26	123		0.479	16.26	217		2.114	15.52
30	March	0.823	14.92	124		0.301	50.89	218		1.031	12.83
31		0.167	2.33	125	July	0.705	0.35	219		0.405	0.99
32		0.323	7.81	126		0.714	0.42	220		0.118	0.34
33		0.329	3.77	127		0.538	0.28	221		0.373	0.49
34		0.132	0.82	128		0.627	0.39	222		1.482	0.47
35		2.014	7.80	129		1.111	2.35	223		0.639	4.78
36		0.516	2.40	130		0.941	1.38	224		0.808	9.01
37		1.331	7.16	131		0.771	1.05	225		0.559	3.26
38		2.159	22.95	132		0.673	0.52	226		0.755	1.35
39		2.909	11.77	133		1.592	4.23	227		1.609	2.45
40		0.981	2.62	134		0.351	2.85	228		1.748	1.20
41		0.698	2.40	135		1.796	3.17	229		0.693	0.58
42		0.803	0.48	136		1.300	1.27	230		0.831	0.71
43		1.942	1.01	137		1.043	1.48	231		0.780	2.60
44		0.105	0.91	138		0.638	3.00	232		0.196	0.38
45		0.685	5.05	139		0.694	0.22	233		0.195	0.38

TABLE I. Continued

Sample	Month	% THC	W index	Sample	Month	% THC	W index	Sample	Month	% THC	W index
46		4.614	15.39	140		0.401	3.46	234		0.278	0.24
47		0.352	1.12	141		0.744	3.24	235		0.208	0.45
48		2.608	8.01	142		0.943	4.05	236		0.768	3.65
49		0.665	3.05	143		1.490	3.05	237		0.028	0.04
50	April	1.264	0.83	144		0.695	0.56	238		0.615	2.90
51		0.458	0.25	145		0.732	0.83	239		0.063	0.17
52		0.965	0.22	146		1.792	0.95	240		0.663	8.36
53		0.536	0.16	147		0.889	0.58	241		0.689	6.89
54		0.690	0.35	148	August	1.869	2.43	242		0.353	0.71
55		0.391	0.18	149		1.746	8.74	243		0.836	1.43
56		0.852	0.24	150		0.995	3.89	244	November	0.381	1.71
57		0.301	5.25	151		1.727	3.20	245		1.249	0.80
58		1.055	2.86	152		0.518	4.78	246		0.699	2.34
59		1.608	3.45	153		0.080	9.29	247		1.425	5.52
60		0.283	2.16	154		0.095	8.89	248		1.321	3.47
61		0.696	8.46	155		0.129	3.92	249		0.504	4.35
62		0.528	1.31	156		1.450	17.50	250		1.082	7.95
63		0.301	31.10	157		1.737	0.70	251		0.765	7.00
64		0.355	28.12	158		0.227	1.64	252		3.321	20.87
65	May	2.211	5.26	159		0.943	3.16	253		0.757	6.58
66		0.120	0.08	160		1.840	4.25	254		1.763	2.81
67		0.817	6.66	161		1.591	4.10	255		1.326	2.55
68		0.454	1.41	162		1.418	3.85	256		0.646	0.53
69		1.426	16.99	163		0.699	0.28	257		0.447	3.42
70		0.531	3.71	164		1.085	2.31	258		1.038	4.06
71		0.416	4.47	165		0.717	0.35	259		0.420	2.50
72		0.659	5.22	166	September	1.770	1.12	260		0.568	8.27
73		0.612	5.11	167		0.906	4.24	261		2.191	1.86
74		0.676	5.89	168		1.081	2.05	262		0.984	0.88
75		0.622	7.53	169		0.962	13.11	263		0.605	0.54
76		0.448	8.09	170		1.770	1.12	264		0.905	0.85
77		0.695	8.04	171		0.900	4.54	265		1.012	10.42
78		0.676	6.11	172		0.952	2.38	266		0.684	3.60
79		0.919	5.00	173		0.925	3.25	267		3.911	6.21
80		0.770	3.12	174		0.826	2.68	268	December	0.060	0.70
81		0.380	3.15	175		0.835	9.35	269		0.486	4.65
82	June	4.479	14.05	176		1.434	7.57	270		0.422	3.73
83		1.662	26.76	177		0.818	9.44	271		2.144	0.34
84		2.333	4.02	178		0.664	5.78	272		0.280	1.11
85		1.003	3.47	179		0.130	2.29	273		1.705	1.90
86		2.290	21.96	180		0.716	8.65	274		0.494	0.59
87		0.734	1.85	181		0.175	0.23	275		1.923	1.44
88		1.358	8.91	182		0.351	0.54	276		1.912	0.78
89		0.310	4.23	183	October	0.190	0.28	277		1.045	1.36
90		4.479	8.70	184		0.060	0.03	278		0.244	0.05

TABLE I. Continued

Sample	Month	% THC	W index	Sample	Month	% THC	W index	Sample	Month	% THC	W index
91		1.782	21.20	185		1.333	4.28	279		0.797	4.98
92		0.688	11.43	186		1.446	1.37	280		2.282	2.46
93		0.480	67.32	187		0.731	0.42	279		0.797	4.98
94		1.609	1.93	188		0.712	0.48	280		2.282	2.46

According to the present work, the Δ^9 -THC content varied from 0.013 to 4.633 % and the Waller classification index from 0.02 to 67.32 % in the 280 cannabis samples seized during 2008 (Table I). The percent of drug, intermediate and fibre-type cannabis during 2008 was 77.5, 14.3 and 8.2, respectively. The most cannabis samples classified as a drug-type were seized in January and in May until September. During 2008, the monthly percent of drug-type cannabis varied from 46.7 to 100 %, of intermediate-type from 0 to 53.3 % and of fibre-type from 0 to 24.6 % (Fig. 4). The percent of drug cannabis varied from 69.2 to 100 % and that of textile cannabis from 0 to 24.6 % during 2008 (Fig. 5). The results showed that the Δ^9 -THC content in the illicitly circulated cannabis slightly decreased from January until December 2008, as did the quality of the drug-cannabis. The reasons for the quality variations could lie in the geographical origin of the cannabis plants, the conditions of plants storage, differing parts of the plants in the samples and the time elapsed between harvesting and chemical analysis. The highest Δ^9 -THC yield reached in the studied samples was 4.633 %.

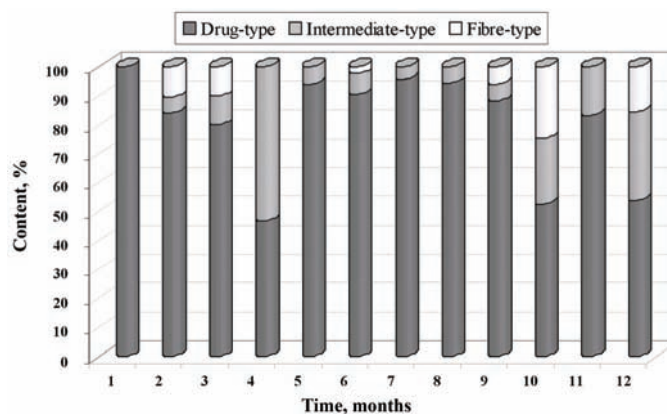


Fig. 4. Percent of drug, intermediate and fibre-type cannabis during twelve months in 2008.

It is well known that there are wide variations in the relative amounts of cannabinoids in cannabis plants. This variation depends on numerous factors. The predominant factors are the genetic characteristics of the seed stock and the environment in which the plant is grown, such as: light, temperature, moisture

and oxygen.^{12,13} Some investigators concluded that the concentration of THC in marihuana is not dependent on the local growing conditions, but on the seed from which it is grown. It was also observed that THC will eventually decompose to CBN and that the original amount of THC present in marihuana can be computed by adding the amount of CBN to the THC present at the time of assay.¹⁴

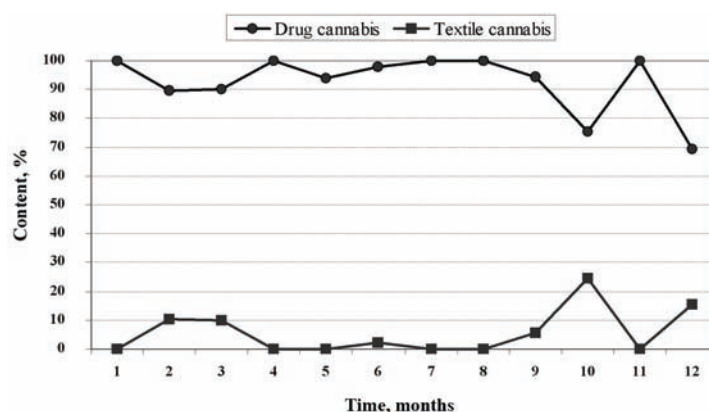


Fig. 5. Percent of drug and textile-type cannabis during twelve months in 2008.

By assaying marihuana for its contents of THC, CBD and CBN, a great deal of information can be obtained regarding the potential source of the sample, its potency as a drug and the approximate time since it was first processed. It would also follow that if many confiscated samples had the same concentration of THC, CBD and CBN, it would be likely that they came from the same source, which could then be sought as a distribution point.

Bearing in mind that seeds are freely transferred from one country to other, some investigators concluded that there is little valid basis for attempts to correlate the cannabinoid content with the country of origin and allocation of cannabis all over the world. However, Faubert Maunder¹⁵ is of opinion that the presence of CBD and its ratio to Δ^9 -THC is useful criterion for indicating the country of origin if the gross appearance of the sample is taken into account. Some investigators found that plants that are drug phenotype generally originate from countries south of latitude 30 deg N. Plants that are fibre phenotype originate north of the same latitude.¹⁴ Cannabis plant material appears on the illicit market in different forms (buds, kilobricks, marihuana and sinsemilla) and that reflects to some extent on its country of origin. The concentration of CBN is a good indication of the age of samples as well as the storage conditions, indicating either old plant material or poor storage conditions.

Diagnostic tools that allow independent descriptions of the sources of cannabis are essential for unravelling market dynamics.¹⁶ In this regard, Ritter¹⁷ called for pursuing multi-disciplinary approaches to understanding drug markets. A no-

vel forensic approach to understanding the cannabis market is the employment of stable isotope analyses of seized cannabis. Stable isotope analysis has the potential to improve significantly the understanding of cannabis trafficking because stable isotopes function as natural recorders revealing aspects of the geographic origin and growth environment of a plant.^{18,19}

Based on the experience of some investigators, a concentration of THC in marihuana from 0.5 to 1.5 % can be considered as a “good” quality marihuana. If the concentration of THC is less than 0.5 %, the marihuana would be of poorer quality and cigarettes with a concentration of THC in excess of 1.5 % would be very good to excellent marihuana. Some attention must be given to the samples with THC content greater than 1.5 %. It is in this range that smoking marihuana can produce a diminution in the ability an individual to perform tasks requiring concentration, coordination and judgment.²⁰

CONCLUSIONS

As cannabis is an illicit drug, it is only available to the public through illegal channels. Consequently, the chemical analysis of confiscated material is important for the understanding of the health problems to the public associated with the use of any form of the drug. The analytical data generated could be employed to show trends in increasing or decreasing potency, to help identify the country of origin whenever possible and to provide information for policymaking decisions at the national and possibly international level. In addition, the analytical data should provide information to the scientific community in studying health problems associated with cannabis use.

ИЗВОД

САДРЖАЈ Δ^9 -ТЕТРАХИДРОКАНАБИНОЛА У УЗОРЦИМА КАНАБИСА ЗАПЛЕЊЕНИМ У НОВОМ САДУ 2008. ГОДИНЕ

МАЈА БУРЕНДИЋ-БРЕНЕСЕЛ, НИКША АЈДУКОВИЋ, КАТАРИНА ШТАЈНИЋ-РИСТИЋ,
ВЛАДИМИР ПИЛИЈА и ИГОР ВЕСЕЛИНОВИЋ

Институт за судску медицину, Клинички центар Војводине, Хајдук Вељкова 7–9, 21000 Нови Сад

Три основна канабиноида Δ^9 -тетрахидроканабинол (Δ^9 -THC), канабидиол (CBD) и канабинол (CBN) су идентификована и квантификована на GCD (GC-EI) инструменту у 280 узорак биљног материјала – канабиса, заплених од стране органа истраге у Новом Саду 2008. године. Заплени узорци су достављени Институту за судску медицину Клиничког центра Војводине, како би се извршила форензичка хемијска анализа узорак. На основу садржаја канабиноида у узорцима извршена је класификација канабиса на три хемијска фенотипа и диференцијација на канабис-дрога и канабис-текстилни тип, применом Waller-овог класификационог индекса. Наведена диференцијација има изузетан форензички значај у утврђивању извесних случајева као противзаконитих. Експериментални резултати у овом раду указују да садржај Δ^9 -THC-а у канабису на илегалном тржишту, благо опада у периоду од јануара до децембра 2008. године, а такође и квалитет канабиса типа дроге. Варијације у квалитету канабиса могу потицати од географског порекла биљки, услова њиховог чувања,

различитих уситњених делова биљке који се могу наћи у заплењеним узорцима или пак од временског периода између бербе и хемијске анализе узорака канабиса.

(Примљено 19. октобра, ревидирано 15. децембра 2009)

REFERENCES

1. M. Pellegrini, E. Marchei, R. Pacifici, S. Pichini, *J. Pharm. Biomed. Anal.* **36** (2005) 939
2. O. Zoller, P. Rhyh, B. Zimmerli, *J. Chromatogr. A* **872** (2000) 101
3. C. Giroud, L. Rivier, *TIAFT Bull.* **26** (1996) 30
4. V. H. Curran, C. Brignell, S. Fletcher, P. Middleton, J. Henry, *Psychopharmacology* **164** (2002) 61
5. H. P. Rang, M. M. Dale, J. M. Ritter, P. K. Moore, *Pharmacology*, 5th ed., Churchill Livingstone, Edinburgh, 2003, p. 608
6. M. Erceg, in *Renaissance of hemp*, R. Kastori, Ed., Research Institute of Field and Vegetable Crops, Novi Sad, 1996, p. 149
7. K. Mechtler, J. Bailer, K. Hueber, *Ind. Crops. Prod.* **19** (2004) 19
8. P. Cappelletto, M. Brizzi, F. Mongardini, B. Barberi, M. Sannibale, G. Nenci, M. Poli, G. Corsi, G. Grassi, P. Pasini, *Ind. Crops. Prod.* **13** (2001) 101
9. F. E. Dussy, C. Hamberg, M. Luginbühl, T. Schwerzmann, A. Briellmann, *Forensic Sci. Int.* **149** (2005) 3
10. I. Barni-Comparini, S. Ferri, F. Centini, *Forensic Sci. Int.* **24** (1984) 37
11. K. Wehr, R. Dieter Maier, *Int. J. Legal Med.* **102** (1989) 509
12. J. E. Pitts, J. D. Neal, T. A. Gough, *J. Pharm. Pharmacol.* **44** (1992) 947
13. E. K. Shibuya, J. E. Souza Sarkis, O. Negrini Neto, M. Z. Moreira, R. L. Victoria, *Forensic Sci. Int.* **160** (2006) 35
14. J. Manno, B. Manno, D. Walsworth, R. Herd, *J. Forensic Sci.* **19** (1974) 884
15. M. J. Faubert Maunder, *J. Pharm. Sci.* **62** (1970) 313
16. J. M. Hurley, J. B. West, J. R. Ehleringer, *Int. J. Drug Policy* **21** (2010) 222
17. A. Ritter, *Int. J. Drug Policy* **17** (2006) 453
18. J. B. West, A. Sobek, J. R. Ehleringer, *PLoS One* **6** (2008) e2447
19. J. B. West, J. M. Hurley, J. R. Ehleringer, *J. Forensic Sci.* **54** (2009) 84
20. C. L. Hart, A. S. Ward, M. Haney, S. D. Comer, R. W. Foltin, M. W. Fischman, *Psychopharmacology* **164** (2002) 407.



J. Serb. Chem. Soc. 75 (7) 903–915 (2010)
JSCS–4016

Determination of natural colorants in plant extracts by high-performance liquid chromatography

RENETA GEVRENOVA*

*Department of Pharmacognosy, Faculty of Pharmacy, Medical University – Sofia,
Dunav str. 2, 1000 Sofia, Bulgaria*

(Received 27 October 2009, revised 12 January 2010)

Abstract: The determination of the colouring compounds apigenin (**1**), lawsone (**2**), juglone (**3**) and indigotin (**4**) in plant extracts using HPLC–UV/Vis methods is reported. The methods were applied to the analysis of **1–4** in ethanolic and propylene glycolic extracts originating, respectively, from chamomile (*Chamomilla recutita* [L] Rauschert, Asteraceae), henna (*Lawsonia inermis* L., Lythraceae), walnut (*Juglans regia* L., Juglandaceae) and natural indigo (*Indigofera* sp., Fabaceae). In the case of the indigo extracts, an optimized acid hydrolysis was applied. HPLC separations were performed on a Hypersil ODS RP18 column using linear gradient elution programs. The detection limits for **1–4** were 0.11, 0.6, 0.10, 0.089 $\mu\text{g mL}^{-1}$, respectively. The procedure did not involve any sample “clean-up” methods. The amounts of the colouring compounds ranged from 0.006 (**3**) to 0.13 mg mL^{-1} (**4**) in the ethanolic extracts and from 0.22 (**2**) to 1.44 mg mL^{-1} (**4**) in propylene glycolic extracts. The proposed HPLC methods are advantageous in terms of sample preparation and the selective separation of the compounds. The plant dye extracts are commonly used in hair colouring formulations. The results indicate that the methods developed may serve for the quantitative control of dyeing plants and cosmetic products.

Keywords: apigenin; indigotin; juglone; lawsone; high-performance liquid chromatography.

INTRODUCTION

Until the mid-19th century, natural dyes were the only source of available colours. They were used for many purposes: to colour natural fibres, to produce inks, watercolours and artist's paints. They also served to colour cosmetic products.¹ Synthetic dyes, being less expensive than natural ones, experienced great progress in a short time. Nevertheless, their utilization presents some risks for the health of consumers. Natural dyes are less toxic, less polluting, less health hazardous and non-carcinogenic. Recently, remarkable interest in natural dyes has

* E-mail: rgevrenova@gmail.com

doi: 10.2298/JSC091027071G

been witnessed in the cosmetic industry. The manufactures offer plant dye extracts, powder pigments and pigment pastes for use in hair colouring and hair highlights. The plant dyes, which meet the growing needs of hair care formulations, such as dyes, shampoos and conditioners, were designed as part of a new range of “environmentally responsible” cosmetic ingredients. Vegetal yellow dyes are flavonoids compounds and notably both luteolin and apigenin (**1**) are largely found in *Reseda luteola*, *Reseda lutea*, *Genista tinctoria*, *Chamomilla recutita*, and *Solidago* spp.^{1,2} Natural henna (*Lawsonia inermis*) produced the most important source of a red dye for hair colouring, *i.e.*, lawsone (2-hydroxy-1,4-naphthoquinone, **2**).^{3–5} Brown to dark brown colour was obtained mainly from *Juglans regia*; the effective substance is juglone (5-hydroxy-1,4-naphthoquinone, **3**).³ Natural indigo provided the most common source of blue pigments. Indigo refers to several species of *Indigofera*. In tropical and sub-tropical areas, the plants most widely used for indigo production were *Indigofera* spp., of which there are over 350 species.^{1,6,7} In temperate climates, the most commonly used species was *Isatis tinctoria* or dyers woad.^{1,8} No natural dye is a pure product and often the exact natural source of a given dye can only be derived from the presence of minor dye components. Toxicological properties of indigo are reported in the literature.⁹ Lawsone has genotoxicity/mutagenicity potential *in vitro* and *in vivo* and no safe threshold for lawsone can be established.¹⁰ The analytical control of dyes is of considerable importance in the cosmetic industry and scientific methods are required to control the quality of hair care formulations. The presence of chemical markers guarantees identity and efficacy of the plant colouring extracts.

In previous analytical studies of plant dyes various methods were used in commercial textile and archaeological dyeing of fibres,^{1,2,11–17} pharmaceuticals,¹⁸ food samples,¹⁹ and colouring compounds in molluscs.^{20–22} Several HPLC methods for analyzing cosmetic colorants^{23–26} and dye precursors of oxidative hair dyes^{4,26} are available in the literature but they were applied to the analysis of synthetic colorants in commercial hair dyeing formulations. Moreover, although HPLC methods for analyzing indigotin (**4**) in different matrices have been published,^{2,11–15,17,20–22} only a few studied on the HPLC analysis of *Isatis tinctoria* leaves and *I. indigotica* roots and leaves have been reported.^{8,27,28}

Reversed-phase liquid chromatography with UV/Vis diode-array detection (DAD) has been used for the identification of **4** in natural organic pigments used in historical art objects.^{12,14,15} Karapanagiotis *et al.* (2006) and Koren (2008) studied molluscan blue and red-purple indigoid vat dyes by HPLC/DAD.^{21,22} Mass spectrometry was applied for the identification of indigoid compounds extracted from objects of historical interest using direct inlet into different ion sources: atmospheric pressure chemical ionization (APCI)¹⁴ and electrospray ionization (ESI-MS)^{13,17} after their separation by HPLC. Puchalska *et al.* identified

indigoid compounds (indigo, indirubin, isoindigo, isoindirubin) of natural dye-stuffs and their natural or synthetic precursors (indican, isatin, indoxyl, 2-indolinone) by LC/ESI-MS in textile fibres of art samples.¹³ A liquid chromatography/electrospray ionization tandem mass spectrometry (LC/ESI-MS/MS) method was developed to determine indican, isatin, indirubin and indigotin in the roots and leaves of *I. indigotica*.²⁸ A qualitative method was devised to analyse indigotin precursors (indican) in leaf extracts of European (*I. tinctoria*) and Chinese (*I. indigotica*) woad using HPLC coupled to an evaporative light scattering detector (ELSD).⁸

The chamomile phenolic fraction is most commonly analyzed by HPLC/DAD and HPLC/MS.^{29,30} In spite of their promising perspectives, HPLC/NMR, capillary electrophoresis (CE) and capillary electrochromatography (CEC) still face some limitations regarding resolution, expensive instruments and time-consuming procedures.^{30–32} High performance liquid chromatography with UV detection is the most commonly used method for the determination of the naphthoquinones juglone in walnut leaves^{33–35} and fruits,^{36,37} and lawsone in natural henna.^{3–5,38} An HPLC/DAD method was used for the simultaneous determination of the naphthoquinones: 1,4-naphthoquinone, lawsone, juglone and plumbagin in plants (*Dionaea muscipula*, *Drosera rotundifolia*, *Drosera spathulata*, *Drosera capensis* and *Paulownia tomentosa*).^{34,35} The quantitative analysis of **2** and henna glycosides can be performed by HPLC^{34,35} and HPTLC.^{39,40} Recently, two chromatographic methods were developed to determine the chemical fingerprinting of *L. inermis*: HPTLC identification followed by densitometric measurements and RP-HPLC.⁵ HPTLC was proposed to control the quality of raw plant materials and formulations based on the title plant. Differential pulse voltammetry (DPV) coupled with a hanging mercury drop electrode (HMDE) and micro flow device were utilized to determine the content of juglone in leaves of *J. regia*.⁴¹

Only a few HPLC methods have hitherto been appropriately validated.^{19,28,31,33,34} Several methods for analyzing plant extract colorants by HPLC are available in the literature, but none of them has been applied to the analysis of **1–4** in propylene glycolic plant extracts. However, **1** has been previously analyzed in so-called “glycolic” extracts (consisting of 92.7 % propylene glycol, 2 % glycerine and 5 % ethanol, w/w) of *Chamomilla recutita* by CE and CEC^{31,32} but the methods used were different from the one described herein. The present work is the first attempt made to use HPLC/UV for the identification of the chemical markers **1–4** in plant colouring extracts for hair care formulations.

The aim of this study was the identification and quantitative determination of the most important colouring components in ethanolic and propylene glycolic plant extracts: chamomile (*Chamomilla recutita*, Asteraceae) extract and apigenin; henna (*Lawsonia inermis*, Lythraceae) extract and lawsone; walnut (*Juglans regia*, Juglandaceae) extract and juglone; natural indigo (*Indigofera* sp., Fab-

ceae) extract and indigotin. For these purposes, it was necessary to optimize the analysis of the commonly used cosmetic colorants by a simple and reliable HPLC method coupled with UV/Vis detection. The ethanolic and propylene glycolic extracts were supplied by a Bulgarian company that manufactures herbal extracts for cosmetic uses. The HPLC methods described herein are of practical interest, allowing the determination of colouring compounds present in hair care formulations defined as “natural”, which should only contain plant extract colorants.

EXPERIMENTAL

Chemicals and reagents

The standard of apigenin was purchased from Extrasynthese (Genay, France) and those of lawsone (97 %), juglone (97 %) and indigotin (95 %) from Sigma–Aldrich (Deisenhofen, Germany). HPLC-grade solvents and analytical-grade chemicals were provided by Merck (Darmstadt, Germany). The water was double distilled. Solvents were filtered through a 0.45 µm filter (Millipore, Bedford, MA, USA) and degassed in an ultrasonic bath before use. Stock solutions (0.4 mg mL⁻¹) of **1–3** were prepared by dissolving 20 mg of each powder in 50 ml methanol. The solutions were stored in a refrigerator. The working standard solutions of appropriate concentration were prepared daily by diluting the stock standard solutions with methanol. The solutions of **4** were freshly prepared in the range 0.2–0.001 mg mL⁻¹ in methanol–dioxane (1:1, v/v) and kept in vials preventing light penetration to avoid decomposition of indigotin.

Extracts

The ethanolic and propylene glycolic extracts from chamomile (*Chamomilla recutita*), henna (*Lawsonia inermis*), walnut (*Juglans regia*) and natural indigo (*Indigofera* sp.) were received directly from a Bulgarian producer. According to the provider, the alcoholic extracts were obtained with 70 % ethanolic–aqueous solution. The ethanolic extracts (10 mL) were evaporated under vacuum at 40 °C and reconstituted with 10 mL methanol. The propylene glycolic extracts were diluted appropriately in MeOH (1 mL extract to 5 mL solvent). All extracts were then submitted to sonication at room temperature for 5 min using a RK 52 H Sonicator (Bandelin electronic, Berlin, Germany) at 120 W, 35 kHz and centrifuged at 10000 rpm for 10 min. The supernatant was collected and filtered through a 0.45 µm filter (Millipore, Bedford, MA, USA) prior to injection.

Acid hydrolysis of the indigo extracts

The samples of natural indigo (1 ml of methanolic or methanolic–propylene glycolic extract, see Section *Extracts*) were hydrolyzed for 15 min at 100 °C in 3 mL of a mixture of 37 % HCl–water (2:1). The extracts were rapidly cooled and centrifuged at 10000 rpm for 10 min. The blue residue after acid hydrolysis indicated the presence of indigotin, which was redissolved in 1 mL methanol/dioxane (1:1, v/v) and filtered through a 0.45 µm filter (Millipore) prior to injection. Indigotin was detected in freshly obtained samples.

HPLC analysis

The chromatographic analyses were performed on a Varian (Walnut Creek, California USA) chromatographic system equipped with a tertiary pump Model 9012, a rheodyne injector with a 20 µl sample loop, a UV/Vis detector Model 9050 set at 335, 340, 249 and 288 nm according to the UV absorption maxima of the compounds **1–4**, respectively. A Varian Star Chromatography workstation and computer software (version 4.5) for controlling the

system and collecting the data were used. A reversed phase Hypersil ODS RP18, 5 μm , 250 \times 4.6 mm I.D., Shandon (Runcom, England) column equipped with a precolumn 30 mm \times 4.6 mm (Varian, USA) filled with the same stationary phase was used.

Gradient program I. The chromatographic separation of **1** was realised using a mobile phase consisting of A) acetonitrile, B) methanol and C) 20 mM potassium dihydrogen phosphate buffer adjusted to pH 3.20 with orthophosphoric acid. The elution program commenced at 15 % A:5 % B:80 % C followed by a linear gradient for 20 min to 30 % A:10 % B:60 % C. The flow rate was 1 mL min⁻¹.

Gradient program II. The chromatographic separation of **2** was performed using a binary solvent system consisting of: A) 3 % methanol in a 20 mM potassium dihydrogen phosphate buffer (adjusted to pH 3.20 with orthophosphoric acid) and B) 45 % methanol in 20 mM potassium dihydrogen phosphate buffer (adjusted to pH 3.20 with orthophosphoric acid). The elution program was from 100 % A to 100 % B in 55 min. The flow rate was 1.3 mL min⁻¹.

Gradient program III. The chromatographic separation of **3** was performed using a binary solvent system consisting of: A) 3 % methanol in a 20 mM potassium dihydrogen phosphate buffer (adjusted to pH 3.20 with orthophosphoric acid) and B) 45 % methanol in 20 mM potassium dihydrogen phosphate buffer (adjusted to pH 3.20 with orthophosphoric acid). The elution program was from 90 % A:10 % B to 10 % A:90 % B in 45 min. The flow rate was 1.2 mL min⁻¹.

Gradient program IV. Chromatographic separation of **4** was carried out using a mobile phase consisted of A) acetonitrile, B) methanol and C) 100 mM ammonium acetate buffer with 30 mM dibutylamine adjusted to pH 6.8 with acetic acid. The elution program commenced at 10 % A: 35 % B: 55 % C followed by linear gradient for 25 min to 10 % A:65 % B:25 % C. The flow rate was 1 mL min⁻¹.

For all programs, the mobile phase was returned to the initial conditions in 5 min and the column was equilibrated for 10 min. The oven temperature was set at 27 °C.

Quantitative analysis

The analysis of the assayed compounds (**1–4**) was performed using the external standard method. Working solutions containing 0.2, 0.1, 0.05, 0.02, 0.01 and 0.001 mg mL⁻¹ of **1–3** were prepared from stock solution, 0.4 mg mL⁻¹ in methanol, respectively. The employed concentrations of **4** were 0.2, 0.1, 0.05, 0.02, 0.01 and 0.001 mg mL⁻¹ and the solutions were prepared in dioxane–methanol (1:1, v/v).

Triplicate analyses were performed for each concentration and the peak area was detected at 335, 340, 249 and 288 nm for **1–4**, respectively. Calibration curves were constructed from the peak areas vs. analyte concentrations. Slope, intercept and other statistics of the calibration lines were calculated by linear regression using the Analytik-Software (Leer, Germany) STL statistics program. The regression equations were, respectively, for compounds **1–4**: $y = 3.38 \times 10^7 x + 7.43 \times 10^4$ ($r^2 = 0.9969$); $y = 6.40 \times 10^6 x + 4.19 \times 10^4$ ($r^2 = 0.9990$); $y = 3.70 \times 10^7 x + 1.05 \times 10^6$ ($r^2 = 0.9936$) and $y = 4.09 \times 10^6 x - 1719$ ($r^2 = 0.9999$).

For every sample, the complete assay procedure was performed in triplicate and the standard deviation calculated.

RESULTS AND DISCUSSION

The principal flavonoid colouring matter is apigenin. It produces the most vibrant and lightfast yellow colour. For standardization purposes of chamomile extracts, apigenin, to which hair colouring property and several therapeutic ac-

tivity have been associated, is the flavonoid of choice.^{1,32,42} The content of this flavonoid in extracts of chamomile flowers was found in a heterogeneous range of values: 106 (methanolic extract), 77 (ethanolic extract) and 11 $\mu\text{g g}^{-1}$ (glycolic extract).³¹ Lawsone and juglone are the most commonly occurring naphthoquinones.³ Natural henna is known to contain 1–2 % lawsone, which is responsible for colouring orange–red. The amount of juglone detected in walnut leaves was about 0.2–0.4 % (fresh weight).⁴¹ Naphthoquinones are not a precursor of oxidative hair dyes. The vegetal blue indigotin is not synthesized directly by the plant; it is a product derived from indole glucoside precursors, which are secondary metabolites.^{1,6,28} *Indigofera* spp. contain a yellowish glycoside indican (indoxyl- β -D-glucoside), which is readily hydrolyzed in aqueous solution by dilute mineral acid or by enzymes to the respective aglycon indoxyl and a sugar. To form indigotin from the precursors, the carbohydrate moiety is cleaved from the indoxyl group and two of the resulting indoxyl molecules combine oxidatively to produce an indigotin molecule. In practice, once the molecule has been hydrolyzed, this combination occurs spontaneously under aerobic conditions and indigotin precipitates from solution and deposits as a blue sediment.

Due to the presence of the glycoside indican in the extracts from indigo (*Indigofera* spp.), its transformation to indigotin was achieved by acid hydrolysis. The final dissolution of indigotin was realised with a mixture of dioxane and methanol (1:1, v/v), which resulted in an increase in the dissolution and stability, in comparison with those previously reported.^{13,19} The limited solubility of indigotin in organic solvents¹⁵ and its instability in these media^{13,19,43} should be mentioned. A study of the solubility of indigotin was performed by Blanc *et al.*¹⁵ It was found that indigotin is soluble in acetic acid and pyridine. To the commonly used methanolic–acidic extraction method for natural indigo in textile fibres, an additional methanol/DMF,¹⁴ DMSO,¹³ acetic acid/SDS,¹⁵ or warm pyridine⁴⁴ extraction step was applied. Moreover, indigotin is unstable in acidic, basic medium and under daylight.^{13,45} The stability of indigotin solutions in DMSO was examined by Puchalska *et al.* It was found that in solutions exposed to daylight at room temperature, a degradation of 50 % of indigotin to isatin was completed after 7 days; after 30 days, only the degradation product could be found.¹³ In a previous study, Altinos *et al.* reported that working solutions (10 mg in 100 mL) of indigotin were prepared in methanol–water (40:60, v/v) for a HPLC method and that the solutions were stable for at least 12 h.¹⁹ In the present study, indigotin was detected in freshly prepared dioxane solutions and extracts and they were stable for at least 3 days (over this period, the *RSD* (area) was 3.16 %). In addition, dioxane is less toxic in comparison with pyridine and DMF, currently evaluated by the International Agency for Research on Cancer (IARC) as carcinogens.

The HPLC analyses were directly performed on the total extracts of chamomile, henna and walnut without any manipulation of the samples. Some authors have reported a sample “clean-up” procedure by solid-phase extraction³² of both ethanolic and propylene glycolic extracts of chamomile as the presence of propylene glycol in the matrix inhibited the absorption of the compounds to the stationary phase. The present method does not involve any sample purification step, the propylene glycolic extracts were diluted appropriately in MeOH and no inhibition of the partitioning caused by the presence of propylene glycol was found.

Preliminary RP-HPLC experiments for the separation of the chamomile extract showed that certain pairs of major aglycones, such as luteolin and quercetin, apigenin and isorhamnetin, were not well resolved by currently used systems consisting of an organic phase (either methanol or acetonitrile) and water/TFA or water/formic acid.^{29,30} Therefore, the effects of various proportions of methanol (A) and acetonitrile (B), ranging from 5 % A:10 % B to 20 % A:30 % B were tested for the separation of the analytes. The proposed HPLC method (gradient program I) enabled the determination of **1** with advantages in terms of retention time (24 min in comparison with 40 min²⁹) and the selective separation of the above-mentioned aglycones and methylated aglycones axillarin and chrysosplenol, well known for their presence in chamomile extracts.²⁹

The structural difference between **2** and **3** is small, originating only from the position of the hydroxyl group. Initial chromatographic runs were gradients that ranged from 3 % methanol to either 30 or 45 % over 45 or 55 min. Eight binary solvent systems were investigated consisting of methanol and either phosphate buffer (20 mM potassium dihydrogen phosphate buffer (adjusted to pH 3.20 with orthophosphoric acid) or an aqueous phase, containing 0.1 % phosphoric acid. The HPLC methods (gradient program II and III) for the separation and quantification of **2** in henna extracts and **3** in walnut extracts were based on a binary gradient system consisting of phosphate buffer containing 3 % methanol and 45 % methanol over 55 and 45 min, respectively. It should be mentioned that the previously reported chemical fingerprinting of *L. inermis* using HPLC enabled the evaluation and comparison of raw plant material only by peak groups at specific and significant t_R values.⁵ The method developed in this study successfully separated **3** from phenolic compounds (phenolic acids, tannins, flavonoids), while in the HPLC method for the simultaneous determination of naphthoquinones in plants,³⁴ the retention times of **2** and **3** were 3 and 5 min, respectively; they were not completely distinguished from the interfering above-mentioned phenolic compounds.

In this report, an HPLC system for the determination of **3** where the chosen mobile phase is compatible with determination of **2** and **1** is reported. The binary mobile phase in gradient programs II and III could be rapidly applied to the determination of **2** and **3**, either as single compounds or in a mixture.

The development of HPLC methods for **1–3** was performed using a mobile phase consisting of organic modifier(s) and pH 3.2 phosphate buffer (gradient programs I–III). The pH was chosen in order to prevent ionization of the phenolic hydroxyl groups of apigenin and naphthoquinones; it was presumed that the studied compounds are neutral molecules at pH 3.2. Indigotin is unstable in acidic and basic medium, hence a buffer of pH 6.8 was chosen for the analysis. Additionally, in the HPLC of indigotin dissolved in dioxane–methanol (1:1, v/v) as eluent with phosphate buffer without dibutylamine, double peaks were observed for each analyte. The addition of dibutylamine to the ammonium acetate buffer at pH 6.8 improved the partition of the analytes between the stationary and mobile phase (gradient program IV). The proposed HPLC method enables the determination of indigotin with advantages in terms of retention time (15 min in comparison with 35 min¹⁵ and 52 min²⁷).

For the HPLC–UV analysis, four wavelengths were specified: indigotin has maximum absorbance at 288 nm, lawsone at 340 nm, juglone at 249 nm and apigenin at 335 nm. These wavelengths allow a sufficient sensitivity of detection for the determined compounds to be obtained. In the case of the natural indigo extracts obtained because of acid hydrolysis, a broad elevation of the baseline was observed; this was assigned to some product of acid hydrolysis of the extract. Peaks of the chemical markers **1–4** were assigned in the HPLC chromatograms by comparing individual peak retention times with those of authentic reference standards and by the spiking technique.

The repeatability was established by injecting standard solutions of the assayed compounds (0.01 mg mL⁻¹) six times. The reproducibility was determined over 10 days by three injections per day of the same solutions. The relative standard deviations (*RSDs*) of the repeatability and the reproducibility were $\leq 2.42\%$ and $\leq 5.71\%$, respectively. The precision of the retention times was evaluated taking into account a triplicate analysis of both standards and plant samples, and the obtained mean values were derived with standard deviation (Table I). In the calibration experiments, the interval of linear response covered the concentration range from 0.001 to 0.4 mg mL⁻¹ (except for indigotin, for which the upper limit was 0.2 mg mL⁻¹). All compounds showed acceptable linearity with correlation coefficients (*r*²) higher than 0.993 within the range of concentrations investigated. The average precision of the entire analytical procedure expressed by the relative standard deviations (*RSDs*) of parallel measurements (*n* = 3) was estimated by measuring the within-day repeatability, being in all cases in the range 1.00–8.48 %. The *RSD* of **3** determined in the walnut extract exceeded 5 %. Taking account of the low amount present in the ethanolic–aqueous extract (0.0059±5.03×10⁻⁴), an *RSD* value of 8 % is acceptable.⁴⁶ The limit of detection (*LOD*) and the limit of quantification (*LOQ*) were calculated according to ICH guidelines based on the standard deviation of the regres-

sion lines of specific calibration curves and their slope using analyte concentrations in the range of the *LOD* and *LOQ*.⁴⁷ The detection (*LOD*) and quantification (*LOQ*) limits determined would permit the quantification of the compounds assayed at ppm levels, since the *LODs* and *LOQs* ranged from 0.089 to 0.6 $\mu\text{g mL}^{-1}$ and from 0.32 to 1.8 $\mu\text{g mL}^{-1}$ for indigotin and lawsone, respectively.

TABLE I. Precision, limit of detection (*LOD*) and limit of quantification (*LOQ*) for the assayed compounds

Compound	($t_R \pm SD$) / min	<i>RSD</i> ^a / %	<i>RSD</i> ^b / %	<i>LOD</i> / $\mu\text{g mL}^{-1}$	<i>LOQ</i> / $\mu\text{g mL}^{-1}$
1	24.24 \pm 0.39	0.06	2.47	0.11	0.36
2	45.04 \pm 0.11	2.42	4.49	0.60	1.80
3	38.09 \pm 0.27	2.16	5.71	0.10	0.32
4	15.00 \pm 0.19	1.54	4.06	0.089	0.32

^aRepeatability ($n = 10$); ^breproducibility tested over 10 days ($n = 3$)

Mulinacci *et al.* described a semi-quantitative study of the flavonoid content of chamomile extracts.²⁹ The *LOD* and *LOQ* of a capillary electrophoretic and a capillary electrochromatographic method for the quantification of **1** in chamomile extracts were 3.80 and 11.5 $\mu\text{g mL}^{-1}$, and 35 and 150 $\mu\text{g mL}^{-1}$, respectively.^{31,32} The proposed HPLC method using UV detection enabled the sensitivity to be increased thirty-fold, whereby values of 0.11 and 0.36 $\mu\text{g mL}^{-1}$ were achieved, respectively. The simultaneous analyses of naphthoquinones by HPLC/DAD³⁴ and DPV⁴¹ were performed by Babula *et al.* and the *LODs* and *LOQs* obtained for **2** were 65 (217) and 5 (16) ng mL^{-1} , respectively, and for **3**, 75 (252) and 18 (60) ng mL^{-1} , respectively. The obtained detection limits for **2** and **3** in the present study were in the same range as those realised in the literature,³⁴ but DPV characteristics were ten-folds better. The sensitivity obtained for **4** with the developed method was higher than that Altinos and Toptan achieved by HPLC with UV detection at 480 nm (0.2 $\mu\text{g mL}^{-1}$).¹⁹

The optimized methods were consequently applied to identify and quantify the colouring compounds **1–4** present in plant extracts originating from extraction with 70 % ethanol and propylene glycol as solvents. The obtained chromatographic profiles are shown in Fig. 1. Although very similar peak profiles were obtained, the amount of the colouring compounds differed considerably among these extracts. The concentrations of the compounds assayed were found to be lower in the ethanolic–aqueous extracts than in propylene glycolic extracts. The amounts of the colouring compounds assayed ranged from 0.006 (**3**) to 0.13 mg mL^{-1} (**4**) in the ethanolic extracts and from 0.22 (**2**) to 1.44 mg mL^{-1} (**4**) in the propylene glycolic extracts (Table II).

The chamomile extract used in hair care formulations is standardized on more than 1.2 % total apigenins; an anti-inflammatory test supports that cha-

momile extract has good anti-inflammatory properties and that it protects cells against UV stress at dosages of 0.1–1.0 %.

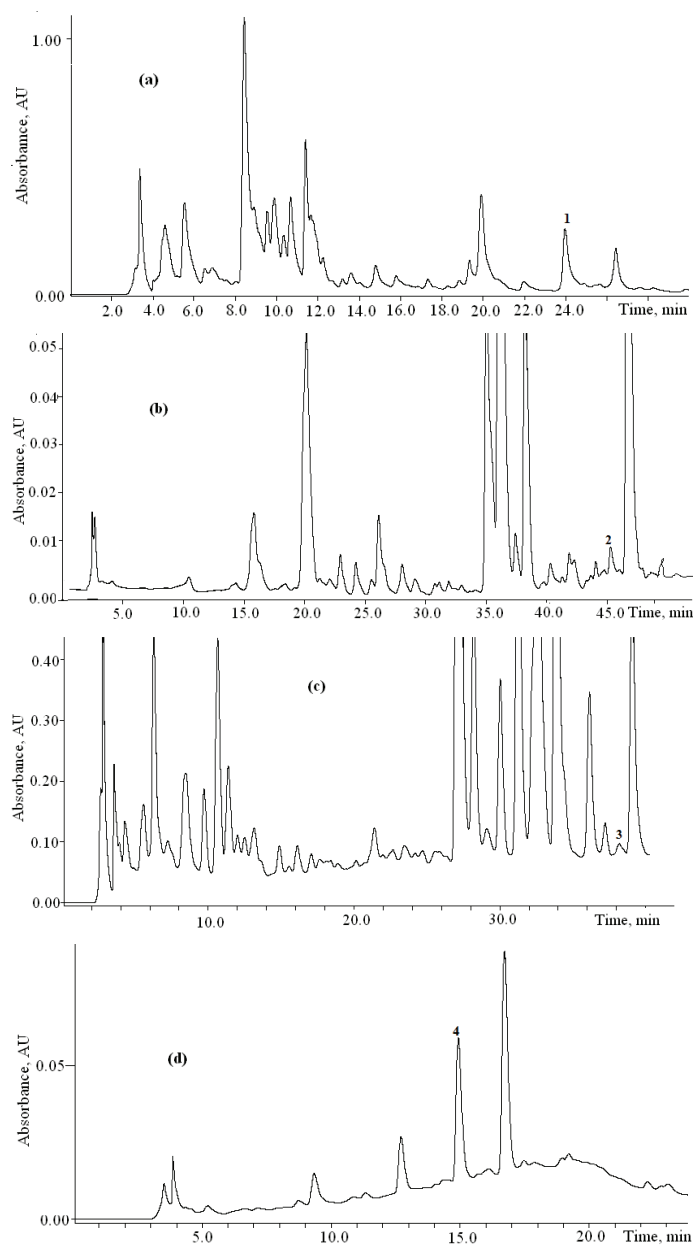


Fig. 1. HPLC chromatograms of a) chamomile propylene glycolic, b) henna ethanolic, c) walnut propylene glycolic and d) natural indigo ethanolic extracts. **1** – apigenin; **2** – lawsone; **3** – juglone and **4** – indigotin. See text for chromatographic conditions.

TABLE II. Content (mg mL^{-1}) of the compounds assayed in ethanolic and propylene glycolic extracts

Compound	Ethanolic extract \pm SD mg mL^{-1}	RSD / %	Propylene glycolic extract \pm SD mg mL^{-1}	RSD / %
1	0.0387 \pm 0.0023	5.82	0.5238 \pm 0.0358	6.83
2	0.0297 \pm 8.02 $\times 10^{-4}$	2.70	0.2192 \pm 0.0066	3.03
3	0.0059 \pm 5.03 $\times 10^{-4}$	8.48	0.3797 \pm 0.0035	1.00
4	0.1250 \pm 0.006	5.08	1.4400 \pm 0.006	4.00

Martinez *et al.* reported in the literature that the total apigenin content in a shampoo was equivalent to 105 ppm (0.0105 %) of a chamomile extract standardized on 1.5 % total apigenins.⁴² Despite its low content in complex formulations (shampoos), the developed specific analytical method was able to successfully quantify the traces of apigenin. It has been proposed that lawsone be used as a non-oxidizing hair colouring agent at a maximum concentration of 1.5 % (typical concentration 1.26%) in the finished cosmetic product. Henna products were found to contain 0.24 % lawsone.⁴ In this study, the concentrations of juglone were found to be very low in all samples. Due to polymerization phenomena, juglone is reported to occur in dry leaves only in vestigial amounts.⁴⁸ A literature survey revealed no data for the presence of juglone and indigotin in hair colouring formulations.

In conclusion, the proposed HPLC methods enable the routine determination of the most employed natural colorants **1–4**, originated from chamomile, henna, walnut and natural indigo extracts, with advantages in terms of sample preparation and the selective separation of the compounds. They could be used for quantitative analysis and quality control of extracts and hair care formulations.

ИЗВОД

ОДРЕЂИВАЊЕ ПРИРОДНИХ БОЈА У ЕКСТРАКТИМА БИЉАКА МЕТОДОМ HPLC

RENETA GEVRENOVA

Department of Pharmacognosy, Faculty of Pharmacy, Medical University – Sofia, Bulgaria

Одређивана су бојена једињења апиџенин (**1**), лосон (**2**), југлон (**3**) и индиготин (**4**) у биљним екстрактима методом HPLC–UV/Vis. Метода је примењена на анализу једињења **1–4** у етанолном и пропиленгликолном екстракту биљака камилица (*Chamomilla recutita* [L] Rauschert, Asteraceae), кана (*Lawsonia inermis* L., Lythraceae), орах (*Juglans regia* L., Juglandaceae) и природном индигу (*Indigofera* sp., Fabaceae). У случају екстракта индига, примењена је оптимизирана кисела хидролиза. HPLC раздвајање је изведено на колони Hypersil ODS RP18, користећи линеарни елуциони градијент. Детекционе границе за **1–4** су 0,11; 0,6; 0,10 и 0,09 $\mu\text{g mL}^{-1}$. Процедура није захтевала методе претходног пречишћавања. Концентрација бојених једињења се кретала од 0,006 (**3**) до 0,13 mg mL^{-1} (**4**) у етанолном екстракту и од 0,22 (**2**) до 1,44 mg mL^{-1} (**4**) у пропиленгликолном екстракту. Предложени HPLC метод има предности у односу на друге методе у припреми узорака и селективном раздвајању једињења. Екстракти биљних боја се користе за бојење косе. Резултати овог рада показују да разви-

јена метода може имати примену у квантитативној контроли биљака за бојење и козметичких производа.

(Примљено 27. октобра 2009, ревидирано 12. јануара 2010)

REFERENCES

1. K. G. Gilbert, D. T. Cookke, *Plant. Growth Regul.* **34** (2001) 57
2. J. Wouters, N. R. Chirinos, *J. Am. Inst. Conserv.* **31** (1992) 237
3. T. Bechtold, in *Handbook of Natural Colorants*, T. Bechtold, R. Mussak, Eds., Wiley, New York, 2009, p. 151
4. S. C. Rastogi, I. M. Worsoe, H. Gitte. G. H. Jensen, *Research Notes from National Environmental Research Institute 175*, National Environmental Research Institute, Roskilde, 2003
5. F. R. Gallo, G. Multari, M. Giambenedetti, E. Federici, *Phytochem. Anal.* **19** (2008) 550
6. J. Balfour-Paul, *Indigo*, British Museum Press, London, 1998, p. 264
7. D. Cardon, *Le monde des teintures naturelles*, Belin Press, Paris, 2003, p. 586
8. K. G. Gilbert, D. J. Hill, C. Crespo, A. Mas, M. Lewis, B. Rudolph, D. T. Cooke, *Phytochem. Anal.* **11** (2000) 18
9. K. H. Ferber, *J. Environ. Pathol. Toxicol. Oncol.* **7** (1987) 73
10. *Scientific committee on consumer products (SCCP). Opinion on Lawsonia inermis (Henna) COLIPA N°C169*, 6th plenary meeting of European Commission Health and Consumer protection, Brussels, Belgium, 2005
11. J. Wouters, A. Verhesken, *J. Soc. Dyers Colour.* **107** (1991) 266
12. B. Szostek, J. Orska-Gawryls, I. Surowiec, M. Trojanowicz, *J. Chromatogr. A* **1012** (2003) 179
13. M. Puchalska, K. Polec-Pawlak, I. Zadrozna, H. Hryszko, M. Jarosz, *J. Mass Spectrom.* **39** (2004) 1441
14. I. Surowiec, A. Quye, M. Trojanowicz, *J. Chromatogr. A* **1112** (2006) 209
15. R. Blanc, T. Espejo, A. Lopez-Montes, D. Torres, G. Crovetto, A. Navalon, J. L. Vilchez, *J. Chromatogr. A* **1122** (2006) 105
16. X. Zhang, R. Laursen, *Int. J. Mass Spectrom.* **284** (2009) 108
17. K. Lech, K. Polec-Pawlak, M. Jarosz, in *Organic Mass Spectrometry in Art and Archeology*, M. P. Colombini, F. Modugno, Eds., Wiley, New York, 2009, p. 365
18. F. A. Fell, G. J. Allan, *Pharm. Anal.* (1981) 291
19. S. Altinos, S. Toptan, *J. Food Comp. Anal.* **16** (2003) 517
20. C. Cooksley, *Molecules* **6** (2001) 736
21. I. Karapanagiotis, V. Villemereuil, P. Magiatis, P. Polychronopoulos, K. Vougianniopoulou, A. L. Skaltsounis, *J. Liq. Chromatogr. Relat. Technol.* **29** (2006) 1491
22. Z. Koren, *J. Soc. Dyers Colour.* **110** (2008) 273
23. L. Gagliardi, G. Cavazzutti, A. Amato, A. Basili, D. Tonelli, *J. Chromatogr. A* **394** (1987) 345
24. L. Gagliardi, A. Amato, G. Cavazzutti, D. Tonelli, *J. Chromatogr. A* **448** (1988) 296
25. J. W. Wegener, J. C. Klamer, H. Govers, U. A. T. Brinkman, *Chromatographia* **24** (1987) 865
26. C. Scarpi, F. Ninci, M. Centini, C. Anselmi, *J. Chromatogr. A* **796** (1998) 319
27. P. Zou, Y. Hong, H. L. Koh, *J. Pharm. Biomed. Anal.* **38** (2005) 514
28. P. Zou, H. L. Koh, *Rapid Commun. Mass Sp.* **21** (2007) 1239

29. N. Mulinacci, A. Romani, P. Pinelli, F. F. Vincieri, D. Prucher, *Chromatographia* **51** (2000) 301
30. B. Weber, M. Herrmann, B. Hartmann, H. Joppe, C. O. Schmidt, H. J. Bertman, *Eur. Food Res. Technol.* **226** (2008) 755
31. F. N. Fonseca, M. F. M. Tavares, *Phytochem. Anal.* **15** (2004) 65
32. F. N. Fonseca, M. F. M. Tavares, C. Horvath, *J. Chromatogr. A* **1154** (2007) 390
33. M. Girzu, D. Fraisse, A. P. Carnat, A. Carnat, J. L. Lamaison, *J. Chromatogr. A* **805** (1998) 315
34. P. Babula, R. Mikelova, V. Adam, R. Kizek, L. Havel, Z. Sladky, *J. Chromatogr. B* **842** (2006) 28
35. P. Babula, R. Mikelova, V. Adam, D. Potesil, J. Zehnalek, R. Kizek, L. Havel, Z. Sladky, *Chem. Listy* **100** (2006) 271
36. M. Colaric, R. Veberic, A. Solar, M. Hudina, F. Stampar, *J. Agric. Food Chem.* **53** (2005) 6390
37. J. Jakopic, R. Veberic, F. Stampar, *Acta Agr. Slov.* **93** (2009) 11
38. G. Hempel, B. Gutsche, *SÖFW J.* **130** (2004) 22
39. T. Kawamura, J. Hasata, K. Okuda, Y. Noro, Y. Takeda, T. Tanaka, *Nat. Med.* **54** (2000) 86
40. S. Nagwa, M. B. Jihan, A. Maha, M. G. Yousry, *J. Sep. Sci.* **30** (2007) 3311
41. P. Babula, D. Huska, P. Hanustiak, J. Baloun, S. Krizkova, V. Adam, J. Hubalek, L. Havel, M. Zemlicka, A. Horna, M. Beklova, R. Kizek, *Sensors* **6** (2006) 1466
42. S. Martinez, S. Gargano, A. Hernandez, S. Alaoui, *Skin Care Forum* **42** (2007) 1
43. N. Kuramoto, T. Kitao, *J. Soc. Dyers Colour.* **95** (1979) 257
44. J. Orska-Gavrys, I. Surowiec, J. Kehl, H. Rejniak, K. Urbaniak-Walczak, M. Trojanowicz, *J. Chromatogr. A* **989** (2003) 239
45. N. P. Boley, N. T. Crosby, R. Roper, L. Somers, *Analyst* **106** (1981) 710
46. L. Huber, *LC/GC Int.* **11** (1998) 96
47. *International Conference on Harmonisation: Draft Guideline on Validation of Analytical Procedures: Definitions and Terminology Availability*, Department of Health and Human Services, Food and Drug Administration, (1995), US Federal Register, Vol. 60, No 40, 1995, p. 11260
48. M. Wichtl, R. Anton, *Plantes therapeutiques*, Tec. & Doc., Paris, 1999, p. 291.



J. Serb. Chem. Soc. 75 (7) 917–927 (2010)
JSCS–4017

Synthetic, structural and biological studies of organosilicon(IV) complexes of Schiff bases derived from pyrrole-2-carboxaldehyde

KIRAN SINGH^{1*} and DHARAM PAL²

¹Department of Chemistry, Kurukshetra University, Kurukshetra-136 119 and

²Department of Applied Sciences, J.I.E.T., Jind-126102, Haryana, India

(Received 16 December 2008, revised 26 April 2010)

Abstract: Selected new organosilicon(IV) complexes having the general formula $R_2SiCl[L]$ and $R_2Si[L]_2$ were synthesized by the reactions of Me_2SiCl_2 with Schiff bases (5-mercapto-4-[(1*H*-pyrrol-2ylmethylene)amino]-*s*-triazole, 5-mercapto-3-methyl-4-[(1*H*-pyrrol-2ylmethylene)amino]-*s*-triazole and 3-ethyl-5-mercapto-4-[(1*H*-pyrrol-2ylmethylene)amino]-*s*-triazole) in 1:1 and 1:2 molar ratios. All of the compounds were characterized by elemental analysis, molar conductance, and IR, UV, ¹H-, ¹³C- and ²⁹Si-NMR spectral studies. All the spectral data suggest an involvement with an azomethine nitrogen in coordination to the central silicon atom. With the help of above-mentioned spectral studies, penta and hexacoordinated environments around the central silicon atoms in the 1:1 and 1:2 complexes, respectively, are proposed. Finally, the free ligands and their metal complexes were tested *in vitro* against some pathogenic bacteria and fungi to assess their antimicrobial properties.

Keywords: antifungal; antibacterial; silicon complexes; *s*-triazole; Schiff bases.

INTRODUCTION

The current research dealing with metal complexes of heteronuclear Schiff bases has expanded enormously and includes diversified subjects comprising their various aspects in bio-coordination and bio-inorganic chemistry. It is known that the presence of metal ions bonded to biologically active compounds may enhance their activity.^{1–6} Heteronuclear Schiff base complexes have found applications as magnetic materials, catalysts and in the field of bio-engineering.^{7–10} Organosilicon compounds of nitrogen- and sulphur-containing ligands are well known for their anticarcinogenic, antibacterial, tuberculostatic, antifungal, insecticidal and acaricidal activities.^{11–16}

* Corresponding author. E-mail: sirohidp@rediffmail.com

doi: 10.2298/JSC081216063S

The interest in organosilicon(IV)^{16–18} compounds is due to their versatile applicability in the pharmaceutical industries. Generally, organosilicon compounds seem to owe their antitumour properties to the immuno–defensive system of the organism.^{19–22} The medical applications and effectiveness of the silatranes in the treatment of wounds and tumours are thought to be related to the role of silicon in the growth of epithelial and connective tissues and hair, where their function is to impart strength, elasticity, and impermeability to water.²³ In view of this, the synthesis of organosilicon(IV) metal complexes of Schiff bases derived from the condensation of pyrrole-2-carboxaldehyde with different triazole derivatives is reported herein. The characterization of the complexes was realised by elemental analysis and spectroscopic (UV, IR, ¹H-, ¹³C- and ²⁹Si-NMR) studies. Their antibacterial and antifungal activities were screened against various fungi and bacteria.

EXPERIMENTAL

Materials and methods

Analytical grade organosilicon chlorides, pyrrole-2-carboxaldehyde, hydrazine hydrate, carbon disulphide, methanol, dimethyl sulphoxide and cyclohexane were purchased from Acros and HiMedia. All the apparatus used during the experimental work were fitted with quick fit interchangeable standard ground joints. Strictly anhydrous conditions were maintained during the synthesis of the metal complexes, since the dichlorodimethylsilane and the product complexes are highly moisture-sensitive.

Silicon was determined gravimetrically as silicon dioxide. Melting points were measured using a capillary melting point apparatus. The molar conductance was measured with a Systronic type 305 conductivity bridge. The electronic spectra of ligands and their metal complexes were recorded in the region 1100–200 nm on a Hitachi U-2000 spectrophotometer, in dry methanol. The IR spectra were recorded on Buck scientific M500 grating spectrophotometer in nujol mulls in the range of 4000–250 cm⁻¹. Multinuclear magnetic resonance spectra (¹H, ¹³C, and ²⁹Si) were recorded on a Bruker 400ACF spectrometer.

Synthesis

4-Amino-5-mercapto-*s*-triazole (AMT), 4-amino-5-mercapto-3-methyl-*s*-triazole (AMMT) and 4-amino-3-ethyl-5-mercapto-*s*-triazole (AEMT) were synthesized by a reported method.²⁴ The ligands, 5-mercapto-4-[(1*H*-pyrrol-2ylmethylene)amino]-*s*-triazole (HL¹), 5-mercapto-3-methyl-4-[(1*H*-pyrrol-2ylmethylene)amino]-*s*-triazole (HL²), 3-ethyl-5-mercapto-4-[(1*H*-pyrrol-2ylmethylene)amino]-*s*-triazole (HL³) were synthesized by the condensation in ethanol of pyrrole-2-carboxaldehyde with AMT, AMMT and AEMT, respectively. The reaction mixture was refluxed for 3–4 h and allowed to cool. The products were filtered, washed and recrystallized from the same solvent and dried. The yields of the ligands HL¹, HL² and HL³ were 80, 77 and 72 %, respectively. The structure of the prepared ligands are given in Fig. 1.

Synthesis of silicon complexes

To a weighed amount of Me₂SiCl₂ in dry methanol was added the required amount of the sodium salt of the ligand HL¹, HL² or HL³ in 1:1 or 1:2 molar ratio. The reaction mixture was refluxed for about 12 h on a fractionating column. The sodium chloride formed during the reaction was removed by filtration. The excess of solvent was removed under reduced pressure

and the complexes were dried *in vacuo* at 35 ± 5 °C after repeated washing with dry cyclohexane. The yields of the newly synthesized silicon complexes ranged from 67–70 %.

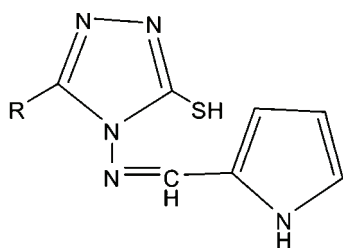


Fig. 1. 5-Mercapto-4-[(1*H*-pyrrol-2ylmethylene)amino]-*s*-triazole (HL¹), 3-methyl-5-mercapto-4-[(1*H*-pyrrol-2ylmethylene)amino]-*s*-triazole (HL²) and 3-ethyl-5-mercapto-4-[(1*H*-pyrrol-2ylmethylene)amino]-*s*-triazole (HL³).

R = H, HL¹; CH₃, HL²; C₂H₅, HL³

In vitro antifungal activity²⁵

Potato dextrose agar medium (PDA) was prepared in flasks and sterilized before being poured into petri plates. The requisite quantity (100 µg/ml) of the standard antibiotic (ampicilline) was added to the medium just before pouring to check the growth of bacteria. Test samples were prepared in different concentrations (10 µg, 50 µg and 100 µg per ml) in dimethyl sulphoxide (DMSO) and 200 µl of each sample was added to PDA plates containing mycelial discs taken from 5–7-day-old cultures of fungi (*Aspergillus flavus* or *A. niger*). These plates were incubated for 5–7 days at 28 ± 1 °C. Control plates underwent the same treatment except for the addition of the test samples. The efficacy of each sample was determined by measuring the radial mycelial growth. The radial growth of the colony was measured in two directions at right angle to each other and the average of two replicates was recorded in each case. Data were expressed as percent inhibition over control calculated from the size of colonies, and subjected to two-way analysis of variance. The percent inhibition was calculated using the formula:

$$\% \text{Inhibition} = (C - T) \times 100 / C$$

where *C* is the diameter of the fungus colony in the control plate after 96 h incubation and *T* is the diameter of the fungus colony in the tested plate after same incubation period.

In vitro antibacterial assay

The newly synthesized ligands and their corresponding metal complexes were screened for their antibacterial activity against test bacteria, namely *Escherichia coli* (MTCC 51) and *Bacillus stearothermophilus*. Their antibacterial activities were determined by reported methods.²⁶ Turbidity of the control was adjusted to 0.5 McFarland standards.²⁷ All the test cultures were streaked on nutrient agar medium (peptone, 10 g l⁻¹; yeast extract, 3.0 g l⁻¹; NaCl, 5.0 g l⁻¹; agar, 2 %) (NAM) and incubated overnight at 37 °C. By preparing bacterial suspension of 3–5 well-isolated colonies of the same morphological type selected from a NAM plate, the cultures were further diluted 10-fold to obtain an inoculum size of 1.2 CFU ml⁻¹. A stock solution of 500 µg ml⁻¹ of each compound were prepared in DMSO and appropriately diluted to obtain final concentrations of 100 and 50 µg ml⁻¹. The requisite quantity of antifungal compound (cyclohexamide) was added to the medium to obtain its desirable final concentration of 100 µg ml⁻¹. Each appropriately diluted 100 µl test sample was spread over the solidified NAM. Separate flasks were taken for each test dilution. The test bacterial culture were spotted in a predefined pattern by aseptically transferring 5 µl of each bacterial culture onto the surface of solidified agar-agar plates and incubated at 35 °C for 24 h.

RESULTS AND DISCUSSION

All the newly synthesized complexes were coloured solids soluble in DMSO, DMF and methanol. The conductivity values measured for 10^{-3} M solutions in anhydrous DMF were in the range $10\text{--}15 \Omega^{-1} \text{ cm}^2 \text{ mol}^{-1}$, which indicates their non-electrolytic nature. The analytical data were in good agreement with the proposed stoichiometry of the complexes. The colour, physical and analytical data of the ligands and their silicon complexes are presented in Table I.

TABLE I. Physical characteristics and analytical data of the ligands and their silicon complexes

Compd.	Empirical formula/ <i>FW</i>	Colour	M.p. °C	Calcd. (Found), %				
				C	N	H	S	Si
HL ¹	C ₇ H ₇ N ₅ S/193	Grey	168–170	43.09 (43.52)	35.57 (36.26)	3.17 (3.62)	15.91 (16.58)	–
Me ₂ SiCl(L ¹)	C ₉ H ₁₂ N ₅ SiClS/285	Bluish	196–198	37.44 (37.89)	24.33 (24.56)	3.98 (4.21)	11.06 (11.22)	9.10 (9.82)
Me ₂ Si(L ¹) ₂	C ₁₆ H ₁₈ N ₁₀ S ₂ Si/442	Dark bluish	183–185	43.79 (42.43)	31.18 (31.67)	3.85 (4.07)	14.35 (14.47)	5.99 (6.33)
HL ²	C ₈ H ₉ N ₅ S/207	Light violet	165–168	46.87 (45.37)	33.26 (33.81)	4.05 (4.34)	15.30 (15.45)	–
Me ₂ SiCl(L ²)	C ₁₀ H ₁₄ N ₅ SiClS/299	Light grey	210–212	39.78 (40.13)	23.13 (23.41)	4.22 (4.68)	10.03 (10.70)	9.12 (9.36)
Me ₂ Si(L ²) ₂	C ₁₈ H ₂₂ N ₁₀ SiS ₂ /470	Dark grey	194–195	45.64 (45.95)	29.41 (29.78)	4.00 (4.68)	13.25 (13.61)	5.04 (5.95)
HL ³	C ₉ H ₁₁ N ₅ S/221	Grey	218–220	48.52 (48.86)	31.09 (31.67)	4.62 (4.97)	14.00 (14.47)	–
Me ₂ SiCl(L ³)	C ₁₁ H ₁₆ N ₅ SiClS/313	Blackish	176–178	42.12 (42.17)	22.30 (22.36)	4.87 (5.11)	10.18 (10.22)	8.27 (8.94)
Me ₂ Si(L ³) ₂	C ₂₀ H ₂₆ N ₁₀ SiS ₂ /498	Blackish	197–199	48.86 (47.19)	27.99 (28.11)	5.18 (5.22)	12.76 (12.85)	5.06 (5.62)

Electronic spectra

The electronic spectra of the ligands (HL¹ and HL²) and their silicon complexes of Si(IV) were studied by dissolving the ligands and their complexes in dry methanol. The electronic spectra of the ligands HL¹ and HL² exhibited maxima at 387 and 358 nm, respectively, which can be assigned to the $n\text{--}\pi^*$ transition of the azomethine group. These bands showed a blue shift in the Si (1:1 and 1:2) complexes and appeared at 370 (Me₂SiL¹Cl), 341 (Me₂Si{L¹}₂), 340 (Me₂SiL²Cl) and 321 nm (Me₂Si{L²}₂), respectively. This clearly indicates the coordination of the azomethine nitrogen atom to the silicon atom. Furthermore, two medium intensity bands at 294 and 223 nm due to $\pi\text{--}\pi^*$ transitions in the ligands remained unchanged in the spectra of the silicon complexes.

IR Spectra

The ligands exhibited a broad band at $\approx 2750\text{ cm}^{-1}$ due to $\nu(\text{S-H})$,²⁸ which disappeared in the spectra of silicon complexes, indicating deprotonation and complexation through the sulphur atom. A new band appears at $\approx 750\text{ cm}^{-1}$, which was assigned to $\nu(\text{C-S})$ and which further confirms the coordination of the ligand through the sulphur atom. Silicon-sulphur bond formation was further supported by a band at $\approx 450\text{ cm}^{-1}$ of $\nu(\text{Si-S})$.²⁹ The sharp and strong band at $\approx 1597\pm 5\text{ cm}^{-1}$, assignable to $\nu(-\text{N}=\text{CH} <)$,³⁰ was shifted to higher wavelength numbers $\approx 1605\pm 5\text{ cm}^{-1}$ in the spectra of the metal complexes, indicating coordination through the azomethine nitrogen to the silicon atom. This shift can be explained by a reduction of the carbon-nitrogen double bond character in the azomethine group. Formation of a silicon-nitrogen bond was further confirmed by the presence of a band at $\approx 575\text{ cm}^{-1}$ of $\nu(\text{Si-N})$.³¹ A strong band in the region of $485\text{--}431\text{ cm}^{-1}$ was assigned to $\nu(\text{M-Cl})$ ³² in the 1:1 metal complexes. A characteristic band at $\approx 3250\text{ cm}^{-1}$, due to $\nu(\text{N-H})$ of pyrrole, was observed in the spectra of the ligands and their silicon complexes. The infrared spectral data of the ligands and their silicon complexes are listed in Table II.

TABLE II. IR Spectroscopic data (cm^{-1}) of the ligands and their silicon complexes

Compd.	$\nu(\text{S-H})$	$\nu(\text{N-H})$	$\nu(-\text{C}=\text{N})$	$\nu(-\text{C-S})$	$\nu_{\text{Si-S}}$	$\nu_{\text{Si-N}}$
HL ¹	2760	3238	1597	–	–	–
Me ₂ SiCl(L ¹)	–	3240	1603	746	443	555
Me ₂ Si(L ¹) ₂	–	3240	1607	749	448	578
HL ²	2744	3251	1611	734	–	–
Me ₂ SiCl(L ²)	–	3255	1620	745	451	545
Me ₂ Si(L ²) ₂	–	3254	1613	–	455	571
HL ³	2768	3256	1593	–	–	–
Me ₂ SiCl(L ³)	–	3260	1597	752	450	535
Me ₂ Si(L ³) ₂	–	3260	1603	757	455	567

¹H-NMR Spectra

To confirm further the bonding pattern in these complexes, the ¹H-NMR spectra of the ligands and their silicon complexes were recorded in DMSO-*d*₆ using TMS as the internal standard. The ¹H-NMR spectroscopic data of the ligands and their silicon complexes are given in Table III. The ¹H-NMR spectra of the ligands showed –SH proton signal at $\delta 13.70\pm 0.15\text{ ppm}$. The disappearance of this signal due to –SH protons in the spectra of the silicon complexes indicates deprotonation of the thiol group, which supported the coordination of silicon through the sulphur atom of the ligand. A signal at $\delta 9.40\pm 0.10\text{ ppm}$ was observed in the spectra of the silicon complexes due to the azomethine protons, which moved downfield in comparison to their original position in the free ligands, thereby indicating the coordination through the azomethine nitrogen to the

silicon atom. A sharp singlet due to $-\text{NH}$ proton (pyrrole) was also observed at δ 11.5–12.0 ppm in the spectra of ligands. Some additional signals at δ 3.5–4.0 ppm (*s*, $-\text{H}$, triazole), δ 2.0–3.5 ppm (*s*, $-\text{CH}_3$, triazole), δ 2.0–3.0 ppm (*q*, $-\text{CH}_2\text{CH}_3$, triazole) and δ 1.0–2.0 ppm (*t*, $-\text{CH}_2\text{CH}_3$, triazole) were observed in the ligands and their silicon complexes. Furthermore, the additional signals in the region δ 0.5–1.0 ppm were due to Me_2Si groups of the complexes.^{33,34}

TABLE III. ^1H -NMR Chemical shifts of the ligands and their silicon complexes

Cmpd.	Aromatic-H	$-\text{NH}$ (pyrrole)	$-\text{SH}$	Azomethine-H	$-\text{H}, -\text{CH}_3, -\text{C}_2\text{H}_5$
HL^1	6.2–7.1	11.4	13.7	9.5	3.5 (<i>s</i>)
$\text{Me}_2\text{SiCl}(\text{L}^1)$	6.1–7.1	11.2	–	9.4	3.4 (<i>s</i>), 0.74 (<i>s</i>)
$\text{Me}_2\text{Si}(\text{L}^1)_2$	6.0–7.2	11.2	–	9.4	3.4 (<i>s</i>), 0.52 (<i>s</i>)
HL^2	6.2–7.1	11.5	13.6	9.4	2.2 (<i>s</i>)
$\text{Me}_2\text{SiCl}(\text{L}^2)$	6.0–7.1	11.4	–	8.4	2.1 (<i>s</i>), 0.86 (<i>s</i>)
$\text{Me}_2\text{Si}(\text{L}^2)_2$	6.1–7.2	11.3	–	8.4	2.1 (<i>s</i>), 0.56 (<i>s</i>)
HL^3	6.0–6.8	11.9	13.3	9.3	2.3 (<i>q</i>), 1.9 (<i>t</i>)
$\text{Me}_2\text{SiCl}(\text{L}^3)$	6.6–7.2	11.6	–	9.1	2.1 (<i>q</i>), 1.7 (<i>t</i>), 0.89 (<i>s</i>)
$\text{Me}_2\text{Si}(\text{L}^3)_2$	6.2–7.1	11.7	–	9.1	2.1 (<i>q</i>), 1.8 (<i>t</i>), 0.50 (<i>s</i>)

^{13}C -NMR Spectra

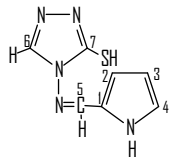
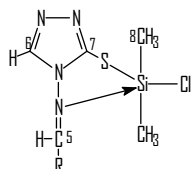
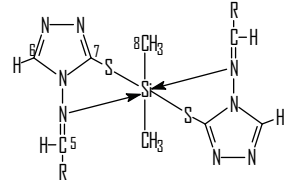
The ^{13}C -NMR spectra of the ligand HL^1 and its corresponding 1:1 and 1:2 silicon complexes were recorded and the data are given in Table IV. The signal due to the azomethine carbon atom of the ligand appears at δ 151.61 ppm. However, in the spectra of the corresponding silicon complexes, the signal appeared at higher δ values. The considerable shifting in the carbon atom attached to the azomethine nitrogen indicates coordination of nitrogen to the central metal atom in the 1:1 and 1:2 metal complexes. Furthermore, the shifting of the ^{13}C resonance that is attached to the sulphur atom in the spectra of the 1:1 and 1:2 silicon complexes, compared to the free ligands, indicates coordination through sulphur to the silicon atom. Additional signals in the ^{13}C -NMR spectra of the silicon complexes were observed at δ 10.32 ppm and δ 8.57 ppm (Si-C) in the 1:1 and 1:2 silicon complexes, respectively.

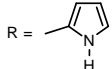
^{29}Si -NMR Spectra

In order to confirm the geometry of the complexes, ^{29}Si -NMR spectra of the complexes were recorded. The value of δ ^{29}Si in the spectra reflects the coordination number of the nucleus in the corresponding silicon complex.^{35,36} In general, ^{29}Si chemical shifts move to lower frequency with increasing coordination number of the nuclei. The spectra show in each case only one sharp singlet indicating the formation of a single species. The ^{29}Si -NMR spectra of the 1:1 and 1:2 silicon complexes exhibited sharp signals at δ -97.38 ppm and δ -107.78 ppm,

which is indicative of a penta- and a hexa-coordinated environment around the silicon atom, respectively.

TABLE IV. ^{13}C -NMR Chemical shifts of the ligands and their silicon complexes

Compd.	C ₁	C ₂	C ₃	C ₄	C ₅	C ₆	C ₇	M-CH ₃
	125.52	124.45	110.37	118.10	151.61	161.26	155.82	-
	125.35	124.21	110.32	118.02	155.99	161.30	152.37	10.32
	125.40	124.11	110.33	118.12	156.12	161.45	152.36	8.57

R = 

Based on the above evidences, it is suggested that the geometries around the silicon atom in the complexes investigated were trigonal bipyramidal and octahedral in the 1:1 and 1:2 ratios, respectively, as shown in Fig. 2.

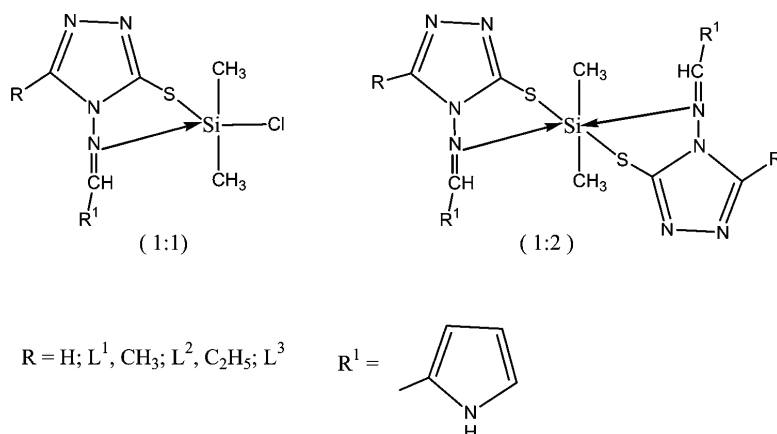


Fig. 2. Proposed structures of the 1:1 and 1:2 complexes.

Biological aspects

The free ligands and their silicon complexes were screened against various fungi and bacteria to assess their potential as antimicrobial agents. The fungicidal and bactericidal activities of free ligands HL¹, HL² and HL³ and their organo-silicon(IV) complexes against various fungi and bacteria are given in Tables V and VI, respectively.

TABLE V. Antifungal screening (average percentage inhibition after 96 h)

Compd.	Concentration, $\mu\text{g ml}^{-1}$	<i>A. flavus</i>	<i>A. niger</i>
C ₇ H ₇ N ₅ S	Control	Nil	Nil
	50	Nil	Nil
	100	Nil	Nil
	500	Nil	Nil
C ₉ H ₁₂ N ₅ SiClS	Control	0.00	0.00
	10	9.20	7.31
	50	29.31	13.55
	100	52.11	37.69
C ₁₆ H ₁₈ N ₁₀ S ₂ Si	Control	0.00	0.00
	10	32.71	19.73
	50	48.14	79.43
	100	84.12	94.71
C ₈ H ₉ N ₅ S	Control	Nil	Nil
	10	Nil	Nil
	50	0.01	0.00
	100	11.10	13.05
C ₁₀ H ₁₄ N ₅ SiClS	Control	0.00	0.00
	10	45.54	35.12
	50	64.72	78.64
	100	89.47	89.41
C ₁₈ H ₂₂ N ₁₀ SiS ₂	Control	0.00	0.00
	10	45.79	35.13
	50	57.89	68.32
	100	84.41	78.62
C ₉ H ₁₁ N ₅ S	Control	0.00	0.00
	10	Nil	Nil
	50	Nil	Nil
	100	Nil	Nil
C ₁₁ H ₁₆ N ₅ SiClS	Control	0.00	0.00
	10	10.87	9.30
	50	26.33	20.55
	100	62.58	47.90
C ₂₀ H ₂₆ N ₁₀ SiS ₂	Control	0.00	0.00
	10	35.40	40.21
	50	62.25	71.43
	100	88.27	90.23

TABLE VI. Antibacterial screening data of the ligands and their metal complexes

Cmpd.	Concentration, $\mu\text{g ml}^{-1}$	Inhibition, %	
		<i>E. coli</i>	<i>B. stearothermophilus</i>
C ₇ H ₇ N ₅ S	50	Nil	Nil
	100	Nil	Nil
	500	14	20
C ₉ H ₁₂ N ₅ SiClS	50	16	31
	100	37	58
	500	63	73
C ₁₆ H ₁₈ N ₁₀ Si ₂	50	21	29
	100	32	47
	500	56	61
C ₈ H ₉ N ₅ S	50	Nil	Nil
	100	Nil	Nil
	500	17	21
C ₁₀ H ₁₄ N ₅ SiClS	50	45	29
	100	83	60
	500	91	83
C ₁₈ H ₂₂ N ₁₀ Si ₂	50	22	19
	100	38	42
	500	55	72
C ₉ H ₁₁ N ₅ S	50	Nil	Nil
	100	11	14
	500	31	38
C ₁₁ H ₁₆ N ₅ SiClS	50	20	13
	100	43	32
	500	68	43
C ₂₀ H ₂₆ N ₁₀ Si ₂	50	24	30
	100	49	40
	500	72	51

The antimicrobial data revealed that the complexes were superior to the free ligands. The activity increased as the concentration increased. These complexes were found to be more potent inhibitor for the growth of *E. coli* among test bacterial cultures and nearly equally sensitive for test fungal cultures. Thus, it can be postulated that further studies of these complexes in this direction could leads to interesting results.

Acknowledgements. This investigation received financial assistance from UGC, New Delhi, India, by providing a Senior Research Fellowship under Rajiv Gandhi National Fellowship Scheme to one of the author (Dharam Pal). The authors are thankful to the Head, RSIC of Panjab University, Chandigarh for providing Metal NMR, C, H and N analyses. They are also thankful to Saurabh Sudha Dhiman, Department of Biotechnology, Kurukshetra University, Kurukshetra, for determining the biological activities.

ИЗВОД

СИНТЕЗА И СТРУКТУРНО И БИОЛОШКО ИСПИТИВАЊЕ ОРГАНОСИЛИЦИЈУМ(IV)-КОМПЛЕКСА ШИФОВИХ БАЗА ДОБИЈЕНИХ ИЗ ПИРОЛ-2-КАРБОАЛДЕХИДА

KIRAN SINGH¹ и DHARAM PAL²¹Department of Chemistry, Kurukshetra University, Kurukshetra-136 119 u ²Department of Applied Sciences, J.I.E.T., Jind-126102, Haryana, India

Одабрани нови органосилицијум(IV)-комплекси, опште формуле $R_2SiCl[L]$ и $R_2Si[L]_2$ синтетизовани су у реакцијама Me_2SiCl_2 са Schiff-овим базама (5-меркапто-4-[(1H-пирол-2-илметил)амино]-s-триазолом, 5-меркапто-3-метил-4-[(1H-пирол-2-илметил)амино]-s-триазолом и 3-етил-5-меркапто-4-[(1H-пирол-2-илметил)амино]-s-триазолом) у 1:1 и 1:2 моларним односима. Сва једињења окарактерисана су помоћу елементарне анализе, моларне проводљивости, IR, UV, ¹H-, ¹³C- и ²⁹Si-NMR спектралним проучавањем. Спектроскопски подаци сугеришу да је азометински азот укључен у координацију са централним силицијумовим атомом. На основу поменутих спектралних података предложена је пента- и хексакоординација око централних силицијумових атома у 1:1, односно 1:2 комплексима. Коначно, слободни лиганди и њихови силицијумови комплекси тестирани су *in vitro* на неке патогене бактерије и гљивице у циљу процене њихових антимикуробних особина.

(Примљено 16. децембра 2008, ревидирано 26. априла 2010)

REFERENCES

1. K. K. Chaturvedi, R. V. Singh, J. P. Tandon, *J. Prakt. Chemie* **327** (1985) 144
2. C. J. Baalal Krishnan, K. Natrajan, *Transition Met. Chem.* **27** (2002) 75
3. X. Zhang, W. H. Li, H. Z. Jia, S. F. Weng, J. G. Wu, in *Proceedings of The Twelfth International Conference on Fourier Transform Spectroscopy*, Waseda University, Tokyo, Japan, 1999, p. 507
4. L. Puccetti, G. Fosolis, V. Daniela, Z. H. Chohan, S. Andrea, C. T. Supuran, *Bioorg. Med. Chem. Lett.* **15** (2005) 3096
5. Z. H. Chohan, M. U. Hassan, K. M. Khan, C. T. Supuran, *J. Enzyme Inhib. Med. Chem.* **20** (2005) 183
6. M. U. Hassan, Z. H. Chohan, A. Scozzafava, *J. Enzyme Inhib. Med. Chem.* **19** (2004) 263
7. H. Y. Zhang, J. Lei, Y. Y. Chen, Q. A. Wu, Y. S. Zhang, L. H. Gao, *Synth. React. Inorg. Met.-Org. Chem.* **31** (2001) 973
8. S. Hong-Jian, L. Xiao-Yan, C. Xue-Gui, L. De-Xin, H. X. X. Bao, *Acta Chim. Sinica* **13** (1992) 1168
9. E. Abele, *Main Group Met. Chem.* **28** (2005) 45
10. W. Ji-Tao, G. Sheng-Hua, L. Xiang-Min, L. Feng-Quan, H. X. X. Bao, *Acta Chim. Sinica* **14** (1993) 645
11. A. Chaudhary, A. Phor, G. K. Aggarwal, R. V. Singh, *Heterocycl. Commun.* **10** (2004) 181
12. M. Gielen, *Tin-Based Antitumor Drugs*, NATO ASI Series, Springer Verlag, Berlin Vol. 37, 1990
13. R. Malhotra, J. Mehta, J. K. Puri, *Cent. Eur. J. Chem.* **5** (2007) 858
14. G. Eng, D. Whalen, P. Musingarimi, J. Tierney, M. Derosa, *Appl. Organomet. Chem.* **12** (1998) 25
15. M. Jain, S. Gaur, S.C. Joshi, R. V. Singh, A. Bansal, *Phosphorus Sulfur Silicon* **179** (2004) 1517

16. G. Deleris, *Met. Based Drugs* **2** (1995) 143
17. P. C. McGowman, *Annu. Rep. Prog. Chem.* **101(A)** (2005) 631
18. R. B. Allen, P. Kochs, G. Chandra, *Handbook Environ. Chem.* **3** (1997) 1
19. C. Saxena, R. V. Singh, *Phosphorus Sulfur Silicon* **97** (1994) 17
20. S. Belwal, H. Tanjea, A. Dandia, R. V. Singh, *Phosphorus Sulfur Silicon* **127** (1997) 49
21. S. Belwal, R. K. Saini, R. V. Singh, *Indian J. Chem.* **37A** (1998) 245
22. M. S. Singh, V. W. Bhagwat, M. D. Raju, S. K. Tiwari, *Indian J. Chem.* **38A** (1999) 716
23. C. Saxena, R. V. Singh, *Synth. React. Inorg. Met.-Org. Chem.* **22** (1992) 1061
24. S. Bala, R. P. Gupta, M. L. Sachdeva, A. Singh, H. K. Pujari, *Indian J. Chem.* **16** (1978) 481
25. Y. L. Nene, P. N. Thapliyal, *Evaluation of Fungicides*, in *Fungicides in Plants Disease Control*, 3rd Ed., Oxford and IBH Publishing, New Delhi, 1993, p. 531
26. P.A. Villanova, *NCCLS, Method for Dilution Antimicrobial Susceptibility Test for Bacteria That Grow Aerobically Approved Standard*, 5th ed., National Committee for Clinical Laboratory Standards, Wayne, PA, 2000
27. J. McFarland, *J. Am. Med. Assoc.* **14** (1907) 1176
28. G. Singh, P. A. Singh, K. Singh, D. P. Singh, R. N. Handa, S. N. Dubey, *Proc. Natl. Acad. Sci. Ind.* **72A** (2002) 87
29. S. Belwal, R. V. Singh, *Appl. Organomet. Chem.* **12** (1998) 39
30. K. Singh, D. P. Singh, M. S. Barwa, P. Tyagi, Y. Mirza, *J. Enzyme Inhib. Med. Chem.* **21** (2006) 557
31. M. Nath, S. Goyal, *Synth. React. Inorg.-Met. Org. Chem.* **30** (2000) 1791
32. A. Chaudhary, R. V. Singh, *Phosphorus Sulfur Silicon* **178** (2003) 615
33. K. Singh, D. Pal, V. Parkash, *Phosphorus Sulfur Silicon* **183** (2008) 2784
34. K. Singh, D. Pal, S. S. Dhiman, *Main Group Chem.* **8** (2009) 47.
35. R. V. Singh, P. Nagpal, *Bioinorg. Chem. Appl.* **3** (2005) 3
36. G. G. Mohamed, M. M. Omar, A. M. Hindy, *Turk. J. Chem.* **30** (2006) 361.



J. Serb. Chem. Soc. 75 (7) 929–934 (2010)
JSCS–4018

Preparation and characterization of novel oxo-centered basic *p*-chlorobenzoic bridging trinuclear complexes

IMAN KHOSRAVI* and MOHAMMAD YAZDANBAKHSH

*Department of Chemistry, Faculty of Science, Ferdowsi University of
Mashhad, Mashhad, Iran*

(Received 25 August 2009, revised 2 February 2010)

Abstract: Three new oxo-centered trinuclear complexes, one of them a mixed-valence complex $[\text{Mn}_3\text{O}(\text{C}_7\text{H}_4\text{O}_2\text{Cl})_6(\text{Py})_3]\text{Py}$ (**1**) and the others, mixed-metal complexes of $[\text{Fe}_2\text{MnO}(\text{C}_7\text{H}_4\text{O}_2\text{Cl})_6(\text{Py})_3]\text{NO}_3$ (**2**) and $[\text{Fe}_2\text{CoO}(\text{C}_7\text{H}_4\text{O}_2\text{Cl})_6(\text{Py})_3]$ (**3**) were synthesized by the direct reaction between metal nitrates and *p*-chlorobenzoic acid. These complexes were characterized by elemental analyses (CHN), atomic absorption spectroscopy and spectral (IR, electronic) studies. These are new type of oxo-bridged mixed-metal complexes in which the carboxylate ligand is *p*-chlorobenzoic acid. The UV spectra of the complexes exhibited a strong band in the region $42,500\text{ cm}^{-1}$ which is related to the ($\pi \rightarrow \pi^*$) transitions of the pyridine ligand. The IR spectra of these compounds showed two strong stretching vibrations bands, indicating a bridging coordination mode of the carboxylic group of the ligand in the complexes.

Keywords: mixed-valence; oxo-centered; trinuclear complexes; spectroscopy; carboxylic ligand; IR spectra.

INTRODUCTION

Trinuclear, oxo-centered, carboxylate complexes of transition metals of general composition $[\text{M}_3\text{O}(\text{O}_2\text{CR})_6\text{L}_3]^{n+}$ and $[\text{M}(\text{III})_2\text{M}(\text{II})\text{O}(\text{O}_2\text{CR})_6\text{L}_3]$ (Fig. 1) have been of interest for several years.^{1,2} Compounds containing metal–oxo–carboxylate fragments exhibit a wide range of structural features and diverse chemical reactions. They have attracted attention as versatile intermediates as precursors to larger assemblies.^{3,4} Interest in these compounds arose for several reasons. Firstly, they form a rare class of compounds, which serve as important models to test theories of magnetic coupling between metal ions in multinuclear systems; likewise the structural variations shown by these metallic clusters have yielded important information on the parameters which govern stability within metal–ligand aggregates.

* Corresponding author. E-mail: khosraviiman@yahoo.com
doi: 10.2298/JSC090825066K

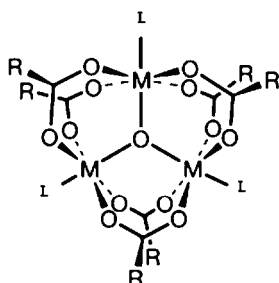


Fig. 1. Structure of the cluster unit $[M_3O(RCOO)_6(L)_3]^{2-}$.

Secondly, the polynuclear structure leads to the formation of mixed-valence and mixed-metal derivative, which give opportunities to study the electronic and magnetic interactions between homo- and heterometal centers in close proximity in a defined geometry. There is also the possibility of generating spin-frustrated species. Thirdly, several of these complexes are active as homogeneous catalysts for a variety of oxidation reactions.^{5,6} In view of this, the spectroscopic, magnetic and redox properties of these complexes have been extensively studied.⁷

Surprisingly, little attention has been paid to the consideration of substitution properties, with only a few reports of comparative studies regarding the redox properties when the terminal ligand L changes. There is interest in establishing how substitution in the carboxylate bridge affects the lability of the terminal ligand and the redox potential of the metal centers. These carboxylate complexes are of additional interest when the carboxylate is unsaturated, because there is a potential scope for further polymerization in the solid state by cross-linking of the substituents.^{8,9}

In this paper, the syntheses and characterization of heterometallic clusters in solution phase are reported.

EXPERIMENTAL

The C, H and N analyses were realized on a Thermo Finnigan Flash model EA1112 elemental analyzer at the Faculty of Science, Ferdowsi University of Mashhad, India. The atomic absorption analyses were performed on a Shimadzu model AA-670 atomic absorption spectrometer. The IR spectra of KBr discs ($4000\text{--}600\text{ cm}^{-1}$) were recorded on a Buck 500 spectrometer. The electronic spectra were registered in the range $600\text{--}200\text{ cm}^{-1}$ on a Perkin-Elmer 1600 spectrometer. The reagents, *p*-chlorobenzoic acid (99%), iron (99%), cobalt (99%) and manganese (99%) nitrate and solvents were obtained commercially from Merck Chemicals and used as received. The nitrogen base (pyridine) was dried following the standard procedures.¹⁰ Sodium *p*-chlorobenzoate was obtained from sodium carbonate and *p*-chlorobenzoic acid in a 1:2 molar ratio and water as solvent.

Preparation of $[Mn_3O(C_7H_4O_2Cl)_6(Py)_3]Py$ (I)

n-Bu₄NMnO₄ was prepared by a literature method.¹¹ *n*-Bu₄NBr (12 g, 37 mmol) was added to an aqueous solution of KMnO₄ (5.0 g, 32 mmol) under vigorous stirring. The immediately formed purple precipitate was collected by filtration, washed thoroughly with distilled water and diethyl ether and dried *in vacuo* at room temperature (yield > 90%).

Warning: *n*-Bu₄NMnO₄ is potentially explosive and must be treated with care!

Mn(O₂CMe)₂·4H₂O (0.80 g, 3.3 mmol) and C₇H₅O₂Cl (3.8 g, 25 mmol) were dissolved in a solvent mixture comprising dry pyridine (3 ml) and absolute EtOH (25 ml). The resulting solution was stirred while solid *n*-Bu₄NMnO₄ (0.46 g, 1.3 mmol) was added in small portions to give a brown-green homogeneous solution, from which the precipitation of a brown-green product began almost immediately. The stirring was continued for 1 h and the product was left undisturbed overnight in a refrigerator. The brown-green precipitate was filtered, washed copiously with cold EtOH, and dried *in vacuo*. Yield: 65 %; m.p.: 190 °C; Anal. Calcd. for C₆₂H₄₄C₁₆Mn₃N₄O₁₃ (FW 1426.7): C, 52.14; H, 3.08; N, 3.92; Mn, 18.6 %. Found: C, 52.22; H, 3.15; N, 3.99; Mn, 18.3 %. IR (selected data, KBr, cm⁻¹): 540 (*m*), 715 (*s*), 1405 (*s*), 1595 (*s*), 2940 (*m*).

Preparation of [Fe₂MnO(C₇H₄O₂Cl)₆(Py)₃]NO₃ (2)

A mixture of Fe(NO₃)₃·9H₂O (1.08 g, 2.68 mmol) and Mn(NO₃)₂·4H₂O (0.34 g, 1.3 mmol), dissolved in 25 ml dry pyridine was refluxed for 10 min and NaC₇H₄O₂Cl (2.0 g, 12 mmol) was added and the reflux continued for 5 h. The resulting deep brown solution was allowed to cool and stored for 2 days at 20 °C. The black crystals were filtered off, washed copiously with Et₂O and dried *in vacuo*. Yield: 75 %; m.p.: 230 °C; Anal. Calcd. for C₅₇H₃₉C₁₆Fe₂MnN₄O₁₆ (FW 1414.5): C, 48.35; H, 2.75; N, 3.95; Fe, 7.8; Mn, 4.3 %. Found: C, 48.95; H, 2.60; N, 3.82; Fe, 7.6; Mn, 4.1 %. IR (selected data, KBr, cm⁻¹): 434 (*m*), 549 (*m*), 715 (*s*), 1410 (*s*), 1598 (*s*), 2900 (*m*).

Preparation of [Fe₂CoO(C₇H₄O₂Cl)₆(Py)₃] (3)

A mixture of Fe(NO₃)₃·9H₂O (1.08 g, 2.68 mmol) and Co(NO₃)₂·6H₂O (0.39 g, 1.3 mmol), dissolved in 25 ml of dry pyridine was refluxed for 10 min and NaC₇H₄O₂Cl (2.0 g, 12 mmol) was added and the reflux continued for 4 h. The resulting dark red solution was allowed to cool and stored for 3 days at 20 °C. The brown crystals were filtered off, washed copiously with Et₂O and dried *in vacuo*. Yield: 70 %; m.p.: 185 °C. Anal. Calcd. for C₅₇H₃₉C₁₆CoFe₂N₃O₁₃ (FW 1356.6): C, 50.41; H, 2.87; N, 3.09; Fe, 8.2; Co, 4.3 %. Found: C, 50.59; H, 2.81; N, 3.20; Fe, 8.1; Co, 4.2 %. IR (selected data, KBr, cm⁻¹): 440 (*m*), 543 (*m*), 710 (*s*), 1402 (*s*), 1600 (*s*), 2950 (*m*).

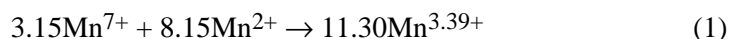
RESULTS AND DISCUSSION

The analytical data for the complexes are given in Table I. They are in close agreement with the calculated data and strongly support the presence of trinuclear metal complexes. Mixed-metal oxo-centered complexes were prepared from metal nitrates and sodium *p*-chlorobenzoate in dry pyridine to obtain the expected products.

TABLE I. Analytical data, color and melting point of the complexes 1–3

Compound	Color	Found (Calcd.), %			M.p., °C
		C	H	N	
1	Brown-green	52.22 (52.14)	3.15 (3.08)	3.99 (3.92)	190
2	Deep-brown	48.95(48.35)	2.60 (2.75)	3.82 (3.95)	230
3	Brown	50.59 (50.42)	2.81 (2.87)	3.20 (3.10)	185

Prior reports of the synthesis and properties of trinuclear oxo-centered Mn complexes are few. The synthetic procedures almost invariably employed polymeric Mn(III) acetate, which can be readily obtained from the oxidation of $\text{Mn}(\text{O}_2\text{CMe})_2 \cdot 4\text{H}_2\text{O}$ with KMnO_4 in hot glacial acetic acid.¹² Reaction of this material with an excess of a neutral donor group L led to discrete units of the formulation $[\text{Mn}_3\text{O}(\text{O}_2\text{CMe})_6(\text{L})_3]^\pm$. As part of our continuing development of *n*- Bu_4NMnO_4 as a reagent for inorganic syntheses in non-aqueous solvents, its use for the synthesis of Mn_3O -type complexes was explored and it was found to work extremely well. The solvents of choice are EtOH and pyridine which ensure solubility of all the reactants; the cleanest reactions are obtained when an excess of carboxylic acid is also present, otherwise low yields or intractable brown gel-like precipitates result. The synthetic strategy was to react together particular ratios of Mn(VII):Mn(II) to yield products in the intermediate metal oxidation state range +2.67 to +3.00 characteristic of Mn_3O units. However, it was noticed that small changes in the Mn(VII):Mn(II) ratio had no noticeable effect on the identity of the products or their yields. As was registered previously,¹³ redox reactions involving solvent, atmospheric oxygen, or reagent impurities could compensate for an excess or lack of Mn(II), for example, over that required to yield the preferred product. A Mn(VII):Mn(II) ratio of 3.15:8.15 has now become the routinely employed stoichiometry and has provided access to complex **1**. This ratio should, in theory, provide an average metal oxidation of +3.39 according to Eq. (1) but cleanly leads instead to either $\text{Mn}_2(\text{III})\text{Mn}(\text{II})$ species, or $\text{Mn}_3(\text{III})$ species:



IR Spectroscopy

The IR spectral data of the complexes are given in Table II. The observed vibrational frequencies, $\nu_{\text{asym}}(\text{COO})$ and $\nu_{\text{sym}}(\text{COO})$, for the carboxylate ligand support the presence of bridging coordinated carboxylates in all the complexes. For the mixed-metal complexes, it appears from the carboxylate stretching frequencies that all six ligands are approximately equivalent and they are best represented as bidentate bridges.¹⁴ For a new series of trinuclear mixed-metal complexes, Cannon *et al.*² assigned the IR spectra and identified the vibrational modes of the central M_3O core. They found that the reduction in site geometry from D_{3h} to C_{2v} lifted the degeneracy of the asymmetric M_3O stretches and two bands were seen. In the IR spectrum of complex **2**, strong bands at 1410 and 1598 cm^{-1} were evident. They are attributed to the $\nu_{\text{sym}}(\text{COO})$ and $\nu_{\text{asym}}(\text{COO})$ modes, respectively. The difference ($\Delta\nu = \nu_{\text{asym}}(\text{COO}) - \nu_{\text{sym}}(\text{COO})$) is 188 cm^{-1} .¹⁵ The presence of ionic nitrate in this complex follows from the IR spectrum through the appearance of a relatively weak band at 1380 cm^{-1} . For the identification of the metal–oxygen bands of the M_3O groups, the IR spectra in the range 800–400

cm^{-1} were used. The strong band observed at 430–560 cm^{-1} is attributed to the $\nu(\text{M}_2\text{M}')$ vibration.¹⁶

TABLE II. Selected IR bands (cm^{-1}) for the complexes **1–3**

Compound	$\nu_{\text{asym}}(\text{COO})$	$\nu_{\text{sym}}(\text{COO})$	$\nu(\text{M}_3\text{O})$	$\nu(\text{C-H})$	$\nu(\text{C-X})$
1	1405	1595	540	2940	715
2	1410	1598	434–549	2900	715
3	1402	1600	440–543	2950	710

Electronic spectroscopy

The electronic spectra of the trinuclear complexes can be interpreted to a good approximation in terms of the individual metal ions, together with ligand–metal charge transfer transitions. The electronic spectra of the complexes were recorded in the range 50000–15000 cm^{-1} in dichloromethane solution. The spectra of the mixed–metal complexes **2** and **3** show the characteristic bands provided by both metal ions. The UV spectra of these complexes exhibited a strong band in the region 42500 cm^{-1} , which is related to the ($\pi \rightarrow \pi^*$) transitions of the pyridine (Py) ligand.¹⁷ The bands are shifted to higher energy when L = pyridine. The electronic spectroscopy data are given in Table III, which can be assigned and characterized based on other literature.¹⁸

TABLE III. Diffuse reflectance spectra of complexes

Compound	Transition $\pi \rightarrow \pi^*$, nm	Transition d \rightarrow d, nm
1	244	470–530
2	247	459–574
3	254	440–558–677(<i>sh</i>)

CONCLUSIONS

In this study, three new oxo-centered basic *p*-chlorobenzoic bridging complexes were prepared by the direct method of reaction between metal nitrate and sodium *p*-chlorobenzoate. These compounds were characterized by elemental analyses (CHN), atomic absorption spectroscopy, as well as by IR and electronic spectroscopy. The IR spectra show two strong bands and the observed stretching vibrations indicated the presence of a bridging coordination mode of carboxylic ligand. In addition, for mixed-metal complexes, the atomic absorption data show a statistical 2:1 disorder of iron and manganese or cobalt atoms, respectively.

ИЗВОД

ДОБИЈАЊЕ И КАРАКТЕРИСАЊЕ НОВИХ ОКСО-ЦЕНТРИРАНИХ ТРИНУКЛЕАРНИХ КОМПЛЕКСА СА МОСТОВНО ВЕЗАНОМ *p*-ХЛОРБЕНЗОЕВОМ КИСЕЛИНОМ

IMAN KHOSRAVI и MOHAMMAD YAZDANBAKHS

Department of Chemistry, Faculty of Science, Ferdowsi University of Mashhad, Mashhad, Iran

Три нова оксо-центрирана тринуклеарна комплекса, мешовито-валентни $[\text{Mn}_3\text{O}(\text{C}_7\text{H}_4\text{O}_2\text{Cl})_6(\text{Py})_3]\text{Py}$ (**1**) и два мешовито-метална $[\text{Fe}_2\text{MnO}(\text{C}_7\text{H}_4\text{O}_2\text{Cl})_6(\text{Py})_3]\text{NO}_3$ (**2**) и $[\text{Fe}_2\text{CoO}(\text{C}_7\text{H}_4\text{O}_2\text{Cl})_6(\text{Py})_3]$ (**3**) су добијена директном реакцијом металног нитрата и *p*-хлорбензоове киселине и окарактерисана елементалном анализом (CHN), атомском апсорпционом спектроскопијом и спектралном (IR, електронском) анализом. Ово је нови тип оксо-мостовних мешовито-металних комплекса са карбоксилатним лигандом *p*-хлорбензоовом киселином. UV спектри ових комплекса имају јаку траку у области 42500 cm^{-1} која припада ($\pi \rightarrow \pi^*$) прелазима пиридинског лиганда. IR спектри садрже две јаке траке вибрација истезања указујући на мостовни начин координације карбоксилатног лиганда.

(Примљено 25. августа 2009, ревидирано 2. фебруара 2010)

REFERENCES

1. J. L. Chen, L. Y. Zhang, L. X. Shi, H. Y. Ye, Z. N. Chen, *Inorg. Chim. Acta* **359** (2006) 1531
2. R. D. Cannon, R. P. White, *Prog. Inorg. Chem.* **36** (1988) 195
3. B. P. Baranwal, T. Fatma, *J. Mol. Struct.* **72** (2005) 750
4. C. Turta, S. Shova, D. Prodius, V. Mereacre, M. Gdaniec, Y. Simonov, J. Lipkowski, *Inorg. Chim. Acta* **657** (2004) 4396
5. C. P. Raptopoulou, Y. Sanakis, A. K. Boudalis, V. Psycharis, *Polyhedron* **24** (2005) 711
6. S. P. Pali, D. E. Richardson, M. L. Hansen, B. B. Iversen, F. K. Larsen, L. Singorean, G. A. Timco, N. V. Gerbelev, K. R. Jennings, J. R. Eyler, *Inorg. Chim. Acta* **23** (2001) 319
7. M. Yazdanbakhsh, I. Khosravi, H. Tavakkoli, *J. Serb. Chem. Soc.* **74** (2009) 401
8. R. E. P. Winpenny, *Adv. Inorg. Chem.* **52** (2001) 1
9. A. K. Boudalis, N. Laloti, G. A. Spyroulias, C. P. Raptopoulou, A. Terzis, *Inorg. Chem.* **41** (2002) 6474
10. D. Gatteschi, R. Sessoli, *Angew. Chem. Int. Ed.* **42** (2003) 268
11. T. Sala, M. V. Sargent, *J. Chem. Soc. Chem. Commun.* **14** (1978) 253
12. M. Soler, E. Rumberger, K. Folting, D. N. Hendrickson, G. Christou, *Polyhedron* **20** (2001) 1365
13. S. G. Baca, H. S. Evans, C. Ambrus, S. T. Malinovskii, I. Malaestean, N. Gerbelev, S. Decurtins, *Polyhedron* **25** (2006) 3617
14. P. T. Maragh, S. E. Thomas, T. P. Dasgupta, *Inorg. Chim. Acta* **358** (2005) 3610
15. M. Yazdanbakhsh, M. H. Alizadeh, H. Z. Khorramdel, W. Frank, *Z. Anorg. Allg. Chem.* **633** (2007) 1193
16. B. P. Baranwal, T. Fatma, A. Varma, *J. Mol. Struct.* **920** (2009) 472
17. J. L. Chen, L. Y. Zhang, L. X. Shi, H. Y. Ye, Z. N. Chen, *Inorg. Chim. Acta* **358** (2005) 859
18. T. J. Mizoguchi, R. M. Davydov, S. J. Lippard, *Inorg. Chem.* **38** (1999) 4098.



J. Serb. Chem. Soc. 75 (7) 935–941 (2010)
JSCS–4019

Synthesis and characterization of a tetraaza macrocyclic ligand and its cobalt(II), nickel(II) and copper(II) complexes

SULEKH CHANDRA^{1*}, MONIKA TYAGI¹ and SWATI AGRAWAL²

¹Department of Chemistry, Zakir Husain College (University of Delhi), JLN-Marg, New Delhi – 110002 and ²Department of Chemistry, Motilal Nehru College (University of Delhi), Benito Juarez Road, New Delhi – 110 021, India

(Received 18 September, revised 7 December 2009)

Abstract: Co(II), Ni(II), and Cu(II) complexes with a tetradentate nitrogen donor [N4] macrocyclic ligand, viz. 6,15-dimethyl-8,17diphenyl-7,16-dihydrodibenzo[*b,i*][1.4.8.11]tetraazacyclotetradecine, were synthesized. Their structures were determined based on elemental analyses, molar conductance and magnetic susceptibility measurements, and IR, ¹H-NMR (ligand) and electronic spectral studies. Based on analytical and molar conductance data, the complexes may be formulated as [M(L)Cl₂] and [M'(L)]Cl₂ (where M = Co(II) and Cu(II), and M' = Ni(II)) due to their non-electrolytic and 1:2 electrolytic nature. Based on spectral studies, an octahedral geometry was assigned for the Co(II) complex, whereas square-planar and tetragonal geometry were proposed for the Ni(II) and Cu(II) complexes, respectively. The synthesized ligand and its complexes were screened for fungicidal activity against two pathogenic fungi (*i.e.*, *Fusarium moniliformae* and *Rhizoctonia solani*) to assess their growth inhibiting potential.

Keywords: tetraaza macrocycle; Co(II), Ni(II) and Cu(II) complexes; characterization.

INTRODUCTION

Transition metal complexes containing macrocycles are of considerable interest in terms of structural and coordination chemistry.¹ The chemical properties of macrocyclic complexes can be tuned to force metal ions to adopt unusual coordination geometries. Transition metal macrocyclic complexes have received much attention as an active part of metalloenzymes² and as biomimetic model compounds,^{3,4} due to their resemblance to natural proteins such as hemerythrin and enzymes. Aza-type ligands appear very promising for potential use as anti-fertile, antibacterial, and antifungal agents as well as due to their other biological properties.^{5–8} Transition metal complexes have received much attention as cata-

* Corresponding author. E-mail: schandra_00@yahoo.com; mnk02tyg@yahoo.co.in
doi: 10.2298/JSC090804069C

lysts in oxidation and epoxidation processes.^{9,10} Structural factors such as ligand rigidity, the type of donor atoms and their disposition have been shown to play significant roles in determining the binding features of macrocyclic ligands toward metal ions.^{11,12} Due to the growing interest in macrocyclic ligands and their transition metal complexes, the synthesis, spectroscopic characterization and antifungal activities of Co(II), Ni(II), and Cu(II) complexes with a 14-membered macrocyclic ligand, *viz.* 6,15-dimethyl-8,17-diphenyl-7,16-dihydrodibenzo[*b,i*][1.4.8.11]tetraazacyclotetradecine (L), are reported in this paper. The preparation and structural formula of the ligand are shown in Fig. 1.

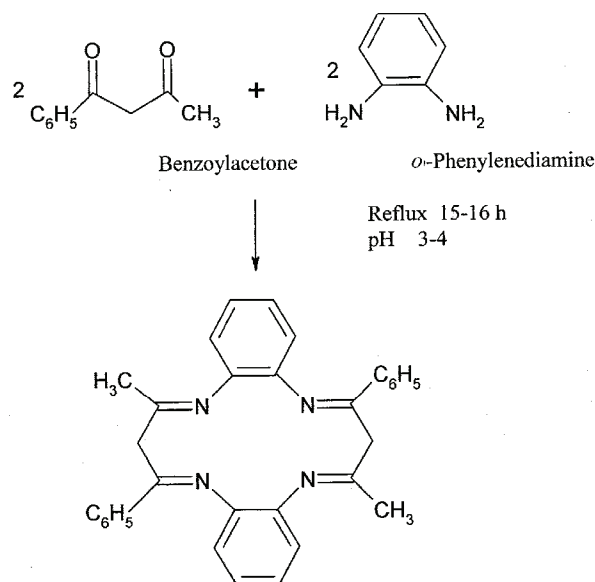


Fig. 1. Preparation and structural formula of the ligand.

EXPERIMENTAL

All the chemicals used were of analytical grade and procured from Sigma–Aldrich (USA) and Fluka (USA). The metal salts were purchased from E. Merck (Germany) and were used as received.

Synthesis of the ligand

A hot ethanolic solution (20 ml) of benzoylacetone (3.24 g, 0.020 mol) and an ethanolic solution (20 ml) of *o*-phenylenediamine (2.16 g, 0.020 mol) were mixed slowly under constant stirring. This mixture was refluxed at 85 ± 5 °C for 15–16 h in the presence of a few drops of concentrated HCl (the pH was 3–4). On cooling, a yellow-coloured compound precipitated out. This was filtered, washed with cold EtOH, and dried under vacuum over P₄O₁₀. Yield: ≈ 75 %; m.p. 196 °C. Anal. Calcd. for C₃₂H₂₈N₄ (FW 468): C, 83.47; H, 6.08; N, 13.91 %. Found: C, 83.52; H, 5.95; N, 13.86 %.

Synthesis of complexes

A hot ethanolic solution (20 ml) of the ligand (0.40 g, 0.0010 mol) and an ethanolic solution (20 ml) of the required metal salt ($\text{CoCl}_2 \cdot 6\text{H}_2\text{O}$, $\text{NiCl}_2 \cdot 2\text{H}_2\text{O}$ or $\text{CuCl}_2 \cdot 2\text{H}_2\text{O}$) (0.0010 mol) were mixed together under constant stirring. This reaction mixture was refluxed at 80–85 °C for 4 h. On cooling, the corresponding coloured complex separated out, which was filtered, washed and recrystallized from 50 % ethanol and dried under vacuum over P_4O_{10} .

Physical measurements

The C and H contents were determined on a Carlo-Erba 1106 elemental analyzer (C. D. R. I. Lucknow, India). The N content of the complexes was determined using the Kjeldhal method.¹³ The metal contents were determined by volumetric analysis.¹⁴ The molar conductance values were measured on an Elico (CM82T) conductivity bridge at 298 K in acetonitrile. The magnetic susceptibility values were measured at room temperature on a Gouy balance using $\text{CuSO}_4 \cdot 5\text{H}_2\text{O}$ as the calibrant. Corrections for diamagnetism were realised using Pascal constants.¹⁵ The $^1\text{H-NMR}$ spectra were recorded on a Hitachi FT-NMR model R-600 spectrometer using CDCl_3 as the solvent. The chemical shifts are given in ppm relative to tetramethylsilane. The IR spectra were recorded as KBr pellets on a FTIR Spectrum BX-II spectrophotometer. The electronic spectra were recorded in acetonitrile on a Shimadzu UV mini-1240 spectrophotometer. The EPR spectra of the complexes were recorded as polycrystalline samples in acetonitrile solution, at liquid nitrogen temperature for Co(II) and at room temperature for the Cu(II) complex using an E4 EPR spectrometer employing DPPH as the g-marker.

Antifungal screening

The *in vitro* antifungal activities of the ligand and its complexes were tested against the pathogenic fungi *Fusarium moniliformae* and *Rhizoctonia solani* using the food poison technique.^{16–20} The percent inhibition was measured according to the formula:

$$\% \text{ Inhibition} = 100(C-T)/C$$

where C and T are the radial diameter of the colony in the control and the treated, respectively.

RESULTS AND DISCUSSION

Based on elemental analyses, the complexes were assigned the compositions shown in Table I. The Co(II) and Cu(II) complexes were non-electrolytes with conductance values of 8–12 $\text{S cm}^2 \text{ mol}^{-1}$ in acetonitrile. However, the molar conductance value of the Ni(II) complex in acetonitrile was 202 $\text{S cm}^2 \text{ mol}^{-1}$, indicating a 1:2 electrolytic nature (the literature range in acetonitrile is 200–300 $\text{S cm}^2 \text{ mol}^{-1}$).²¹ Thus, these complexes may be formulated as $[\text{M}(\text{L})\text{Cl}_2]$ and $[\text{M}'(\text{L})\text{Cl}_2]$, where $\text{M} = \text{Co}(\text{II})$ or $\text{Cu}(\text{II})$ and $\text{M}' = \text{Ni}(\text{II})$, $\text{L} = 6,15\text{-dimethyl-}8,17\text{-diphenyl-}7,16\text{-dihydrodibenzo}[b,i][1.4.8.11]\text{tetraazacyclotetradecine}$.

The $^1\text{H-NMR}$ spectrum of the ligand (L) gave no signal corresponding to primary amine protons. This suggests the derivatization of carbonyl groups. A multiplet in the δ range 2.20–2.64 ppm may be attributed to the imine methyl and methylene protons of benzoyl acetone (6H, $\text{CH}_3\text{-C=N}$ and 4H, $\text{N=C-CH}_2\text{-C=N}$, respectively). Another multiplet in the δ range 7.28–7.52 ppm is assigned to aromatic ring protons.²²

TABLE I. Yield, molar conductance (Λ_M) in acetonitrile, elemental analysis data and some physical properties of the prepared complexes (L = 6,15-dimethyl-8,17-diphenyl-7,16-dihydrodibenzo[*b,i*]1.4.8.11[tetraazacyclotetradecine])

Complex	$\Lambda_M / S^1 \text{ cm}^2 \text{ mol}^{-1}$	Colour	M.p. °C	Yield %	Found (Calcd.), %			
					M	C	H	N
[Co(L)Cl ₂]	8	Shiny	278	66	9.84	64.43	4.78	9.34
C ₃₂ H ₂₈ CoN ₄ Cl ₂		pink			(9.87)	(64.32)	(4.69)	(9.38)
[Ni(L)Cl ₂]	202	Shiny	292	71	9.83	65.40	4.64	9.44
C ₃₂ H ₂₈ NiN ₄ Cl ₂		red			(9.88)	(65.34)	(4.68)	(9.39)
[Cu(L)Cl ₂]	12	Bluish	284	73	9.42	63.62	4.62	9.32
C ₃₂ H ₂₈ CuN ₄ Cl ₂		green			(9.46)	(63.83)	(4.65)	(9.30)

The IR spectrum of the free ligand exhibited no bands corresponding to a free primary diamine or a free keto group. This suggests complete condensation of the amino groups with the keto groups.²³ The bands at 1594 and 1566 cm⁻¹ were due to $\nu(\text{C}=\text{N})$ vibrations of the phenyl, and methyl, groups, respectively. The strong and sharp absorption bands appearing in the regions 2800–3049 and 1402–1466 cm⁻¹ in the spectra of all of the complexes may be due to C–H stretching and bending vibrations, respectively.²⁴ On complexation, the position of the $\nu(\text{C}=\text{N})$ band shifted by 18–34 cm⁻¹ to lower wavenumbers. This indicates coordination through the N atoms of the imine groups.²⁵

At room temperature, the Co(II) and Cu(II) complexes showed magnetic moments of 4.86 and 1.99 μ_B , corresponding to 3 and 1 unpaired electrons, respectively, while the Ni(II) complex was diamagnetic as expected for a square-planar d⁸ system²⁶ (Table II).

TABLE II. Magnetic moments at room temperature (μ_{eff}) and electronic spectral data of the complexes (L = 6,15-dimethyl-8,17-diphenyl-7,16-dihydrodibenzo[*b,i*]1.4.8.11[tetraazacyclotetradecine])

Complex	μ_{eff} / μ_B	$\lambda_{\text{max}} / \text{nm}$	$\epsilon / \text{dm}^3 \text{ mol}^{-1} \text{ cm}^{-1}$
[Co(L)Cl ₂]	4.86	830	55
		677	69
		532	90
[Ni(L)Cl ₂]	Diamagnetic	735	49
		478	87
		402	127
[Cu(L)Cl ₂]	1.99	876	52
		534	65
		356	153

The electronic spectrum of the Co(II) complex exhibited absorption bands at 830, 677 and 532 nm, which may be assigned to the transitions $^4T_{1g}(\text{F}) \rightarrow ^4T_{2g}(\text{F})$ (ν_1), $^4T_{1g} \rightarrow ^4A_{2g}$ (ν_2) and $^4T_{1g}(\text{F}) \rightarrow ^4T_{2g}(\text{P})$ (ν_3), respectively.²⁷ The Ni(II) complex displayed an electronic spectrum with transitions at 735, 478

and 402 nm. These bands may be assigned to the transitions ${}^1A_{1g} \rightarrow {}^1A_{2g}(G)$ (ν_1), ${}^1A_{1g}(D) \rightarrow {}^1B_{2g}(G)$ (ν_2) and ${}^1A_{1g}(D) \rightarrow {}^1E_g(G)$ (ν_3), respectively.²⁸ The Cu(II) complex displayed bands at 876 nm and 534 nm, which may be assigned to the transitions ${}^2B_{1g} \rightarrow {}^2A_{1g}$ ($d_{x^2-y^2} \rightarrow d_{z^2}$) (ν_1), ${}^2B_{1g} \rightarrow {}^2B_{2g}$ ($d_{x^2-y^2} \rightarrow d_{zy}$) (ν_2). The third band at around 356 nm may be due to charge transfer²⁹ (Table II).

The EPR spectrum of the Co(II) complex (Table III) was recorded as a polycrystalline sample and in acetonitrile solution at liquid nitrogen temperature (77 K). In both cases, the g -values were almost identical. The large deviation in g values from the free electron value ($g = 2.0023$) is due to a large angular momentum contribution. The EPR spectrum of the Cu(II) complex was recorded at 300 K as a polycrystalline sample and in acetonitrile solution, on the X-band at the frequency of 9.3 GHz under a magnetic field strength 3400 G. The polycrystalline spectrum showed a well-resolved anisotropically broad signal. The analysis of the spectra give g_{\parallel} 2.08–2.11 and g_{\perp} 2.02–2.08 (Table III). The trend $g_{\parallel} > g_{\perp} > 2.0023$ observed for the complex under study indicates that the unpaired electron is localized in the $d_{x^2-y^2}$ orbital of the Cu(II) ion.³⁰ Based on the spectral studies, the following geometries may be suggested for the complexes (Fig. 2).

TABLE III. EPR spectral data of the complexes (L = 6,15-dimethyl-8,17-diphenyl-7,16-dihydrodibenzo[*b,i*][1.4.8.11]tetraazacyclotetradecine)

Complex	T / K	Polycrystalline			DMSO solution	
		g_{\parallel}	g_{\perp}	g_{iso}	g_{\parallel}	g_{\perp}
[Co(L)Cl ₂]	77	2.3387	2.0174	2.1245	2.3294	2.0052
[Cu(L)Cl ₂]	298	2.1182	2.0269	2.0842	2.0834	2.0890

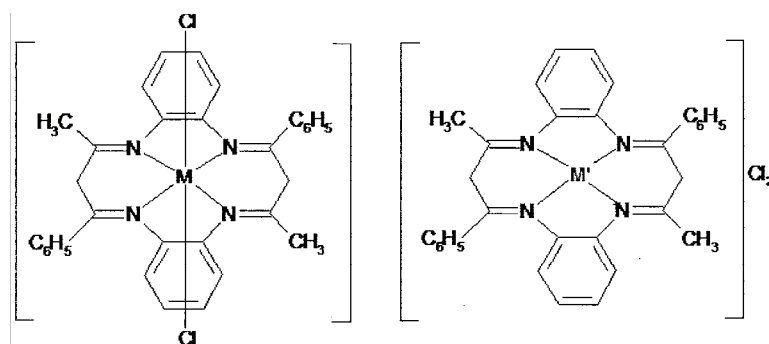


Fig. 2. Suggested geometries of the complexes, where M = Co(II) and Cu(II), and M' = Ni.

Antifungal screening

The results of the antifungal screening showed that the tested complexes exhibited higher activities than the ligand towards the inhibition of the test fungi under the *in vitro* test conditions. The minimum inhibitory concentration (MIC) of the test compounds against both fungi was 500 ppm, at which concentration

100 % inhibition was observed. The compounds showed fungal inhibition in the following order: benzoylacetone < *o*-phenylenediamine < L < Ni(II) complex < Cu(II) complex < Co(II) complex (Table IV).

TABLE IV. Fungicidal screening data of the ligand and complexes at 125 and 250 ppm concentrations after 8 days at 30±2 °C (L = 6,15-dimethyl-8,17-diphenyl-7,16-dihydrodi-benzo[*b,i*][1.4.8.11]tetraazacyclotetradecine)

Compound	Fungal inhibition, %			
	<i>F. moniliformae</i>		<i>R. solani</i>	
	125	250	125	250
Benzoylacetone	32	45	35	49
<i>o</i> -Phenylenediamine	47	59	52	61
L	54	66	56	70
[Co(L)Cl ₂]	67	82	71	83
[Ni(L)Cl ₂]	61	72	63	75
[Cu(L)Cl ₂]	63	75	68	79
Standard (mancozeb)	82	84	85	86

CONCLUSIONS

The present study revealed octahedral, square-planar and tetragonal geometry for the Co(II), Ni(II) and Cu(II) complexes, respectively. The ligand acts in a tetradentate manner coordinating through four nitrogens of the azomethine groups in an N N N N fashion. Moreover, the fungicidal data revealed that the complexes were superior to the free ligand in the inhibition of the tested fungi. It is proposed that concentration plays a vital role in increasing the degree of inhibition; the activity increased with increasing concentration of the complexes.

Acknowledgement. The authors are thankful to the DRDO, New Delhi for financial support.

ИЗВОД

СИНТЕЗА И КАРАКТЕРИСАЊЕ ТЕТРААЗА МАКРОЦИКЛИЧНОГ ЛИГАНДА И ЊЕГОВИХ КОБАЛТ(II)-, НИКЛ(II)- И БАКАР(II)- КОМПЛЕКСА

SULEKH CHANDRA,¹ MONIKA TYAGI¹ и SWATI AGRAWAL²

¹Department of Chemistry, Zakir Husain College (University of Delhi), JLN-Marg, New Delhi – 110002

²Department of Chemistry, Motilal Nehru College (University of Delhi),

Benito Juarez Road, New Delhi – 110 021, India

Синтетизовани су Co(II), Ni(II) и Cu(II) комплекси са макроцикличним лигандом са тетраденатним азотним дономом (N₄), као што је 6,15-диметил-8,17-дифенил-7,16-дихидроди-бензо[*b,i*][1.4.8.11]тетраазациклотетрадецин. Њихове структуре су одређене на основу елементалне анализе, мерења електричне моларне проводљивости и магнетне суспектибилности, као и ИЦ, ¹H-NMR (лиганд) и електронских спектра. Према аналитичким подацима и моларној електричној проводљивости, а због њихове неелектролитичке или 1:2 електролитичке природе, комплекси могу да се формулишу као [M(L)Cl₂] и [M'(L)]Cl₂ (где су M = Co(II), Cu(II) и M' = Ni(II)). На основу спектралних проучавања комплексу Co(II) приписана је октаедарска геометрија, док је за Ni(II) и Cu(II) предложена квадратно-планарна и тетра-

гонална геометрија. Испитивана је и активност синтетизованог лиганда и његових комплекса према две патогене гљивице (*Fusarium moniliformae* и *Rhizoctonia solani*) да би се утврдило њихово инхибиторско деловање.

(Примљено 18. септембра, ревидирано 7. децембра 2009)

REFERENCES

1. Q. Wang, K. Z. Tang, W. S. Liu, Y. Tang, M. Y. Tan, *J. Solid State Chem.* **182** (2009) 31
2. H. Yan Li, J. Wu, W. Huang, Y. H. Zhou, H. R. Li, Y. X. Zheng, J. L. Zuo, *J. Photochem. Photobiol.* **208A** (2009) 110
3. S. Chandra, D. Shukla, L. K. Gupta, *J. Indian Chem. Soc.* **85** (2008) 800
4. J. Yao, W. Dou, W. Liu, J. Zheng, *Inorg. Chem. Commun.* **12** (2009) 430
5. Z. H. A. El-Wahab, *J. Coord. Chem.* **43** (2009) 231
6. A. Chaudhary, N. Bansal, A. Garjraj, R. V. Singh, *J. Inorg. Biochem.* **96** (2003) 393
7. D. P. Singh, R. Kumar, V. Malik, P. Tyagi, *J. Enzyme Inhib. Med. Chem.* **22** (2007) 177
8. R. C. Sharma, R. Vats, S. Singh, S. Agarwal, *J. Inst. Chem.* **74** (2007) 119
9. Y. W. Ren, H. Guo, C. Wang, J. J. Liu, H. Jiao, J. Li, F. X. Zang, *Transition Met. Chem.* **31** (2006) 611
10. M. Salavati-Niasari, M. R. Adaryni, S. Heydarzadeh, *Transition Met. Chem.* **30** (2005) 445
11. M. Liu, W. B. Yuan, Q. Zhang, L. Yan, R. Yang, *Spectrochim. Acta* **70A** (2008) 1114
12. S. Chandra, M. Tyagi, S. Rani, S. Kumar, *Spectrochim. Acta* **75A** (2010) 835
13. I. L. Finar, *Organic Chemistry*, 6th ed., Longman Group Ltd., London, 1973, p. 4
14. V. I. Vogel, *Quantitative Inorganic Analysis*, ELBS, London, 1962, p. 536
15. R. S. Drago, *Physical Methods in Chemistry*, W. B. Saunders Co., London, 1977, p. 413
16. S. Chandra, M. Tyagi, *J. Indian Chem. Soc.* **85** (2008) 42
17. S. Chandra, M. Tyagi, *Int. J. Chem. Sci.* **7** (2009) 116
18. S. Chandra, M. Tyagi, *J. Serb. Chem. Soc.* **73** (2008) 27
19. N. K. Singh, M. K. Biyala, R. V. Singh, *Transition Met. Chem.* **29** (2004) 681
20. R. K. Agarwal, S. Prasad, *Bioinorg. Chem. Appl.* **3** (2005) 271
21. W. G. Geary, *Coord. Chem. Rev.* **7** (1971) 110
22. P. S. Kalsi, *Spectroscopy of Organic Compounds*, New Age International (P) Ltd., New Delhi, India, (1999)
23. S. Chandra, L. K. Gupta, *J. Saudi Chem. Soc.* **8** (2004) 77
24. K. Nakamoto, *Infrared Spectra of Inorganic and Coordination Compounds*, Wiley Interscience, New York, 1970
25. S. Chandra, L. K. Gupta, *Spectrochim. Acta* **60A** (2004) 3079
26. S. Chandra, L. K. Gupta, *Spectrochim. Acta* **61A** (2005) 1181
27. S. Chandra, A. Gautam, M. Tyagi, *Russ. J. Coord. Chem.* **35** (2009) 27
28. A. B. P. Lever, *Crystal Field Spectra, Inorganic Electronic Spectroscopy*, 1st ed., Elsevier, Amsterdam, 1968, p. 249
29. S. Chandra, A. Gautam, M. Tyagi, *Transition Met. Chem.* **32** (2007) 1079
30. S. Chandra, S. Raizada, M. Tyagi, P. K. Sharma, *Spectrochim. Acta* **69A** (2008) 816.



J. Serb. Chem. Soc. 75 (7) 943–950 (2010)
JSCS–4020

Cyclic conjugation in benzo-annelated triphenylenes

SVETLANA JEREMIĆ, SLAVKO RADENKOVIĆ and IVAN GUTMAN*#

Faculty of Science, University of Kragujevac, P. O. Box 60, 34000 Kragujevac, Serbia

(Received 1 December 2009)

Abstract: Cyclic conjugation in benzo-annelated triphenylenes was studied by means of the energy effect (*ef*) and the π -electron content (*EC*) of the six-membered rings. A regularity that was earlier discovered in the case of acenaphthylene and fluoranthene congeners is now shown to hold also for benzo-annelated triphenylenes: Benzenoid rings that are annelated angularly with regard to the central six-membered ring Z_0 of triphenylene increase the intensity of the cyclic conjugation in Z_0 , whereas linearly annelated benzenoid rings decrease the cyclic conjugation in Z_0 . The *ef*- and *EC*-values are strongly correlated, yet in a non-linear manner.

Keywords: cyclic conjugation; energy effect of cyclic conjugation; triphenylene; benzo-annelated triphenylene.

INTRODUCTION

Whereas benzenoid hydrocarbons have been in the focus of interest of theoretical organic chemistry for almost a whole century,^{1–3} a systematic study of the structurally closely related acenaphthylene and fluoranthene congeners have only started quite recently.⁴ (Recall that these latter polycyclic conjugated molecules differ from benzenoids by possessing one five-membered ring). In a series of recent works^{4–14} various structure-property relations for acenaphthylenes and fluoranthenes were established. The most remarkable of these seem to be the regularities found for the intensity of cyclic conjugation in the five-membered ring: benzenoid rings that are annelated angularly (resp. linearly) with regard to the five-membered ring increase (resp. decrease) the intensity of the cyclic conjugation in it. These, so-called PCP- and linear rules, were first recognized within studies of the energy effects (*ef*) of the individual rings,^{6–8,10} but were eventually corroborated by several independent theoretical approaches.^{9,12–14} It was shown that fully analogous regularities hold for acenaphthylene and fluoranthene analogs, in which instead of a 5-membered ring, there is some other odd-membered ring.¹⁵

* Corresponding author. E-mail: gutman@kg.ac.rs

Serbian Chemical Society member.

doi: 10.2298/JSC091201068J

Bearing the above in mind, the obvious question that emerges is whether there similar regularities exist also for ordinary benzenoid hydrocarbons. The aim of this work was to provide an answer. In order to arrive at clear and conclusive results, the class of benzo-annelated triphenylenes (*cf.* Fig. 1) was chosen for study.

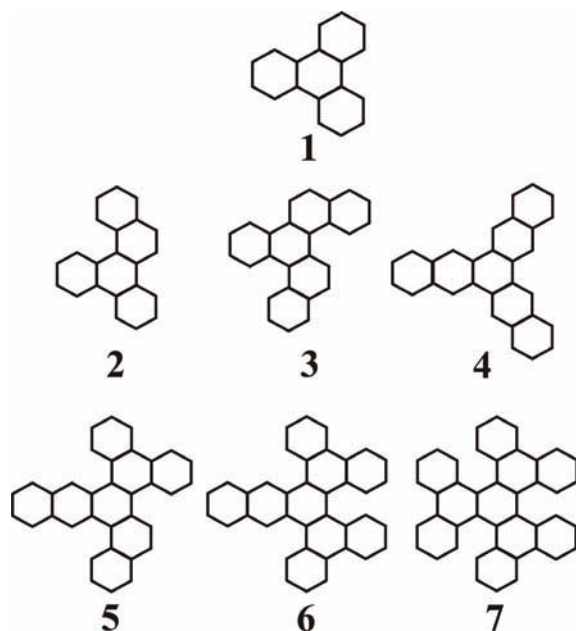


Fig 1. Triphenylene (**1**) and some of its benzo-annelated derivatives: **2–7** are examples of mono-, di-, tri-, tetra-, penta-, and hexa-benzo annelated species. There are 2, 7, 10, 7, 2, and 1 distinct, symmetry-non-equivalent, mono-, di-, tri-, tetra-, penta-, and hexa-benzo-triphenylene isomers, *cf.* Table 1.

TRIPHENYLENE AND ITS BENZO-ANNELATED DERIVATIVES

The reason for considering cyclic conjugation in triphenylene and its benzo-annelated derivatives is the following. First of all, the members of this class of benzenoid hydrocarbons are stable, easy-to-synthesize compounds, most of which have been known for a long time.^{16,17} All members of this class have a central six-membered ring (denoted by Z_0), surrounded by three disjoint six-membered rings. To these latter rings, one or more benzene rings are annelated, each either in an angular or in a linear constellation with regard to Z_0 (*cf.* Fig. 2). In all benzo-annelated triphenylenes, the manner in which the central ring Z_0 is attached to its neighbors is exactly the same. Therefore, the very strong first-neighbor effects^{18,19} on the cyclic conjugation in Z_0 are equal in all members of the class considered, and thus may be disregarded.

Throughout this paper, an abbreviated naming of the benzo-annelated triphenylenes is employed. In Fig. 3, it is shown how the carbon-carbon bonds of triphenylene are labeled by a_1 – a_6 (for angular annelation), and by l_1 – l_3 (for linear annelation). Then, the structure of a benzo-annelated triphenylene is determined by indicating the sites of annelation. For instance, compounds **2–7**, depicted in

Fig. 1, are coded as a_1 , a_2a_4 , $l_1l_2l_3$, $a_1a_2a_4l_3$, $a_1a_2a_3a_4l_3$ and $a_1a_2a_3a_4a_5a_6$, respectively.

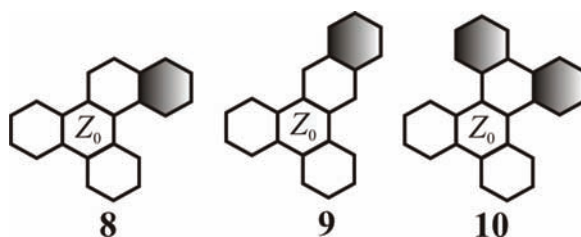


Fig. 2. Types of benzo-annulation: angular (8), linear (9), and geminal (10).

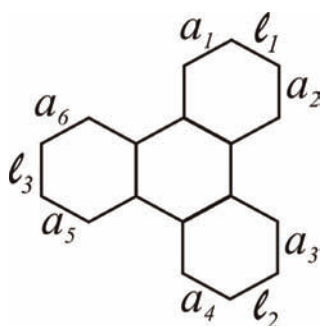


Fig. 3. Labeling of the sites of triphenylene used for denoting its benzo-annulated derivatives; for details, see text.

QUANTIFYING THE CYCLIC CONJUGATION IN A RING

A variety of theoretical methods has been proposed for assessing the intensity of cyclic conjugation in individual rings of a polycyclic conjugated molecule.^{1,2} In this work, the molecular-orbital-based energy effect (ef) and the Kekulé-structure-based π -electron content (EC) are applied. The former method was conceived already in the 1970s^{20–22} and eventually much applied. For details of the ef -method, see the review²³ and the recent works.^{6–8,10,14,15,24–28} The idea of using Kekulé structures for distributing the π -electrons of a polycyclic conjugated molecule into its rings was suggested by Randić and Balaban²⁹ in 2004, and then elaborated and applied in numerous papers.^{30–38} As will be seen in the subsequent section, in the case of benzo-annulated triphenylenes, the ef - and EC -values are strongly correlated, which confirms that they measure one and the same physico-chemical property of the underlying rings.

NUMERICAL WORK

Using in-house software, the energy effects and π -electron contents of all six-membered rings of triphenylene and all its benzo-annulated congeners were calculated. In Table I are given the (for this study most important) ef - and EC -values of the central ring Z_0 . The numerical values of the other energy effects and π -electron contents can be obtained from the authors upon request.

TABLE I. Energy effects (ef) and π -electron contents (EC) of the central ring Z_0 of triphenylene (**1**) and its benzo-annelated derivatives. The benzo-annelated species are labeled according to Fig. 3

Molecule	$ef(Z_0)$	$EC(Z_0)$
1	0.0242	2.0000
a_1	0.0304	2.2857
l_1	0.0204	1.6923
a_1a_2	0.0360	2.5000
a_1a_3	0.0390	2.5909
a_1a_4	0.0390	2.5909
a_2a_3	0.0389	2.5909
l_1a_3	0.0249	1.9500
l_1a_4	0.0249	1.9500
l_1l_2	0.0179	1.4211
$a_1a_2a_3$	0.0466	2.8158
$a_1a_2a_4$	0.0467	2.8158
$a_1a_3a_5$	0.0511	2.9143
$a_1a_3a_6$	0.0510	2.9143
$a_1a_2l_2$	0.0289	2.1471
$a_1a_3l_3$	0.0310	2.2258
$a_1a_4l_3$	0.0310	2.2258
$a_2a_3l_3$	0.0309	2.2258
$a_1l_2l_3$	0.0212	1.6552
$l_1l_2l_3$	0.0161	1.1786
$a_1a_2a_3a_4$	0.0562	3.0455
$a_1a_2a_3a_5$	0.0616	3.1475
$a_1a_2a_3a_6$	0.0615	3.1475
$a_1a_2a_4a_5$	0.0617	3.1475
$a_1a_2a_3l_3$	0.0364	2.4340
$a_1a_2l_2a_5$	0.0365	2.4340
$a_1a_2l_2l_3$	0.0242	1.8367
$a_1a_2a_3a_4a_5$	0.0748	3.3832
$a_1a_2a_3a_4l_3$	0.0432	2.6484
$a_1a_2a_3a_4a_5a_6$	0.0910	3.6190

What first requires checking is whether the ef - and EC -values yield consistent results. That this is indeed the case can be seen from Fig. 4; although not linear, the correlation between ef and EC is remarkably good and, of course, positive. This means that the (stabilizing) energy effect of the cyclic conjugation is proportional to the amount of π -electrons in the underlying ring. In other words, both ef and EC indicate to the same regularities for the structure-dependency of cyclic conjugation in the central ring of triphenylene congeners; these regularities are discussed in due detail in the subsequent section.

The correlation between the ef - and EC -values of the annelated benzenoid rings is shown in Fig. 5. Here the data points lie on three nearly parallel lines, each line pertaining to one of the three annelation modes shown in Fig. 2. Such a clustering of the data-points was expected, in view of the results of earlier investigations.^{35,36}

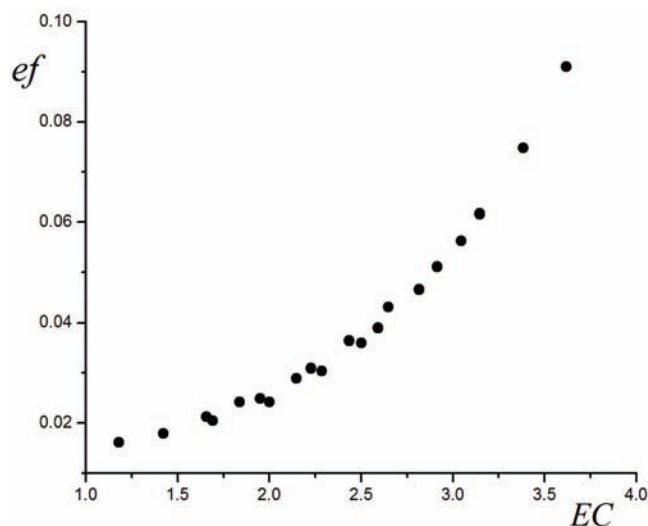


Fig. 4. The energy effect (ef) of the central ring Z_0 of triphenylene congeners vs. its π -electron content (EC).

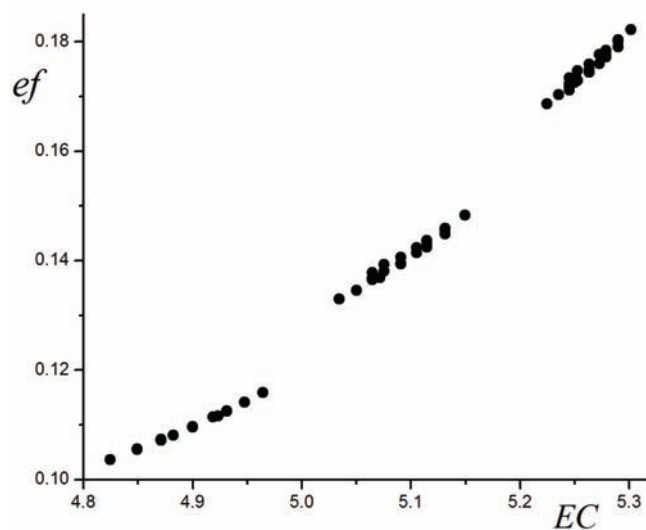


Figure 5. The energy effects (ef) of the annelated marginal rings of triphenylene congeners vs. their electron contents (EC). The clustering of the data points reflects the three modes of annelation (*cf.* Fig. 2): linear (lower line), angular (middle line), and geminal (upper line).

RESULTS AND DISCUSSION

The data collected in Table I clearly, and without a single exception, confirm the validity of the following regularities.

Rule 1 (angular effect)

Six-membered rings annelated in an angular mode (*cf.* Fig. 2) increase both the energy effect and the π -electron content of the central ring. The larger the number of angularly annelated six-membered rings is, the greater are the *ef*- and *EC*-values.

Examples. The *ef*-values of triphenylene and its a_1 , a_1a_3 , and $a_1a_3a_5$ derivatives are 0.0242, 0.0304, 0.0390, and 0.0511, respectively; the *EC*-values of the same species are 2.0000, 2.2857, 2.5909, and 2.9143, respectively.

Rule 2 (linear effect)

Six-membered rings annelated in a linear mode (*cf.* Fig. 2) decrease both the energy effect and the π -electron content of the central ring. The larger the number of linearly annelated six-membered rings is, the smaller are the *ef*- and *EC*-values.

Examples. The *ef*-values of triphenylene and its l_1 , l_1l_2 , and $l_1l_2l_3$ derivatives are 0.0242, 0.0204, 0.0179, and 0.0161, respectively; the *EC*-values of the same species are 2.0000, 1.6923, 1.4211, and 1.1786, respectively.

As a consequence of Rules 1 and 2, the minimal and maximal *ef*-values are found for the $l_1l_2l_3$ and $a_1a_2a_3a_4a_5a_6$ species, equal to 0.0161 and 0.0910, respectively. The corresponding *EC*-values are 1.1786 and 3.6190, also minimal and maximal.

Rule 3

The effect of a geminally annelation (*cf.* Fig. 2) is slightly weaker than the effect of two six-membered rings attached to different hexagons.

Examples. $ef(a_1a_2) = 0.0360$ whereas $ef(a_1a_3) = 0.0390$; $EC(a_1a_2) = 2.5000$ whereas $EC(a_1a_3) = 2.5909$, $ef(a_1a_2l_3) = 0.0289$ whereas $ef(a_1a_3l_3) = 0.0310$; $EC(a_1a_2l_3) = 2.1471$ whereas $EC(a_1a_3l_3) = 2.2258$.

If an equal number of angularly and linearly annelated marginal benzenoid rings are present, then their effect on the cyclic conjugation roughly cancels out. For example, $ef(a_2l_2) = 0.0249$ and $ef(a_1a_2l_2l_3) = 0.0242$, as compared with $ef = 0.0242$ for the parent triphenylene. Similarly, $EC(a_2l_2) = 1.9500$ and $EC(a_1a_2l_2l_3) = 1.8367$, which are nearly equal to $EC = 2.0000$ for triphenylene.

Rule 4 (isoarithmicity)

The energy effect and the π -electron content depend on the number of angularly and linearly annelated benzenoid rings, but are insensitive to their actual position. The respective *ef*-values are nearly equal, whereas the *EC*-values are strictly equal.

Examples. $ef(a_1a_3) = 0.0390$, $ef(a_1a_4) = 0.0390$, $ef(a_2a_3) = 0.0389$, and $EC(a_1a_3) = EC(a_1a_4) = EC(a_2a_3) = 2.5909$. Similarly, $ef(a_1a_3l_3) = 0.0310$,

$ef(a_1a_4l_3) = 0.0310$, $ef(a_2a_3l_3) = 0.0309$, and $EC(a_1a_3l_3) = EC(a_1a_4l_3) = EC(a_2a_3l_3) = 2.2258$.

Additional examples illustrating the above Rules 1–4 can be envisaged by inspecting the data in Table I. For more details on the concept of isoarithmicity,³⁹ see a recent article.⁸

As a final remark, it should be mentioned that with present-day knowledge, it can be seen that the results obtained in an earlier work,⁴⁰ in which benzo-derivatives of perylene were examined, are tantamount to Rule 1. In the time when the work⁴⁰ was created, this fact was been recognized.

Acknowledgement. The authors thank the Ministry of Science and Technological Development of the Republic of Serbia for partial support of this work, through Grant No. 144015G.

ИЗВОД

ЦИКЛИЧНА КОНЈУГАЦИЈА У БЕНЗО-АНЕЛИРАНИМ ТРИФЕНИЛЕНИМА

СВЕТЛАНА ЈЕРЕМИЋ, СЛАВКО РАДЕНКОВИЋ И ИВАН ГУТМАН

Природно–математички факултет Универзитета у Крагујевцу

Циклична конјугација у бензо-анелираним трифениленима проучавана је помоћу енергетског ефекта (ef) и π -електронског садржаја (EC) шесточланих прстенова. Показано је да једна правилност, раније откривена код једињења аценафтиленског и флуорантенског типа, важи и у случају анелираних трифенилена: Бензеноидни прстен који је анелиран ангуларно у односу на централни шесточлани прстен Z_0 трифенилена, појачава интензитет цикличне конјугације у Z_0 , док линеарно анелирани бензеноидни прстен умањује цикличну конјугацију у Z_0 . Нађено је да постоји добра корелација између ef и EC , иако корелација није линеарна.

(Примљено 1. децембра 2009)

REFERENCES

1. I. Gutman, S. J. Cyvin, *Introduction to the Theory of Benzenoid Hydrocarbons*, Springer-Verlag, Berlin, 1989
2. M. Randić, *Chem. Rev.* **103** (2003) 3449
3. A. T. Balaban, P. V. R. Schleyer, H. S. Rzepa, *Chem. Rev.* **105** (2005) 3436
4. I. Gutman, J. Đurđević, *MATCH Commun. Math. Comput. Chem.* **60** (2008) 659
5. J. Đurđević, S. Radenković, I. Gutman, *J. Serb. Chem. Soc.* **73** (2008) 989
6. I. Gutman, J. Đurđević, A. T. Balaban, *Polycyclic Arom. Comp.* **29** (2009) 3
7. J. Đurđević, I. Gutman, J. Terzić, A. T. Balaban, *Polycyclic Arom. Comp.* **29** (2009) 90
8. A. T. Balaban, J. Đurđević, I. Gutman, *Polycyclic Arom. Comp.* **29** (2009) 185
9. J. Đurđević, I. Gutman, R. Ponec, *J. Serb. Chem. Soc.* **74** (2009) 549
10. I. Gutman, J. Đurđević, *J. Serb. Chem. Soc.* **74** (2009) 765
11. I. Gutman, J. Đurđević, S. Radenković, A. Burmudžija, *Indian J Chem.* **37A** (2009) 194
12. S. Radenković, J. Đurđević, I. Gutman, *Chem. Phys. Lett.* **475** (2009) 289
13. J. Đurđević, S. Radenković, I. Gutman, S. Marković, *Monatsh. Chem.* **140** (2009) 1305
14. A. T. Balaban, T. K. Dickens, I. Gutman, R. B. Mallion, *Croat. Chem. Acta*, accepted
15. I. Gutman, S. Jeremić, V. Petrović, *Indian J. Chem.* **48A** (2009) 658

16. E. Clar, *Polycyclic Hydrocarbons*, Academic Press, London, 1964
17. J. R. Dias, *Handbook of Polycyclic Hydrocarbons. Part A. Benzenoid Hydrocarbons*, Elsevier, Amsterdam, 1987
18. I. Gutman, *Rep. Mol. Theory* **1** (1990) 115
19. I. Gutman, B. Furtula, S. Jeremić, N. Turković, *J. Serb. Chem. Soc.* **70** (2005) 1199
20. I. Gutman, S. Bosanac, *Tetrahedron* **33** (1977) 1809
21. J. Aihara, *J. Am. Chem. Soc.* **99** (1977) 2048
22. W. C. Herndon, *J. Am. Chem. Soc.* **104** (1982) 3541
23. I. Gutman, *Monatsh. Chem.* **136** (2005) 1055
24. I. Gutman, S. Stanković, J. Đurđević, B. Furtula, *J. Chem. Inf. Model.* **47** (2007) 776
25. I. Gutman, S. Stanković, *Monatsh. Chem.* **139** (2008) 1179
26. I. Gutman, J. Đurđević, B. Furtula, B. Milivojević, *Indian J. Chem.* **47A** (2008) 803
27. I. Gutman, B. Furtula, *Polycyclic Arom. Comp.* **28** (2008) 136
28. A. T. Balaban, J. Đurđević, I. Gutman, *Polycyclic Arom. Comp.* **29** (2009) 185
29. M. Randić, A. T. Balaban, *Polycyclic Arom. Comp.* **24** (2004) 173
30. A. T. Balaban, M. Randić, *J. Chem. Inf. Comput. Sci.* **44** (2004) 50
31. A. T. Balaban, M. Randić, *New J. Chem.* **28** (2004) 800
32. A. T. Balaban, M. Randić, *J. Chem. Inf. Comput. Sci.* **44** (2004) 1701
33. I. Gutman, T. Morikawa, S. Narita, *Z. Naturforsch.* **59a** (2004) 295
34. A. T. Balaban, M. Randić, *J. Math. Chem.* **37** (2005) 443
35. B. Furtula, I. Gutman, N. Turković, *Indian J. Chem.* **44A** (2005) 9
36. I. Gutman, S. Milosavljević, B. Furtula, N. Cmiljanović, *Indian J. Chem.* **44A** (2005) 13
37. A. T. Balaban, M. Randić, *New J. Chem.* **32** (2008) 1071
38. S. Stanković, J. Đurđević, I. Gutman, R. Milentijević, *J. Serb. Chem. Soc.* **73** (2008) 547
39. A. T. Balaban, *MATCH Commun. Math. Comput. Chem.* **24** (1989) 29
40. I. Gutman, N. Turković, J. Jovičić, *Monatsh. Chem.* **135** (2004) 1389.



J. Serb. Chem. Soc. 75 (7) 951–963 (2010)
JSCS–4021

Synthesis and characterization of ammonium phosphate fertilizers with boron

ANGELA MAGDA^{1*}, RODICA PODE¹, CORNELIA MUNTEAN¹,
MIHAI MEDELEANU¹ and ALEXANDRU POPA²

¹Faculty of Industrial Chemistry and Environmental Engineering, "Politehnica" University of Timișoara, Victoria Square 2, 300006 Timișoara and ²Institute of Chemistry Timișoara of the Romanian Academy, M. Viteazul Ave, 24, 300223-Timișoara, Romania

(Received 28 February 2009, revised 26 April 2010)

Abstract: The concentration of boron, an essential micronutrient for plants, presents a narrow range between deficiency and toxicity. In order to provide the boron requirement for plants, and to avoid toxicity problems, boron compounds are mixed with basic fertilizers. Sodium borate pentahydrate was used as a boron source. Ammonium orthophosphates fertilizers with boron were prepared by neutralizing phosphoric acid with ammonia and addition of variable amounts of sodium tetraborate pentahydrate to the reaction mixture at a $\text{NH}_3:\text{H}_3\text{PO}_4$ molar ratio of 1.5. The fertilizers obtained with boron contents ranging from 0.05 to 1 % (w/w) were fully characterized by chemical analysis, thermal analysis, X-ray diffraction and infrared spectrophotometry. The studies showed that up to 500 °C, regardless of the boron content, no significant changes concerning thermal stability and nutritional properties occurred. Above 500 °C, an increase of thermal stability with an increase of the boron content was observed. X-Ray diffraction of a heat-treated sample containing 5 % (w/w) boron indicated the appearance of boron orthophosphate, BPO_4 , as a new crystalline phase, and the disappearance of the previous structures above 500 °C, which explains the increase in thermal stability.

Keywords: sodium borate pentahydrate; fertilizer; micronutrient; diammonium hydrogen phosphate; ammonium dihydrogen phosphate; boron orthophosphate.

INTRODUCTION

Boron is an essential micronutrient for all vascular plants. Boron deficiency causes rapid biochemical, physiological and anatomical aberrations. It is very important to maintain a continuous supply of boron for efficient agricultural production.^{1–5} Boron has restricted mobility in many plants and is freely mobile in others. In the majority of plant species, the boron distribution between plant or-

* Corresponding author. E-mail: angela.magda@gmail.com
doi: 10.2298/JSC090228064M

gans indicates a restricted transport of boron. Thus, symptoms of boron deficiency occur mainly in the growing organs of plants. On the other hand, boron is highly mobile in some plants.⁶ For example, under similar soil conditions, pistachio contains the highest boron concentration in the leaves and the lowest in fruit and seeds (leaf 130, hull 33, shell 2 and kernel 1 ppm/dry product). This indicates that boron is not transported from the leaves to the fruit and seeds. Unlike pistachio, apple trees grown under same conditions have the highest boron concentrations in the hull (51 ppm/dry product) and fruit (54 ppm/dry product), and lower boron concentration in the leaves (41 ppm/dry product) and shell (34 ppm/dry product).

The concentration of boron in leaves of different ages on the same plant provides evidence of boron mobility in plants. Thus, a higher boron concentration in older (basal) leaves than younger (apical) leaves indicates a restricted transport of boron. For example in tomato, the boron concentration (ppm/dry product) is 721 in basal leaves, 318 in middle and 94 in apical leaves. In contrast, higher boron concentration in younger leaves indicates boron mobility. For example in apple trees, boron concentration (ppm/dry product) in basal leaves is 50, middle leaves 56 and apical leaves 70.

Correction of boron deficiency is affected by boron mobility or immobility in plants. Boron is applied directly to developing tissues, such as flowers, in order to ensure an adequate boron supply during the time of their development. On the other hand, foliar sprays can be applied to boron-mobile species at any time when functional leaves are present. The applied boron corrects current deficiencies, and assures boron supply to future developing flowers and fruit tissues.⁷

Boron is required in small amounts. In order to maintain the recommended application rate, boron compounds are mixed with a basic fertilizer.^{3,8} A very efficient boron-containing fertilizer, boron phosphate, BPO_4 , when incorporated into soil, slowly releases soluble boron over a period of time corresponding at least to the critical uptake period of the usual crop. BPO_4 is not soluble in water; hence, there is no possibility of rainfall washing it from the soil.⁹

In the present study, ammonium phosphates with a variable boron content ranging from 0.1 to 1 % (w/w) were prepared by neutralizing phosphoric acid with ammonia and introducing sodium borate pentahydrate in variable amounts into the reaction mixture. In connection with a previous report,¹⁰ in order to obtain heat-resistant fertilizers which undergo a minimum loss of ammonia, sodium borate was added to the reaction mixture at 1.5 $NH_3:H_3PO_4$ molar ratio. The pH of the reaction mixture was proved to be the controlling parameter of the neutralization process.^{10,11} Thus, the dependence of pH on the $NH_3:H_3PO_4$ molar ratio was monitored. In addition, a boron free sample was prepared under the same conditions.

The objective of the present study was to examine to what extent the thermal and nutritive properties of boron-containing fertilizers are affected by changing the amount of sodium borate pentahydrate added to the reaction mixture. Consequently, the dried products were fully characterized by chemical analysis, thermal analysis, X-ray diffraction analysis and infrared spectroscopy. Another objective of the study was to investigate the possible formation of new chemical compounds of boron with phosphates from the system. With this end in view, an additional product containing a larger amount of boron (5 % w/w) was prepared.

EXPERIMENTAL

All employed reagents were of analytical grade. Volumes of 50 mL phosphoric acid, 43.5 % P_2O_5 (obtained from Merck phosphoric acid, 64.47 % w/w P_2O_5 , with a minimum purity of 99 % w/w) were neutralized with a 25 % ammonia solution ("Reactivul" – București, with a minimum purity of 99 %) under continuous stirring at 20 °C up to a pH of about 8.0. Crystalline sodium tetraborate pentahydrate (Merck, with a minimum purity of 99.8 % $Na_2B_4O_7$) was added in variable quantities to the reaction mixture at a 1.5 $NH_3:H_3PO_4$ molar ratio. The fertilizers obtained were dried at 60 °C. During the neutralization process with the addition of sodium tetraborate pentahydrate, the dependence of the pH of the reaction mass on the molar ratio $NH_3:H_3PO_4$ was measured using a Denver instrument 250 pH-meter.

The P_2O_5 content in the dried products was determined by gravimetric analysis.¹² The gravimetric determination of phosphorus was accomplished by its precipitation as magnesium ammonium phosphate hexahydrate $MgNH_4PO_4 \cdot 6H_2O$ using a magnesium mixture as the precipitation reagent (55 g $MgCl_2$ + 70 g NH_4Cl dissolved in 250 cm³ of a 10 % ammonia solution). The precipitate was converted by calcination at 1000 °C into magnesium pyrophosphate $Mg_2P_2O_7$ and weighed in that form. The nitrogen in the ammonia was determined by spectrophotometric analysis in the presence of Nessler reagent ($\lambda = 425$ nm)¹³ and the boron content was determined by spectrophotometric analysis with Carmine Acid reagent ($\lambda = 630$ nm).^{14,15} UV-Vis Spectra were recorded on a Cary 50 spectrophotometer.

Thermogravimetric, TG, and differential TG, DTG, curves were obtained on a computer controlled Netzsch TG 209 apparatus with a K(NiCr-Ni) thermocouple, in a platinum crucible, at a linear heating rate of 10 °C min⁻¹, in the temperature range 20–990 °C, under a dynamic atmosphere (nitrogen, 5 mL min⁻¹), on samples of about 10 mg.

X-Ray powder diffraction patterns were recorded on a Bruker D8 Advance diffractometer, in Bragg-Brentano geometry, with graphite monochromatized $CuK-\alpha$ ($\lambda = 1.5418$ Å) radiation.

The infrared spectra in KBr matrix were run on a Jasco 410 spectrophotometer in the wave number range 4000–400 cm⁻¹.

The sample containing 5 % boron was calcined for 2 h at 500 °C in a Nabertherm oven with a heating rate of 10 °C min⁻¹.

RESULTS AND DISCUSSION

The following samples were obtained through the neutralization of phosphoric acid with ammonia solution and sodium tetraborate pentahydrate addition to the reaction system:

- sample 1, with 0.05 % boron;
- sample 2, with 0.1 % boron;

- sample 3, with 0.5 % boron;
- sample 4, with 1 % boron;
- sample 5, with 5% boron and
- sample 6, without boron.

The boron content was expressed as g boron/100 g diammonium hydrogen phosphate.

Dependency of the pH of the reaction system on the $\text{NH}_3:\text{H}_3\text{PO}_4$ molar ratio

The pH of the reaction mixture was measured during the preparation of samples 1–4. The dependency of the pH of the reaction mixture on the $\text{NH}_3:\text{H}_3\text{PO}_4$ molar ratio is shown in Fig. 1.

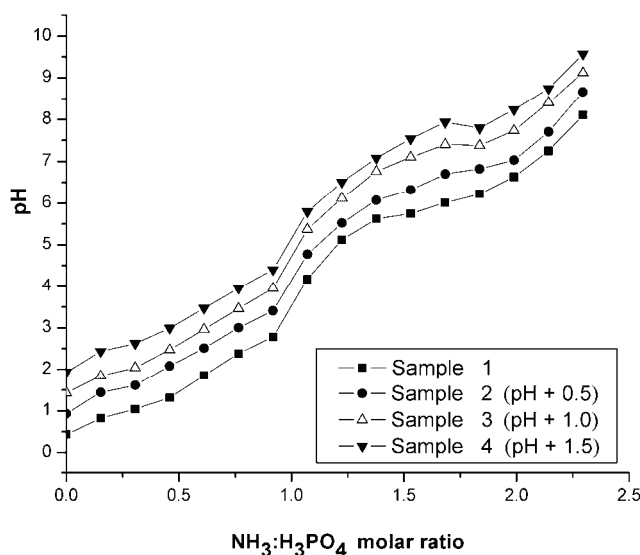


Fig. 1. Dependency of the pH on the $\text{NH}_3:\text{H}_3\text{PO}_4$ molar ratio during the synthesis of samples 1–4.

The curves shown in Fig. 1 have similar profiles. The pH values corresponding to similar $\text{NH}_3:\text{H}_3\text{PO}_4$ molar ratios were very similar for the 4 samples. In order to distinguish the curves and to obtain a higher accuracy of the figure, the experimental pH values corresponding to samples 2–4 were offset 0.5, 1, and 1.5 pH-units, respectively. Each curve has two inflection points corresponding to completion of ammonium dihydrogen phosphate (ADP), and diammonium hydrogen phosphate (DHP) formation. The experimental pH values and the $\text{NH}_3:\text{H}_3\text{PO}_4$ molar ratio corresponding to the inflections points are given in Table I.

The pH value and the $\text{NH}_3:\text{H}_3\text{PO}_4$ molar ratio corresponding to the first inflection point are similar for each neutralization curve. This was also the case for the second inflection point. Consequently, up to a limit of 1 % B in the final

product, the neutralization process was not significantly influenced by the addition of sodium tetraborate pentahydrate to the reaction mixture.

TABLE I. $\text{NH}_3:\text{H}_3\text{PO}_4$ molar ratio and pH values at the inflection points of the pH vs. $\text{NH}_3:\text{H}_3\text{PO}_4$ molar ratio curves during the synthesis of samples 1–4

Sample	Inflection point 1		Inflection point 2	
	$\text{NH}_3:\text{H}_3\text{PO}_4$ molar ratio	pH	$\text{NH}_3:\text{H}_3\text{PO}_4$ molar ratio	pH
1	1	3.56	1.84	6.40
2	1	3.66	1.84	6.40
3	1	3.67	1.82	6.33
4	1	3.68	1.85	6.53

Chemical composition

The chemical composition of samples 1–4 are given in Table II.

The $\text{N}:\text{P}_2\text{O}_5$ mass ratio, corresponding to the samples 1–4, ranges from 0.38 to 0.39. Thus, in accordance with literature data,^{10,11,16} a DHP and ADP mixture is obtained. The addition of sodium tetraborate up to a limit of 1% (w/w) boron in the final product did not significantly change the content of macronutrients N and P in the products obtained.

TABLE II. The chemical composition of samples 1–4

Sample	P_2O_5 Content, %	$\text{N}-\text{NH}_4$ Content, %	Mass ratio $\text{N}:\text{P}_2\text{O}_5$	Boron content, %
1	52.3	20	0.38	0.07
2	50.5	19.9	0.39	0.1
3	50.3	19	0.38	0.5
4	49.4	19.1	0.38	0.9

Thermal analysis

The thermogravimetric curves (TG and DTG) obtained by heating samples 1–4 from 20 to 990 °C at a heating rate of 10 °C min^{-1} are shown in Figs. 2–5, respectively.

TG and DTG analysis showed that the thermal decomposition of sample 2–4 began at 30 °C and proceeded up to about 990 °C. The DTG curves showed four processes associated with mass loss. Sample 1 was relatively stable up to 65 °C. Above this temperature, thermal decomposition proceeded up to about 900 °C. The mass losses of samples 1–4 and the corresponding temperature ranges are shown in Table III in comparison to similar data obtained by heating sample 6 (ammonium phosphate without boron) in the same temperature range.¹¹

The first process with mass loss (samples 2–4), observed within the temperature range 30–65 °C was assigned to the partial dehydration of sodium borate pentahydrate; the mass loss increased with increasing boron content. No ammonia was released; hence the nutritional properties of the obtained fertilizers were not affected. Sample 1 was stable up to 65 °C.

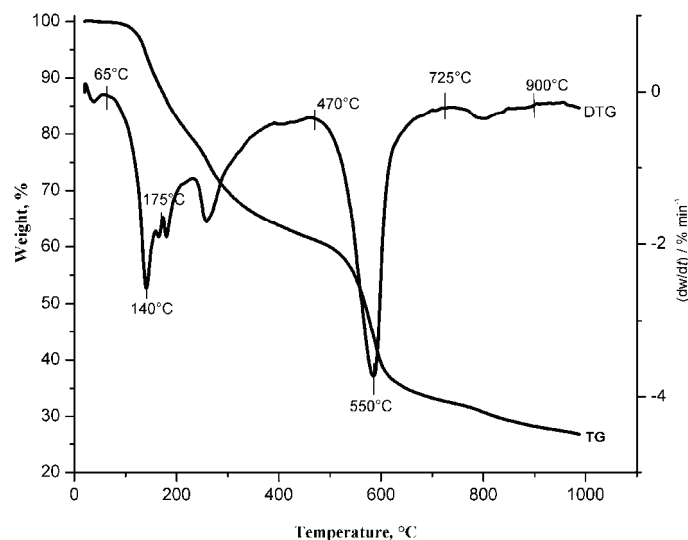


Fig. 2. Thermal gravimetric curves (TG and DTG) of sample 1.

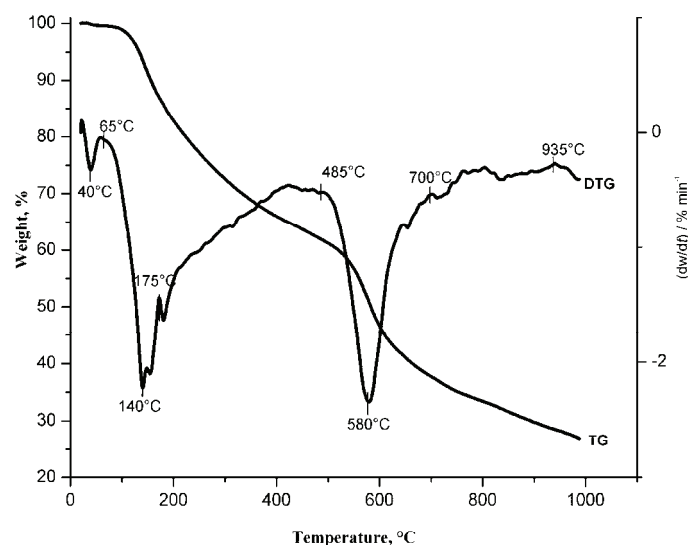


Fig. 3. Thermal gravimetric curves (TG and DTG) of sample 2.

The second process with mass loss (samples 1–4) occurred from 65 °C up to around 500 °C and developed in two stages. In the first stage, the mass loss was assigned to DHP decomposition with ammonia release and ADP formation (reaction (1)). In the second stage, the mass loss was assigned to the decomposition of ADP to ammonium metaphosphate, according to equations 2 and 3, which is in agreement with literature data,^{17,18} and to the liberation of constitution water during polycondensation processes.^{19,20} The TG curves showed continuous mass

loss; thus, the processes occurred in a very complex manner, which could not be separated into individual reactions:

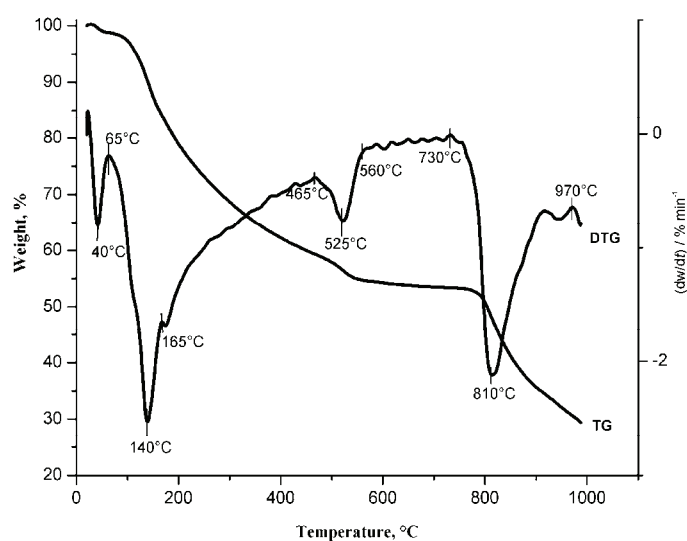
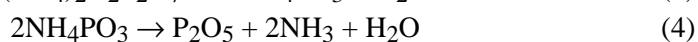
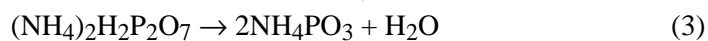
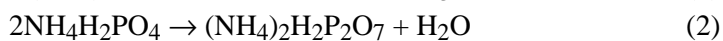
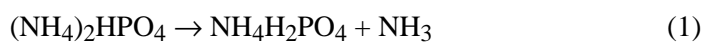


Fig. 4. Thermal gravimetric curves (TG and DTG) of sample 3.

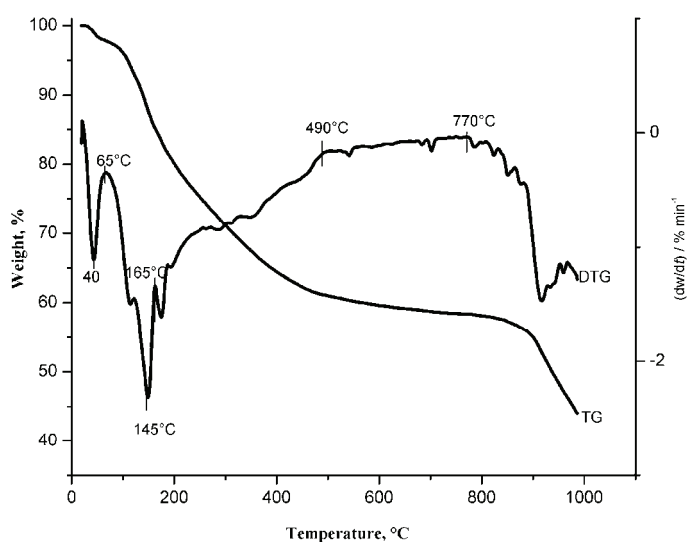


Fig. 5. Thermal gravimetric curves (TG and DTG) of sample 4.

TABLE 3. Mass losses on heating for samples 1–4, 6

Sample	Temp. range °C	Mass loss %	Temp. range °C	Mass loss %	Temp. range °C	Mass loss %	Temp. range °C	Mass loss %	Final residue %
1	30–65	–	65–470	39	470–725	28	725–900	4.7	27
2	30–65	0.13	65–485	38	485–700	24.5	700–935	8.5	27
3	30–65	0.44	65–465	40	465–560	4.2	730–970	22.7	29.5
4	30–65	0.87	65–490	37	490–770	–	770–990	14	44
6	30–65	–	65–490	37	490–700	43	750–850	5	12.5

On the DTG curve of sample 1 (Fig. 2), an endothermic peak at about 250 °C appears, which could be assigned to the mass loss described by reaction (2), which was particularly separated from the other processes.

Up to about 500 °C, the thermal behavior of samples 1–4 was not influenced by the addition of sodium tetraborate. The boron-containing samples underwent similar mass losses (ammonia nitrogen) within similar temperature ranges as those for the boron-free sample 6.

Consequently, on processing the obtained fertilizers up to 500 °C, their nutritional properties were not affected by the addition of boron, in comparison with the ammonium phosphates without boron.

The third process with mass loss occurred in the temperature interval from around 500 up to around 700 °C. The mass loss, assigned to sublimation of P₂O₅, decreased with increasing content of boron. The mass loss of the boron-free sample 6 within 490 and 700 °C was 43 %. Sample 1 lost 28 % mass between 470 and 725 °C, the mass loss of sample 2 within the temperature range 485–700 °C was 24.5 %. Sample 3 lost only 4.2 % mass between 465 and 560 °C, while between 560 and 730 °C no mass loss was registered. Sample 4 was stable within 490 and 770 °C, the decomposition processes were shifted towards higher temperatures.

The fourth process with mass loss occurred on further heating of samples 1–4 up to 990 °C. An increase of mass loss with increasing boron content was observed. The mass loss was assigned to the decomposition of the polycondensation products.^{19,20} The completion of the decomposition process was shifted towards higher temperatures from sample 1 to sample 3. The decomposition of sample 4 was not completed at 990 °C.

Increasing the boron content resulted in an increase of the thermal stability of the obtained fertilizers at temperatures above 500 °C.

X-Ray diffraction

The X-ray diffraction patterns of samples 1, 3 and 4 together with that of sample 6 (ammonium phosphate without boron)¹¹ for comparison are given in Fig. 6.

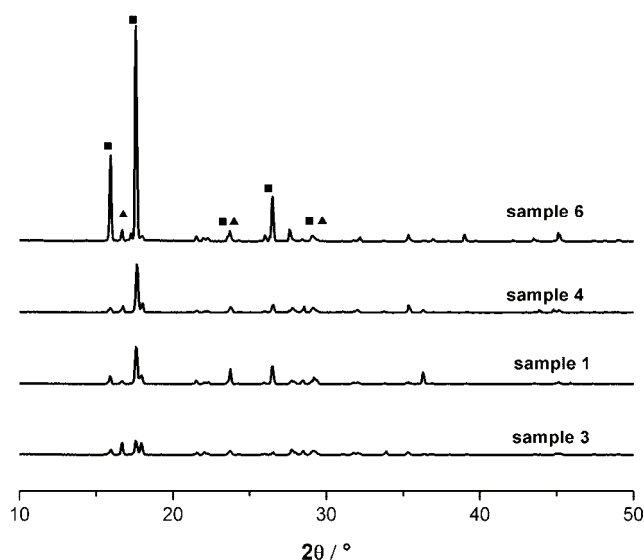


Fig. 6. X-Ray diffraction pattern of samples 1, 3, 4 and 6; ■ – $(\text{NH}_4)_2\text{HPO}_4$; ▲ – $\text{NH}_4\text{H}_2\text{PO}_4$.

Two crystalline phases were detected in all the three boron-containing samples: monoclinic diammonium hydrogen phosphate²¹ and tetragonal ammonium dihydrogen phosphate.²²

Regardless of the boron content, no new crystalline phases could be detected by X-ray diffraction in any of the three samples. Therefore, ammonium phosphate with boron concentration of up to 1 % (w/w) may be utilized as fertilizers, without any structural changes in comparison to the fertilizers without boron.

FTIR Analysis

The infrared spectrum of sample 4, having the maximum boron content in the series, was compared with the spectrum of boron-free ammonium phosphates (sample 6). The spectra are shown in Fig. 7.

According to literature data,^{23–25} the following four bands are observed in the infrared spectrum of BPO_4 : 1085, 925, 615 and 550 cm^{-1} . The IR spectrum of sample 4 showed three absorption bands at 1080, 950 and 550 cm^{-1} , which eventually could be assigned to the B–O–P link, present in boron orthophosphate, BPO_4 . However, as can be seen, the IR spectrum of sample 4 was almost the same as the IR spectrum of sample 6. This could be explained by the low concentration of boron and by overlapping with the IR bands assigned to ammonium phosphate. The difference spectrum between sample 6 and sample 4 was recorded in order to emphasize the boron presence (spectrum 4, Fig. 7). Although a weak band at around 933 cm^{-1} appeared, the other three bands (1085, 615 and 550 cm^{-1}) were not observed, which confirms the overlapping of the bands. In conclusion,

no B–O–P or B–P bonds that could eventually affect the assimilation boron by plants were detected in the infrared spectrum of sample 4.

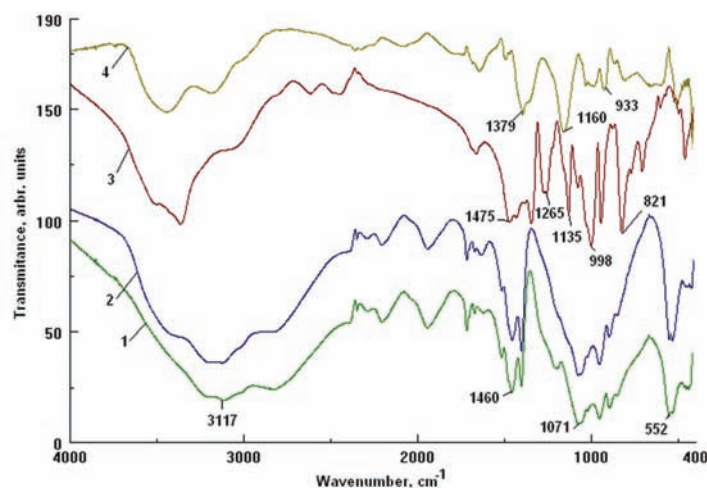


Fig. 7. Infrared spectra: 1) sample 6; 2) sample 4; 3) sodium tetraborate; 4) sample 4 minus sample 6.

X-Ray diffraction and infrared spectrum of heat treated fertilizer

A possible explanation of the increase in thermal stability above 500 °C with increasing boron content was the formation of a new chemical combination of boron with the phosphates present in the system. In order to investigate the new structure, product **5** with a higher boron content (5 %) was calcined at 500 °C. The calcined product was investigated by X-ray diffraction and infrared spectroscopy. The X-ray patterns are shown in Fig. 8.

The X-ray pattern after calcination at 500 °C indicated the disappearance of the previous structures and the appearance of BPO₄, boron orthophosphate,²⁶ which explains the increase of thermal stability with increasing boron content.²⁴ In addition, the formation of BPO₄ induced an improvement in the efficiency the fertilizer.^{9,27}

The infrared spectrum of product 5 is shown in Fig. 9.

The IR spectrum of sample 5 showed all the bands assigned to boron phosphate, slightly shifted towards higher frequencies, which confirms the XRD data. In addition, some bands appeared, assigned as γ_{as} PO₂ (1276 cm⁻¹),²⁸ γ_s P–O–P (766 cm⁻¹)²⁹ and δ PO₂ (511 cm⁻¹)²⁹ vibrations, characteristic of polyphosphates.

In conclusion, in addition to the already studied methods,^{9,23,24} boron orthophosphate may be obtained by calcination at 500 °C of the neutralization products of phosphoric acid with ammonia and addition of boron tetraborate to the reaction system.

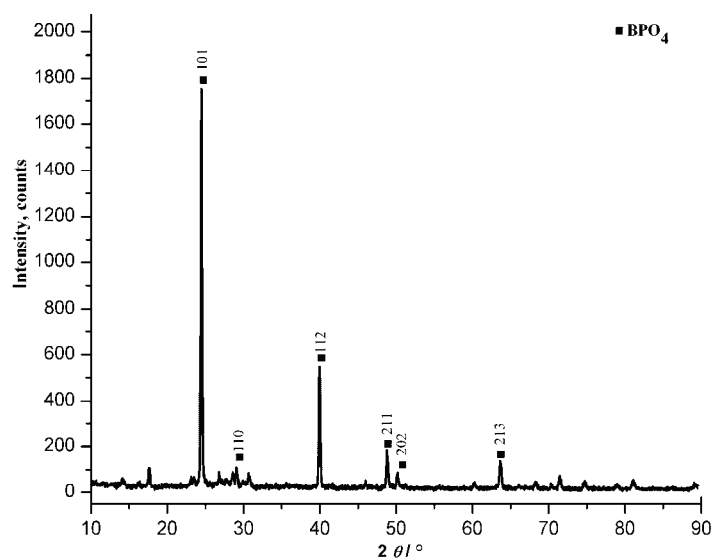


Fig. 8. X-Ray diffraction pattern of the sample calcined at 500 °C; ■ – BPO₄.

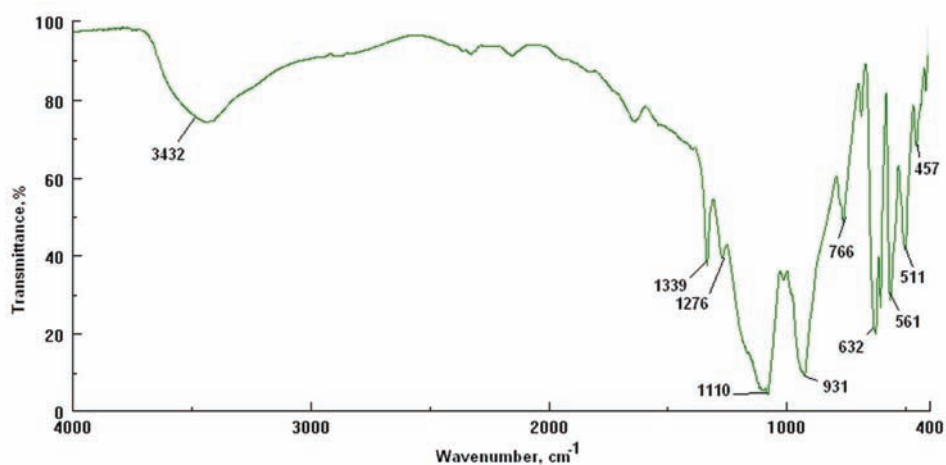


Fig. 9. Infrared spectrum of the sample calcined at 500 °C.

CONCLUSIONS

The pH of the reaction mixture represents a control parameter which enables the proper management of the neutralization process of phosphoric acid with ammonia in presence of sodium tetraborate pentahydrate. Up to a concentration of 1 % boron in the final product, the addition of sodium tetraborate did not significantly influence the neutralization process.

Chemical analysis of the products obtained showed that the addition of sodium tetraborate up to a content of 1 % boron in the final product did not signi-

ificantly change the nutritional properties of the fertilizers in respect to the content of nitrogen and phosphorus.

Thermal analysis showed that up to 500 °C, regardless of boron content, no significant differences in thermal behavior of the boron-containing fertilizers in comparison with the boron free-fertilizer were observed. The thermal stability of the products obtained during their processing up to 500 °C was not changed. Moreover, the products underwent similar mass losses (ammonia nitrogen); hence their nutrition qualities were not altered. Above 500 °C, the thermal stability of fertilizers increased with increasing boron content.

X-Ray diffraction analysis showed that no structural changes of the obtained products occurred with increasing content of boron, compared with boron-free ammonium phosphates.

The infrared spectra did not positively confirm the formation of new chemical compounds of boron with the phosphates present in the system.

In conclusion, the addition of sodium tetraborate pentahydrate to the reaction mass of phosphoric acid with ammonia at a $\text{NH}_3:\text{H}_3\text{PO}_4$ molar ratio equal to 5, up to a limit of 1 % boron in the final products, did not result in any changes of structure and nutritional properties of the obtained products compared with boron-free ammonium phosphates.

On calcination at 500 °C of a 5 % boron-containing fertilizer, boron phosphate, which is a quality fertilizer with high contents of boron and phosphorus and a slow release of boron, was obtained.

ИЗВОД

СИНТЕЗА И КАРАКТЕРИСАЊЕ АМОНИЈУМ-ФОСФАТНОГ ЂУБРИВА СА ДОДАТКОМ БОРА

ANGELA MAGDA¹, RODICA PODE¹, CORNELIA MUNTEAN¹, MIHAI MEDELEANU¹ и ALEXANDRU POPA²

¹*Faculty of Industrial Chemistry and Environmental Engineering, "Politehnica" University of Timișoara, Victoria Square No. 2, 300006 Timișoara, Romania* и ²*Institute of Chemistry Timișoara of Romanian Academy, M. Viteazul Ave, No. 24, 300223-Timișoara, Romania*

Бор је један од основних микро-нутрицијената биљака, али је према концентрацији узан опсег између дефицитарности и токсичности. Да би се обезбедила потреба биљака за бором и избегао проблем токсичности, једињења бора се мешају са основним ђубривом. У овом раду је као извор бора коришћен натријум-борат пентахидрат; у реакциону смешу са молским односом $\text{NH}_3:\text{H}_3\text{PO}_4$ 1,5 за добијање амонијум-ортофосфатног ђубрива неутрализацијом фосфорне киселине амонијаком, додаване су променљиве количине натријум-тетраборат пентахидрата. Ђубриво које садржи 0,05–1 % w/w бора потпуно је окарактерисано хемијском анализом, термичком анализом, дифракцијом X-зрака и инфрацрвеном спектрофотометријом. Испитивања су показала да до температуре 500 °C, без обзира на садржај бора, не долази до значајних промена термичке стабилности и нутрификационих својстава, а изнад ње повећава се термичка стабилност са повећањем садржаја бора. Дифракција X-зрака термички третираних узорака који садрже 5 % w/w бора, указала је на присуство бор-ортофосфата, BPO_4 , као

нове кристалне фазе и нестајање претходних структура изнад температуре 500 °C, што објашњава повећање термичке стабилности.

(Примљено 28. фебруара 2009, ревидирано 26. априла 2010)

REFERENCES

1. L. Bolanos, K. Lukaszewski, I. Bonilla, D. Blevins, *Plant Physiol. Biochem.* **42** (2004) 907
2. D. G. Blevins, K. M. Lukaszewski, *Annu. Rev. Plant. Physiol. Plant. Mol. Biol.* **49** (1998) 481
3. V. M. Shorrocks, *Plant Soil* **193** (1997) 121
4. M. Tanaka, T. Fujiwara, *Pflügers Arch – Eur. J. Physiol.* **456** (2008) 671
5. A. M. Acuna, *Udo Agricola* **5** (2005) 10
6. P. H. Brown, B. J. Shelp, *Plant Soil* **193** (1997) 85
7. *Boron mobility in various plant species*, U.S. Borax Inc., – L.T. – AC10-AN-204_U.S., 2002
8. A. Iovi, C. Iovi, P. Negrea, *Chemistry and Technology of Fertilizers with Microelements*, Politehnica Publishing House, Timișoara, 2000, p. 5 (in Romanian)
9. L. F. Ray, U. S. Patent 3655357 (1972)
10. A. Magda, C. Muntean, P. Negrea, L. Lupa, G. Bandur, A. Iovi, *Chem. Bull. “Politehnica” Univ. Timișoara* **52** (2007) 66
11. A. Magda, C. Muntean, A. Iovi, M. Jurca, L. Lupa, M. Simon, V. Pode, *Rev. Chim.* **60** (2009) 226
12. C. G. Macarovici, *Inorganic quantitative chemical analysis*, Editura Academiei R.S.R., Bucuresti, 1979, p. 436 (in Romanian)
13. *Die Untersuchung von Wasser*, E. Merck, Darmstadt, 1989, p. 4.
14. L. Martony, A. Nimara, I. Eremia, T. Simionescu, *Rev. Chim.* **36** (1985) 57
15. Z. Borlan, C. Hera, *Methods for the Fertility State Appreciation in the View of the rational Use of Fertilisers*, Ceres Publishing House, București, 1973, p. 280 (in Romanian)
16. R. Radovet, A. Iovi, M. Stefanescu, R. Pode, P. Negrea, C. Iovi, *Chem. Bull., “Politehnica” Univ. Timișoara* **45** (2000) 67
17. A. Abdel-Kader, A. A. Ammar, S. I. Saleh, *Thermochim. Acta* **176** (1991) 293
18. S. Liidakis, G. Katsigiannis, T. Lymperopoulou, *Thermochim. Acta* **453** (2007) 136
19. P. Melnikov, A. L. Guirardi, M. A. C. Secco, E. Nogueira de Aguiar, *J. Therm. Anal. Calorim.* **94** (2008) 163
20. J. Pérez, E. Pérez, B. del Vas, L. Garcia, J. L. Serrano, *Thermochim. Acta* **443** (2006) 231
21. *JCPDS International Centre for Diffraction Data*, 29-0111
22. *JCPDS International Centre for Diffraction Data*, 37-1479
23. A. Baykal, M. Kizilyalli, M. Toprak, R. Kniep, *Turk. J. Chem.* **25** (2001) 425
24. P. Kmecl, P. Bukovec, *Acta Chim. Slov.* **46** (1999) 161
25. R. Kniep, H. Engelhardt, C. Hauf, *Chem. Mater.* **10** (1998) 2930
26. *JCPDS International Centre for Diffraction Data*, 34-0132
27. A. Nimară, A. Iovi, C. Mateescu, E. Princz, L. Martony, *Rev. Chim.* **44** (1993) 738
28. J. F. Ferraro, K. Krishnan, *Practical Fourier Infrared Spectroscopy*, Academic Press Inc., New York, 1990, p. 203
29. R. M. Silverstein, G. C. Bassler, T. C. Morrell, *Spectrometric Identification of Organic Compounds*, 5th Ed., Wiley, New York, 1991, p. 387.



J. Serb. Chem. Soc. 75 (7) 965–973 (2010)
JSCS–4022

Singlet oxygen generation by higher fullerene-based colloids

SVETLANA P. JOVANOVIĆ^{1*}, ZORAN M. MARKOVIĆ¹, DUŠKA N. KLEUT¹,
VLADIMIR D. TRAJKOVIĆ², BRANKA S. BABIĆ-STOJIĆ¹, MIROSLAV D.
DRAMICANIN¹ and BILJANA M. TODOROVIĆ MARKOVIĆ¹

¹Vinča Institute, P.O. Box 522, 11001 Belgrade and ²Institute of Microbiology
and Immunology, School of Medicine, University of Belgrade,
Dr. Subotića 1, 11000 Belgrade, Serbia

(Received 17 June 2009, revised 26 April 2010)

Abstract: In this paper, the results of the synthesis and characterization of higher fullerene-based colloids is presented. The generation of singlet oxygen ¹O₂ (¹Δ_g) by fullerene water-based colloids (*n*C₆₀, *n*C₇₀ and *n*C₈₄) was investigated. It was found by electron paramagnetic resonance spectroscopy that the generation of singlet oxygen was the highest by the *n*C₈₄ colloid. The amplitude of the electron paramagnetic resonance (EPR) signal was two orders of magnitude higher than the amplitude of the EPR signals which originated from *n*C₆₀ and *n*C₇₀. The surface morphology and the structure of the particles of the water-based colloids were investigated by atomic force microscopy (AFM). The AFM study showed that the average size of the *n*C₆₀, *n*C₇₀ and *n*C₈₄ were 200, 80 and 70 nm, respectively. In addition, the particle size distribution of the *n*C₆₀, *n*C₇₀ and *n*C₈₄ colloids was determined by dynamic light scattering (DLS) measurements.

Keywords: higher fullerene; colloid; electron paramagnetic resonance spectroscopy; atomic force microscopy; dynamic light scattering.

INTRODUCTION

For more than 20 years, fullerenes have attracted the attention of researchers from many different fields. Their application is possible in many areas (biomedicine, electronics) because of their unique properties.^{1–6} Whereby, their photophysical properties are the most interesting for medical applications. Pristine fullerenes, C₆₀ [60-*I*_h] and C₇₀ [70-*D*_{5h}], effectively produce singlet oxygen (¹Δ_g) by absorbing light energy.⁷ The photosensitized production of singlet oxygen involves four steps: a) absorption of light; b) formation of the triplet state of the photosensitizer; c) trapping of the triplet state by molecular oxygen; d) energy transfer from the triplet state to molecular oxygen.⁸ In photodynamic therapy

* Corresponding author. E-mail: svetlanajovanovic@vinca.rs
doi: 10.2298/JSC090617062J

(PDT) of cancer, fullerenes could be used as photosensitizers.⁹ Photodynamic therapy (PDT) is one of the non-invasive treatments applicable with reduced side effects for various types of tumors.¹⁰ Chemical modification by PEG of appropriate molecular weight and terminal structures enables water-insoluble C₆₀ to dissolve in water and automatically accumulate in a tumor. The PDT effect of C₆₀-PEG-Gd was significant when light irradiation was performed 3 h or longer after injection, whereas no effect was observed 1 h after injection.¹¹

Biomedical applications demand fullerene in a water soluble form. Several methods have been developed to disperse these otherwise hydrophobic carbon compounds in water.¹² There are different methods for creating colloidal nanocrystalline fullerenes (*n*C₆₀, *n*C₇₀ and *n*C₈₄).^{13–15} Variations such as the solvent used, temperature, fullerene concentration and mixing regime affect the size, structure and charge characteristics of fullerene-based colloids. Differences in size, structure and surface chemistry of *n*C₆₀ produced by various procedures could have important implications for the interpretation of data from environmental transport and toxicity studies.

In a previous study, it was shown that *n*C₆₀ intercalated with different solvents produce singlet oxygen at different rates.¹⁶ With regard to their capacity to generate ROS and cause mitochondrial depolarization followed by necrotic cell death, *n*C₆₀ suspensions are ranked in the following order: THF/*n*C₆₀ > EtOH/*n*C₆₀ > aqua/*n*C₆₀. Mathematical modeling of singlet oxygen (¹Δ_g) generation indicates that the ¹Δ_g-quenching power (THF/*n*C₆₀ < EtOH/*n*C₆₀ < aqua/*n*C₆₀) of the solvent intercalated in the fullerene crystals determines their ability to produce ROS and cause cell damage.

In this study, singlet oxygen generation of fullerene-based colloids was investigated. The photophysical properties of higher fullerenes remain poorly understood, largely because of the challenge posed by multiple isomeric forms of these compounds.¹⁷ Singlet oxygen was detected by electron paramagnetic resonance (EPR) spectroscopy, following the formation of stable nitroxide radicals, TEMPO (2,2,6,6-tetramethylpiperidine-1-oxyl).¹⁸ Using atomic force microscope (AFM), individual particles and group of particles can be visualized and unlike other microscopy techniques, AFM offers visualization in three dimensions. Based on dynamic light scattering (DLS) analysis, it was found that the average size of the higher fullerene colloidal particles was about 40 nm.

EXPERIMENTAL

C₆₀ (99.9 % purity), C₇₀ (99 % purity) and mixture of higher fullerenes (C₈₄ (40 %), C₇₆ (20 %), C₇₈ (20 %) and C₇₀ (20 %) - further in the text C₈₄) were purchased from MER corporation, Tuscon, USA. The preparation procedure of *n*C₆₀ and *n*C₇₀ were described in previous studies.^{16,19} Freshly distilled THF of HPLC purity (Carlo Elba, Milan, Italy) was used as the solvent. During the preparation of *n*C₈₄/THF, powder of the higher fullerenes was added to THF at a concentration of 10 mg L⁻¹. The THF/C₈₄ mixture was purged with nit-

rogen to remove any dissolved oxygen and stored overnight in the dark while being continuously stirred to ensure a homogeneous mixture. The THF/C84 solution was then filtered through a 0.5 μm PTFE filter to remove any excess of solid material. An equal amount of MilliQ water was then added to the THF/C84 filtrate at a rate of 1 L min^{-1} under continuous stirring. The THF was removed from the solution using a rotary evaporator operated at 45 $^{\circ}\text{C}$. The concentrations of fullerene particles in water were determined from the absorption spectra. The concentration of the THF/*n*C84 suspension was approximately 6 mg L^{-1} .

Silicon was used as the substrate. The drop of fullerene-based colloids was deposited on silicon substrates and dried in air. The morphology of the three different colloids was investigated by means of a Quesant AFM. A conventional Si cantilever was used for all measurements under ambient conditions. Imaging was realized in the non-contact dynamic mode. In this mode, the cantilever oscillates close to resonance and the tip only slightly touches the surfaces. All images were processed for better quality.

The particle size distributions of the C^{60} , C^{70} and higher fullerene suspensions were obtained using a Brookhaven Instruments light scattering system equipped with a BI-200SM goniometer, a BI-9000AT correlator, a temperature controller and a Coherent INNOVA70C argon-ion laser.

EPR Spectroscopy was used to monitor the generation of singlet oxygen in the aqueous solutions. The EPR experiments were performed at room temperature using a Varian E-line spectrometer operating at a nominal frequency of 9.5 GHz. A mixture containing 0.18 mL TMP (Sigma) and different fullerene-based colloids with a concentration of 2 mg L^{-1} was thoroughly ultrasonicated and incubated at room temperature for 24 h. Aliquots (7 μL) of the TMP-fullerene mixtures were then transferred into 3 mm i.d. quartz tubes and the Tempol signal was analyzed by EPR. Quantification of the signals was realized by calculating the mean value of the amplitudes of the EPR signals and the data are expressed in arbitrary units.

RESULTS AND DISCUSSION

Surface morphology

In addition to yielding three-dimensional topographic images of investigated objects, AFM has also become an invaluable tool for studying important properties of a specimen.²⁰ The surface morphology of the prepared fullerene-based colloids deposited on freshly cleaned silicon substrates was observed by atomic force microscopy. The size and shape of particles of the three different fullerene-based colloids were determined by AFM. The colloids were diluted to a concentration of approximately 0.1 mg L^{-1} to prevent agglomeration of particles during the course of drying and to enable the detection of single particles. The AFM images of the particles of the *n*C₆₀, *n*C₇₀ and *n*C₈₄ colloids are presented in Figs. 1a–1f. As can be observed from Fig. 1, the average sizes of the *n*C₆₀, *n*C₇₀ and *n*C₈₄ particles based on surface profile analysis were 200 nm, 80nm and 70 nm, respectively.

Despite the precautions, the particles formed agglomerates on certain areas of the silicon substrate. It is considered that most of the aggregates were formed during drying but preformed aggregates, maintained by van der Waals attraction, in the colloid are also possible.²¹ Brant *et al.* observed that aggregate formation resembled a crystal growth process rather than undirected particle aggregation.²²

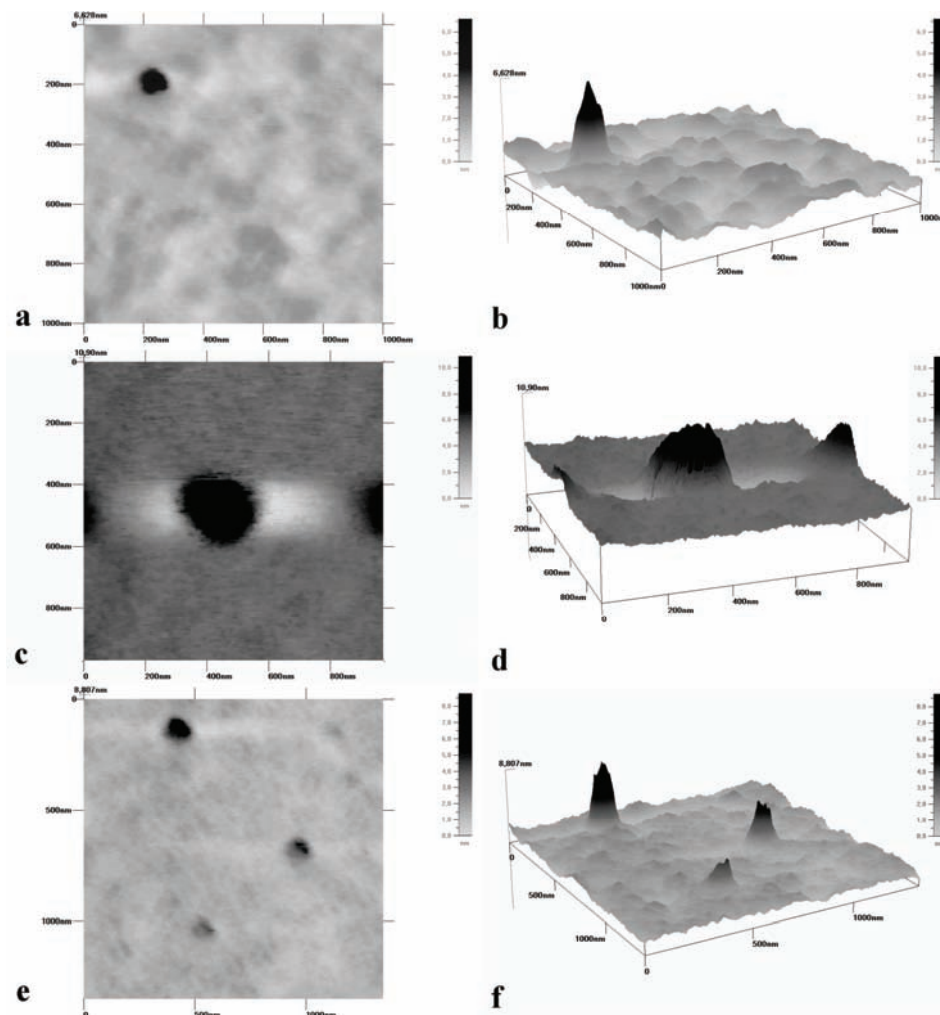


Fig. 1. Top and 3D views of AFM images of C₆₀, C₇₀ and C₈₄ particles, respectively.

Dynamic light scattering (DLS)

Dynamic light scattering measurements were performed to examine the particle size distribution of the three different fullerene-based colloids and the formation of aggregates in the specimens. Based on data presented in Fig. 2, it could be concluded that the sizes of most of the C₆₀ particles were between 100–150 nm. The DLS measurements of the C₇₀ and C₈₄ particles showed that the sizes were approximately the same, between 40–50 nm. Less than 10 % of the C₇₀ particles had a diameter in the range from 80 to 100 nm. The mean lateral diameter measured by AFM were larger than the real mean diameters measured by DLS because of convolution of the tip.²⁰

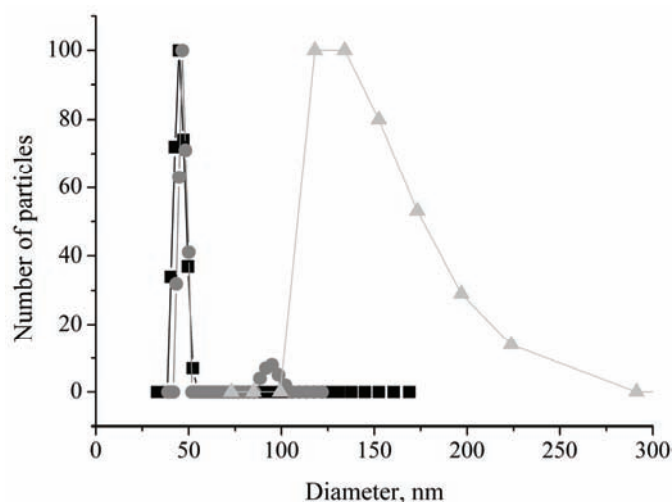


Fig. 2. Particle size distribution of different fullerene particles in the colloids: (●) C₇₀ particles, (▲) C₆₀ particles, (■) C₈₄ particles.

The results obtained by AFM measurements and by DLS for particle size distribution were in a good agreement.

Electron paramagnetic resonance (EPR)

Electron paramagnetic resonance (EPR) is a non-optical technique in which energy transfer between the intrinsic magnetism of an unpaired electron and an external magnetic field is measured with a sensitive microwave detection system. An EPR spectrum is recorded by measuring the strength of the microwave signal when the magnetic field is swept over a small range.²³

The reaction of $^1\Delta_g$ with a stable molecule can generate a moderately long-lived free radical. In addition, $^1\Delta_g$ can react with a spin label, an organic molecule with an unpaired electron. Determination of the structure of the adduct by EPR provides an unambiguous identification. The spin label TEMP was employed as a spin label probe. The reaction of $^1\Delta_g$ with TEMP leads to the free radical TEMPO.¹⁸

The results of EPR measurements of the three different fullerene-based colloids are presented in Fig. 3. In a previous study, it was established that singlet oxygen was generated by nC_{60} .¹⁹ These experimental results were confirmed by a theoretical model.¹⁶ In this study, generation of singlet oxygen by nC_{84} was observed. The amplitude of EPR signal produced by nC_{84} is significantly higher than the ones caused by nC_{60} and nC_{70} . This is for the first time that the generation of singlet oxygen by C_{84} particles in an aqueous solution is shown. The observed formation rates of Tempo were about two orders of magnitude faster for nC_{84} than for nC_{60} and nC_{70} .

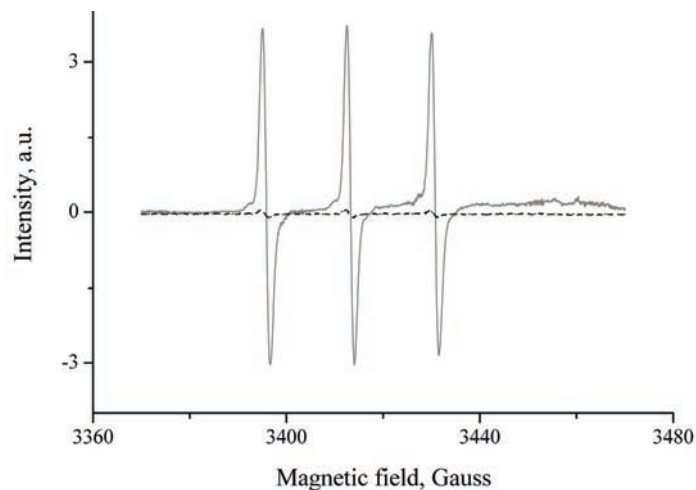


Fig. 3. EPR Spectra of the three different fullerene-based colloids: (···) nC_{60} , (---) nC_{70} and (—) nC_{84} .

Experimentally, seven C_{84} isomers are formed in standard fullerene soot.²⁴ Of these, the two most abundant isomers are $D_2(IV)$ (*ca.* 50 %) and $D_{2d}(II)$ (*ca.* 25 %). The triplet lifetime of $D_2(IV)$ C_{84} is 640 μs , which represents the second longest time found to date among fullerenes. The triplet lifetimes of C_{60} and C_{70} in toluene at room temperature are 143 μs and 11.8 ms, respectively.²⁵ The energies of the lowest lying triplet states of C_{60} and C_{70} are 1.62 and 1.54 eV, respectively.^{26,27}

Despite the fact that C_{70} has a longer triplet lifetime than C_{60} , the present results demonstrate that nC_{60} and nC_{70} produce almost equal amounts of singlet oxygen. One of the reasons for such behavior is the fact that C_{70} quenches singlet oxygen much better than C_{60} .²⁸ According to literature data, the rates of singlet oxygen quenching for C_{60} and C_{70} are $6.1 \times 10^4 \text{ L mol}^{-1} \text{ s}^{-1}$ and $3 \times 10^6 \text{ L mol}^{-1} \text{ s}^{-1}$, respectively.^{29,30} Based on a theoretical model of singlet oxygen generation by nC_{60} and nC_{70} ,¹⁶ the concentration of neutral oxygen inside nC_{60} and nC_{70} is in the range of 10^{14} to 10^{17} cm^{-3} , and nC_{70} produces only 5 % more singlet oxygen than nC_{60} .

Booth *et al.* recently showed the presence of a peak at around 0.97 eV in the emission spectrum of $C_{84}\{D_2(IV)\}$, which was assigned to luminescence emission to $^1\Delta_g$ molecular oxygen.³¹ According to measurement of energies, the lowest lying triplet state of $D_2(IV)$ and $D_{2d}(II)$ are 0.99 and 0.94 eV.³¹ No significant emission from $^1\Delta_g$ was observed for $D_{2d}(II)$.³¹ Up to now, it was considered that the higher fullerenes produce a significantly lower amount of the reactive form of molecular oxygen $^1O_2(^1\Delta_g)$ than C_{60} and C_{70} .³²

The extremely high generation of singlet oxygen by nC_{84} compared to nC_{60} and nC_{70} could be, at the moment, explained by two facts. The first one is that the total energy of the triplet state of excited $C_{84}\{D_2(IV)\}$ is almost identical to the excitation energy of neutral oxygen, 1.6 eV.³¹ Therefore, the process of energy transfer from C_{84} to neutral oxygen can proceed without collision with a third body, necessary to take the excess of energy.

The second fact is that the area of the channels in the unit cell of a C_{84} nanocrystal that permits diffusion of neutral oxygen within the unit cell is rather larger than for the unit cell of C_{60} or C_{70} . It was reported that a face-centered cubic structure was dominant for C_{60} , C_{70} and C_{84} .^{33–35} Zubov *et al.* assumed free rotation of the nearly spherical fullerene molecules in the unit cells at room temperature.³⁶

The distances, a , among the nearest fullerene molecules in a unit cell (C_{60} , C_{70} and C_{84}) and the surface area of one channel between the fullerene molecules in the unit cell are listed in Table I, from which it can be seen that the distances between the C_{84} molecules are the largest. Since there are six channels per unit cell, the total surface area for the diffusion of neutral oxygen is 9 times larger for C_{84} than for C_{60} .

TABLE I. Parameters of fullerene nanocrystals

Property	C_{60}	C_{70}	C_{84}
a / nm	1.417	1.501	1.59
Surface area of one channel ($\times 10^{18} \text{ m}^2$)	0.431	0.4835	0.5425

CONCLUSIONS

In this work, the generation of singlet oxygen by a water-based nC_{84} colloid was demonstrated for the first time. The rate of singlet oxygen generation by the nC_{84} colloid was two orders of magnitude higher than those of the nC_{60} and nC_{70} colloid. Experimental conformation was obtained by EPR spectroscopy.

Acknowledgment. This research was supported by the Ministry of Science and Technological Development of the Republic of Serbia (Project No. 145073).

ИЗВОД

СТВАРАЊЕ СИНГЛЕТНОГ КИСЕОНИКА У ВОДЕНИМ КОЛОИДИМА ВИШИХ ФУЛЕРЕНА

СВЕТЛАНА П. ЈОВАНОВИЋ¹, ЗОРАН М. МАРКОВИЋ¹, ДУШКА Н. КЛЕУТ¹, ВЛАДИМИР Д. ТРАЈКОВИЋ², БРАНКА С. БАБИЋ-СТОЈИЋ¹, МИРОСЛАВ Д. ДРАМИЋАНИН¹ И БИЉАНА М. ТОДОРОВИЋ МАРКОВИЋ¹

¹"Винча" Институт за нуклеарне науке, б.п.р. 522, 11001 Београд и ²Институт за микробиологију и имунологију, Медицински факултет, Универзитет у Београду, Др. Суботића 1, 11000 Београд

У овом раду су приказани резултати анализе синтетисаних фулеренских колоида. Фулереи C_{60} , C_{70} и C_{84} су коришћени за синтезу водених колоидних раствора. Електронском парамагнетном резонантном спектроскопијом (EPR) селективно је праћено стварање синглетног кисеоника и утврђено је да највећа количина синглетног кисеоника настаје у колоиду

nC_{84} . EPR сигнал колоида nC_{84} има двоструко већу амплитуду у односу на амплитуде EPR сигнала колоида nC_{60} и nC_{70} . Испитана је структура, облик и величина честица добијених колоида микроскопом атомских сила (AFM). На основу AFM анализа утврдили смо да је просечна величина честица 200, 80 и 70 nm за фулеренске колоиде nC_{60} , nC_{70} и nC_{84} редом. DLS мерењима такође су испитане величине честица и потврђени резултати добијени AFM испитивањем.

(Примљено 17. јуна 2009, ревидирано 26. априла 2010)

REFERENCES

1. S. Bosi, T. Da Ros, G. Spalluto, M. Prato, *J. Med. Chem.* **38** (2003) 913
2. S. C. Tsang, Y. K. Chen, P. J. F. Harris, M. L. H. Green, *Nature* **372** (1994) 159
3. J. S. Shil, Y. C. Chao, M. F. Sung, G. J. Sau, C. S. Chiou, *Sensors Actuators B* **76** (2001) 347
4. Q. H. Wang, A. A. Setlur, J. M. Lauerhaas, J. Y. Dai, E. W. Scelig, R. P. H. Chang, *Appl. Phys. Lett.* **72** (1998) 2912
5. P. Innocenti, G. Brusatin, *Chem. Mater.* **13** (2001) 3126
6. G. V. Andrievsky, V. K. Klochkov, E. I. Karyankina, N. O. Medlov-Petrosyan, *Chem. Phys. Lett.* **300** (1999) 392
7. J. W. Arbogast, C. S. Foote, *J. Am. Chem. Soc.* **113** (1991) 8886
8. M. Belousova, N. G. Mironova, M. S. Yurev, *Opt. Spectrosc.* **98** (2005) 349
9. T. J. Dougherty, C. J. Gomer, B. W. Henderson, G. Jori, D. Kessel, M. Korbelik, J. Moan, Q. Peng, *J. Natl. Cancer Inst.* **90** (1998) 889
10. Y. Tabata, Y. Murakami, Y. Ikada, *Jpn. J. Cancer Res.* **88** (1997) 1108
11. J. Liu, S. Ohta, A. Sonoda, M. Yamada, M. Yamamoto, N. Nitta, K. Murata, Y. Tabata, *J. Control. Release* **117** (2007) 104
12. J. D. Fortner, D. Y. Lyon, C. M. Sayes, A. M. Boyd, J. C. Falkner, E. M. Hotze, L. B. Alemany, Y. J. Tao, W. Guo, K. D. Ausman, V. L. Colvin, J. B. Hughes, *Environ. Sci. Technol.* **39** (2005) 4307
13. G. V. Andrievsky, M. V. Kosevich, O. M. Vovk, V. S. Shelkovsky, L. A. Vaschchenko, *Chem. Commun.* (1995) 1281
14. S. Deguchi, G. A. Rossitza, K. Tsujii, *Langmuir* **17** (2001) 6013
15. J. Brant, J. Labille, J. Y. Bottero, M. R. Wiener, *Langmuir* **22** (2006) 3878
16. Z. Marković, B. Todorović Marković, D. Kleut, N. Nikolić, S. Vranješ Djurić, M. Misirkić, L. Vučićević, K. Janjetović, A. Isaković, L. Harhaji, B. Babić Stojić, M. Dramićanin, V. Trajković, *Biomaterials* **28** (2007) 5437
17. F. Diederich, R. L. Whetten, *Acc. Chem. Res.* **25** (1992) 119
18. B. Vilenko, M. Lekka, A. Sienkiewicz, P. Marcoux, A. J. Kulik, S. Kasas, S. Catsicas, A. Graczyk, L. Forro, *J. Phys. Condens. Matter.* **17** (2005) S1471
19. A. Isaković, Z. Marković, B. Todorović-Marković, N. Nikolić, S. Vranješ-Djurić, M. Mirković, M. Dramićanin, L. Harhaji, N. Raičević, Z. Nikolić, V. Trajković, *Tox. Sci.* **91** (2006) 173
20. M. Rasa, B. W. M. Kuipers, A. P. Philipse, *J. Colloid Interface Sci.* **250** (2002) 303
21. A. Rao, M. Schoenenberger, E. Gneco, T. Glatzel, E. Meyer, D. Brandlin, L. Scandela, *J. Phys: Conf. Ser.* **61** (2007) 971
22. J. Brant, H. Lecoanet, M. Wiesner, *J. Nanopart. Res.* **7** (2005) 545

23. I. Kruk, *Environmental Toxicology and Chemistry Oxygen Species*, Springer, Berlin, 1998, p. 26
24. T. J. S. Dennis, T. Kai, K. Asato, T. Tomiyama, H. Shinohara, T. Yoshida, Y. Kobayashi, H. Ishiwatari, Y. Miyake, K. Kikuchi, Y. Achiba, *J. Phys. Chem.* **103** (1999) 8747
25. K. D. Ausman, R. B. Weisman, *Res. Chem. Intermed.* **23** (1997) 431
26. J. W. Arbogast, A. P. Darmanyan, C. S. Foote, Y. Rubin, F. N. Diederich, M. M. Alvarez, S. J. Anz, R. L. Whetten, *J. Phys. Chem.* **95** (1991) 11
27. S. P. Sibley, S. M. Argentine, A. H. Francis, *Chem. Phys. Lett.* **188** (1992) 187
28. V. Bagrov, I. M. Belousova, O. B. Danilov, V. M. Kiselev, T. D. Murave'va, E. S. Sasnov, *Opt. Spectrosc.* **102** (2007) 52
29. G. Black, E. Dunkle, E. A. Dorko, L. A. Schlie, *J. Photochem. Photobiol. A* **70** (1993) 147
30. A. Krasnovky, C. S. Foote, *J. Am. Chem. Soc.* **115** (1993) 6013
31. E. C. Booth, S. M. Bachilo, M. Kanai, T. John, S. Dennis, R. B. Weisman, *J. Phys. Chem. C* **111** (2007) 17720
32. L. Juha, B. Ehrenberg, S. Couris, E. Koudoumas, S. Leach, V. Hamplová, Z. A. Müllerová, P. Kubát, *Chem. Phys. Lett.* **335** (2001) 539
33. N. Yao, C. F. Klein, S. K. Behal, M. M. Disko, R. D. Sherwood, D. M. Cox, *Phys. Rev. B* **45** (1992) 11366
34. Y. Saito, Y. Ishikawa, A. Ohshita, H. Shinohara, H. Nagashima, *Phys. Rev. B* **46** (1992) 1846
35. Y. Saito, T. Yoshikawa, N. Fujimoto, H. Shinohara, *Phys. Rev. B* **489** (1993) 9182
36. V. I. Zubov, N. P. Tretiakov, I. V. Zubov, *Eur. Phys. J. B* **17** (2000) 629.



J. Serb. Chem. Soc. 75 (7) 975–985 (2010)
JSCS–4023

Development and application of a validated HPLC method for the analysis of dissolution samples of mexiletine hydrochloride capsules

DRAGAN M. MILENOVIĆ^{1*#} and ZORAN B. TODOROVIĆ^{2#}

¹"Zdravlje-Actavis" Company, Analytical Department, R & D, Vlajkova 199, 16000 Leskovac,
and ²Faculty of Technology, Bulevar oslobođenja 124, 16000 Leskovac,
University of Niš, Serbia

(Received 28 July 2009, revised 16 February 2010)

Abstract: The aim of this work was to develop and validate a simple, efficient, sensitive and selective method for the analysis of dissolution samples of mexiletine hydrochloride capsules by HPLC without the necessity of any time-consuming extraction, dilution or evaporation steps prior to drug assay. Separation was performed isocratically on a 5 μm LiChrospher 60, RP-Select B column (250 \times 4 mm ID) using the mobile phase buffer–acetonitrile (60:42, v/v) at a flow rate of 1.2 mL min⁻¹ and UV detection at 262 nm. The elution occurred in less than 10 min. The assay was linear in the concentration range 50–300 $\mu\text{g mL}^{-1}$ ($r^2 = 0.9998$). The validation characteristics included accuracy, precision, linearity, specificity, limits of detection and quantification, stability, and robustness. Validation acceptance criteria were met in all cases (the percent recoveries ranged between 100.01 and 101.68 %, $RSD < 0.44$ %). The method could be used for the determination of mexiletine hydrochloride and for monitoring its concentration in *in vitro* dissolution studies.

Keywords: mexiletine hydrochloride; dissolution; method validation; HPLC.

INTRODUCTION

Mexiletine hydrochloride is an orally active class I anti-arrhythmic agent. Chemically it is 1-methyl-2-(2,6-xylyloxy)-ethylamine hydrochloride (Fig. 1). Mexiletine hydrochloride has been shown to be effective in the suppression of induced ventricular arrhythmias, including those induced by glycoside toxicity and coronary artery ligation. It is available in capsule form.¹

Mexiletine hydrochloride is a white powder, freely soluble in water and in ethanol, slightly soluble in acetonitrile and practically insoluble in diethyl ether.²

* Corresponding author. E-mail: dmilenovic@actavis.rs

Serbian Chemical Society member.

doi: 10.2298/JSC090728065M

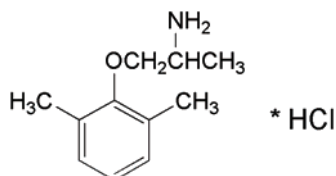


Fig. 1. Chemical structure of mexiletine hydrochloride.

Various analytical methods have been reported in the literature for the quantitative determination of mexiletine hydrochloride in human plasma or serum. These methods are quite limited and typically involve a derivatization step.³⁻⁷ The literature on HPLC analysis of mexiletine hydrochloride in raw materials and pharmaceutical preparations is rather poor.^{1,2,8-14} Due to their high sensitivity and selectivity, analytical methods such as liquid chromatography were previously reported to be used for the determination of active substances in dissolution samples.¹⁵⁻²¹

As is known, dissolution testing is a regular quality control procedure in good manufacturing practice, and dissolution data are also a substantial parameter for the evaluation of the bioavailability of drugs. The dissolution test has emerged in the pharmaceutical field as a very important tool for the characterization of the performance of a drug product. It provides measurements of the bioavailability of a drug and can demonstrate bioequivalence from batch-to-batch as well. In addition, dissolution is a requirement for regulatory approval for product marketing. To the best of our knowledge there are only two references for the determination of the amount of mexiletine hydrochloride dissolved from capsules (derivative spectrophotometry and sequential injection method) during dissolution studies.^{9,14}

The aim of the present work was to develop and validate a simple, efficient, sensitive and selective method for the analysis of dissolution samples of mexiletine hydrochloride capsules by HPLC. The analytical methods reported were validated in terms of specificity, linearity, accuracy, precision, stability and robustness.²²

EXPERIMENTAL

Chemicals and reagents

Mexiletine hydrochloride, working certified standard, 100.39 % purity, was purchased from Medichem S.A. (Barcelona, Spain). Acetonitrile (HPLC gradient grade) was purchased from J. T. Baker (Deventer, Holland). Potassium dihydrogen phosphate and ortho-phosphoric acid 85 %, suprapur, were purchased from Merck KgaA (Darmstadt, Germany). Purified water was obtained using an Arium Laboratory Equipment (RO, UV) from Sartorius A.G. (Göttingen, Germany). The mobile phase was filtered through a 0.45 µm Sartorius membrane filter (Göttingen, Germany). Capsules of mexiletine hydrochloride, containing 200 mg of active substances, were obtained in-house and commercially.

Equipment

The HPLC system consisted of a binary pump G1312A, an manual injector G1328A, a thermostated column compartment G1316A and a UV detector G1314A, all 1100 Series, from Agilent Technologies, which was controlled by HP Chemstation software (Waldbroon, Germany). An Erweka DT700LH dissolution apparatus (USP II) (Heusenstamm, Germany) was used. The employed Transsonic 470/H ultrasonic bath was from Elma, (Singen, Germany). The CP224S – OCE analytical balance was from Sartorius A.G. (Gottingen, Germany); the repeatability (standard deviation) of the balance: ± 0.0001 g.

Chromatographic conditions

Separation was achieved on a LiChrospher 60, RP-Select B column 250×4 mm, 5 μm (Merck). The elution was isocratic at 1.2 mL min⁻¹ using a mobile phase of buffer – acetonitrile (60 : 42, v/v). The column temperature was maintained at 30 °C. The injection volume was 20 μL with UV detection at 262 nm.

The buffer was prepared by dissolve 1.28 g dodecyl sodium sulfate and 4.00 g of anhydrous sodium dihydrogen phosphate in 600 mL of water (pH 4.5).

Dissolution

A calibrated dissolution apparatus (USP II) was used with the paddles turning at 50 rpm and a bath temperature maintained at 37±0.5 °C. Nine hundred milliliter freshly prepared and degassed water was used as the dissolution medium.⁹

Six capsules were evaluated for each tested drug product. Dissolution samples were collected manually at 10, 15, 20, 30 and 45 min. At each time point, a 10 mL sample was removed from each vessel and filtered through a filter (0.45 μm) into glass vials and analyzed by HPLC.

The amount of mexiletine hydrochloride in the test samples was calculated, as percentage dissolved, from the measured peak area for the test samples, which were compared with the peak area for a standard mexiletine hydrochloride solution.

Preparation standard solutions

Mexiletine hydrochloride stock solution I of 1 mg mL⁻¹ was prepared in water using a working certified standard, by accurately weighing the mexiletine hydrochloride standard (approximately 25 mg) and transferring it into a 25 mL volumetric flask. Calibration standard solutions were prepared by diluting the stock solution I (50–300 $\mu\text{g mL}^{-1}$).

A system suitability standard solution, which contained 222 $\mu\text{g mL}^{-1}$, was prepared by measuring 22.2 mg mexiletine hydrochloride and diluting with purified water to 100 mL.

RESULTS AND DISCUSSION

Selection and optimization of analytical method

UV Spectrophotometry and HPLC are most commonly used for the analysis of dissolution samples. UV is the more preferable choice when compared to HPLC because of the time required for the analysis of the sample. In cases when the interference is higher than 2 %, it is recommended to choose another wavelength, second derivative, baseline subtraction or HPLC. Regarding interference from excipients, sensitivity issues, automated system and regulatory agencies, an HPLC method for the determination of mexiletine hydrochloride after dissolution is recommended, especially if it has a short retention time.

In order to obtain the best chromatographic conditions, the wavelength for detection, the column and the mobile phase composition must be adequately selected.

The starting point for the development of the assay of mexiletine hydrochloride were the chromatographic conditions given in the United States Pharmacopoeia (USP).⁹ The USP method utilizes a mobile phase of MeOH and acetate buffer (pH 4.8) (60:40, v/v), UV detection at 254 nm, column Purospher STAR RP18e (250×4.6 mm, 5 μm) and a flow rate of 1 mL min⁻¹. An initial attempt resulted in an acceptable retention time (about 8 min), the USP tailing factor was 1.7, but there was interference from the body of the capsules (Fig. 2).

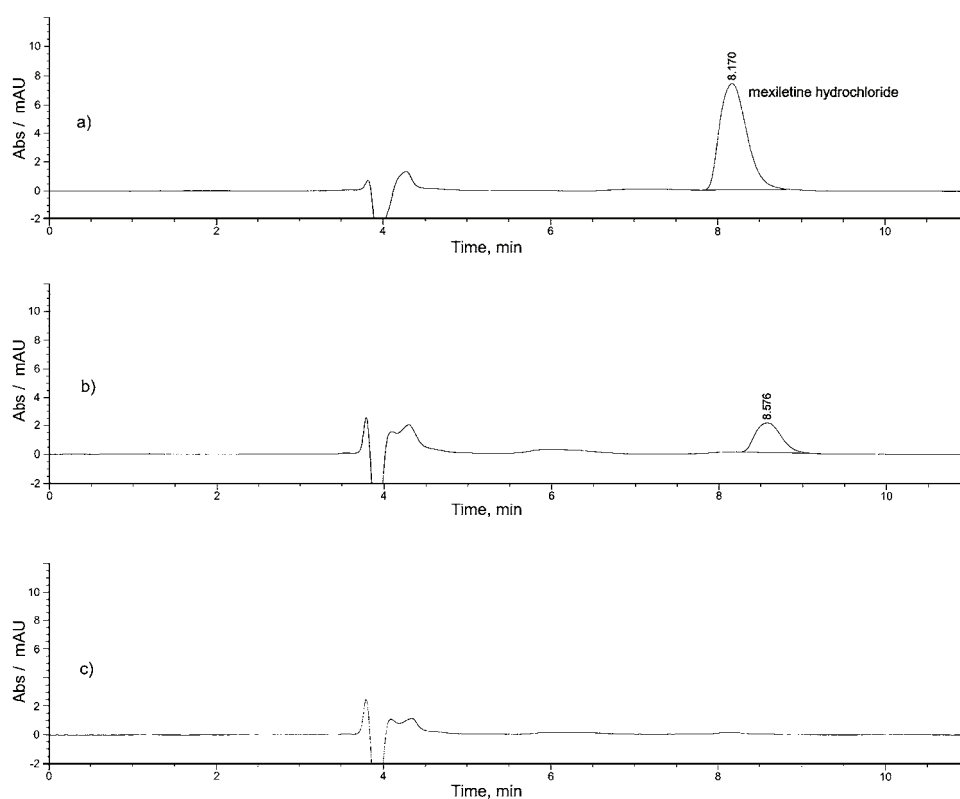


Fig. 2. Chromatograms obtained from: a) the standard solution of mexiletine hydrochloride (200 μg mL⁻¹), b) excipient mixture and c) background sample, using the initial chromatographic conditions.

In order to resolve this problem, the conditions set by the Japanese Pharmacopoeia (UV detection at 210 nm, column 150×4 mm, packed with octyl-silicized silica gel for liquid chromatography, about 7 μm in particle diameter, mobile phase buffer and acetonitrile (60:42, v/v)) were modified in terms of wave-

length, buffer composition and column.² A LiChrospher 60, RP Select B, 250×4 mm, 5 µm column was used at 30 °C with a mobile phase flowrate of 1.2 mL min⁻¹. A detection wavelength of 262 nm was selected for the analysis because the drug has sufficient absorption and low quantities of mexiletine hydrochloride may be detected correctly. Furthermore, the calibration curves obtained at 262 nm show good linearity. Regarding the mobile phase, one buffer solution was without an ion-pairing reagent, but every subsequent phase (four in total), contained a different ion-pairing reagent: sodium hexane sulfonate, sodium heptane sulfonate, sodium octane sulfonate and dodecyl sodium sulfate, used in the same molar quantity, respectively (0.004 mol L⁻¹). The obtained results are given in Table I.

TABLE I. Comparative data on the effect of the different ion-pairing reagents (concentration of mexiletine hydrochloride was 200 µg mL⁻¹)

Ion-pairing reagent	Retention time, min	Capacity factor	USP Tailing	Number of plates	Width at half height	Symmetry
Without an ion-pairing reagent	2.756	0.826	1.843	1924	0.251	0.410
Sodium hexane sulfonate	2.898	0.845	1.775	3205	0.259	0.475
Sodium heptane sulfonate	3.021	0.923	1.737	3237	0.261	0.477
Sodium octane sulfonate	3.455	1.200	1.598	4153	0.268	0.556
Sodium dodecyl sulfate	13.754	4.789	1.168	12154	0.420	1.104

In order to select the proper reagent, alkyl chain lengths must be taken into consideration. The chain lengths enable selective separation of the analyte. The longer the chain, the greater is the retention (about 14 minutes for dodecyl sodium sulfate), but the features of the peak are better (the USP tailing factor decreased from 1.8 for sodium hexane sulfonate to 1.2 for dodecyl sodium sulfate).

In order to obtain the shortest retention time with the best features of peak and the highest efficiency, the quantity of dodecyl sodium sulfate and sodium dihydrogen phosphate were optimized. Finally, the aforementioned composition of the mobile phase, described in Experimental part was chosen as the mobile phase (buffer–acetonitrile (60:42, v/v)). The retention time was about 9 min (USP tailing factor 1.0, number of plates per column above 12000). When compared to Japanese Pharmacopoeia, using the same flow (1.2 mL min⁻¹) the retention time was obviously shorter.

Taking into account the above-mentioned facts, peak characteristics and retention time that is short enough, for further work, the method given in the Experimental Part was chosen (*i.e.*, the method given in the Japanese Pharmacopoeia was modified concerning the employed wavelength, buffer composition and column).

Validation of the method

The method was validated according to the ICH guidelines (International Conference on Harmonization).²² The following validation characteristics were determined: specificity, linearity, accuracy, precision, limits of detection and quantification, stability and robustness.

Suitability test. System suitability was determined from six replicate injections of the system suitability standard solution before sample analysis. According to the USP, the acceptance criteria are less than 2 % relative standard deviation (*RSD*) for the peak area, column efficiency (*N*) greater than 2000 column plates and USP tailing factor less than 2.0. The system suitability test ensures the validity of an analytical procedure. All critical parameters tested met the USP acceptance criteria. For this method, the *RSD* of the mean peak area was below 1.8 %, the mean USP tailing factor was 1.0 and *N* (column efficiency) was above 12000 plates per column.

Specificity. The specificity was evaluated by preparing a placebo sample of a commercial formulation of capsules in their usual concentrations. The placebo contained corn starch, silicon dioxide, magnesium stearate and body capsule. This sample was transferred to a vessel with 900 mL of the dissolution medium and stirred at 50 rpm using the paddle for 60 minutes (USP apparatus II) at a temperature of 37 °C. Aliquots of this solution (10 mL) were filtered and analyzed by HPLC.

The specificity analysis revealed that the developed HPLC method did not suffer interference from the formulation excipients, since no other peak was registered at the retention time of mexiletine hydrochloride (Fig. 3).

Linearity. Standard calibration curves were prepared with six calibrators over the mexiletine hydrochloride concentration range of 50–300 $\mu\text{g mL}^{-1}$ (50, 100, 150, 200, 250, 300 $\mu\text{g mL}^{-1}$), with triplicate determination at each level. The data of peak area vs. drug concentration were treated by linear least square regression analysis. Values of the slope, the intercept and the coefficient of determination of the calibration curve for mexiletine hydrochloride are given in Table II. The high value of the coefficient of determination indicated good linearity.

Precision and accuracy. To test the precision and accuracy of the method, solutions containing all excipients in amounts equivalent to one capsule were spiked with a known amount of mexiletine hydrochloride. Taking into consideration the excellent solubility of mexiletine hydrochloride in the dissolution media suggested by the USP, 80, 100 and 120 % were chosen as the three concentration levels for the testing of the accuracy and precision. The determination of mexiletine hydrochloride was realized six times under the same operating conditions over a short period of time (assay working concentrations of 177.78, 222.22 and 266.66 $\mu\text{g mL}^{-1}$ mexiletine hydrochloride, respectively). The precision and accuracy of the chromatographic method, reported as *RSD* (%) and recovery (%),

respectively, were assessed by estimating the repeatability of the results for six replicate injections at three different concentration levels. The recovery, 95 % confidence interval, and *RSD* values obtained per each level illustrated the good precision and accuracy of the method (Table III).

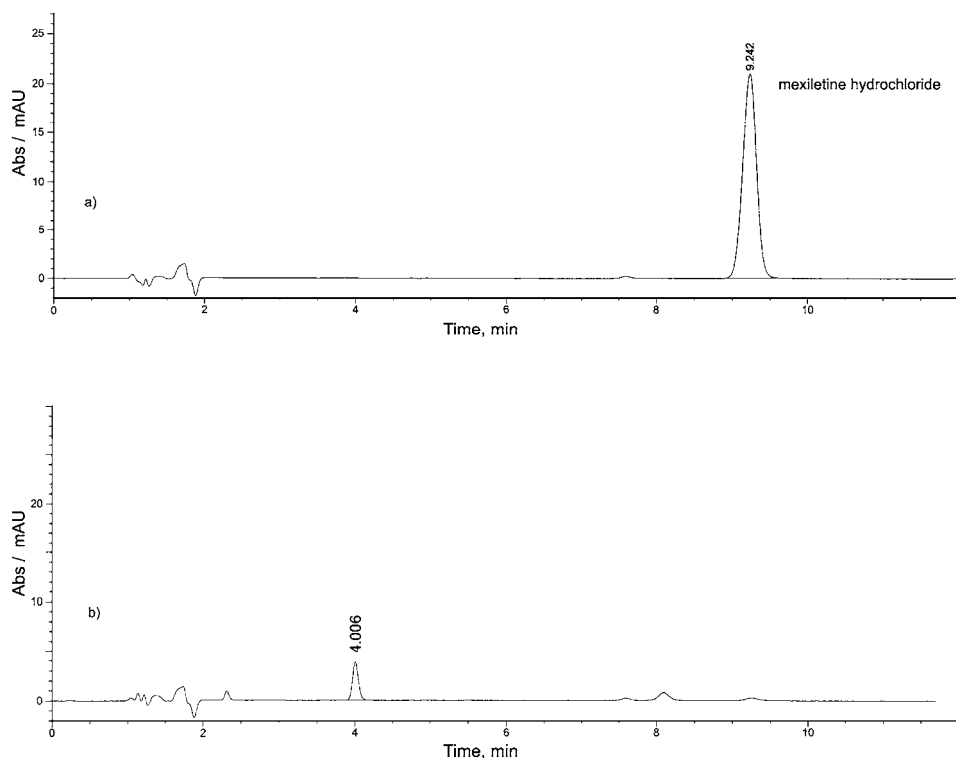


Fig. 3. Chromatograms obtained from: a) the standard solution of mexiletine hydrochloride ($222 \mu\text{g mL}^{-1}$) and b) excipient mixture, using the selected chromatographic conditions.

TABLE II. Linear regression data in the analysis of mexiletine hydrochloride

Statistical parameters	Obtained values
Concentration range, $\mu\text{g mL}^{-1}$	50.00–300.00
Regression equation	$y = 1.1772x + 3.497$
Coefficient of determination	$r^2 = 0.9998$
<i>a</i> (y-intercept)	1.1772 ± 0.243
<i>b</i> (slope)	3.497 ± 0.472
<i>S</i> (<i>a</i>) – error in intercept	0.74
<i>S</i> (<i>b</i>) – error in slope	0.02

The intermediate precision of the method was investigated by making ten consecutive injections of a standard solution on two different days by different analysts using two different HPLC instruments. On both days, the *RSD* values

were calculated for the peak area responses obtained for the mexiletine hydrochloride peaks. The data obtained suggested that the method exhibited an acceptable intermediate precision with less than 2.0 % *RSD* for the mexiletine hydrochloride standard solution (Table IV).

TABLE III. Precision and accuracy results obtained for the drug product

Concentration level, %	95 % Confidence interval, %	Recovery, %	<i>RSD</i> / % (<i>n</i> = 6)
80	101.47–101.89	101.68	0.26
100	99.66–100.36	100.01	0.44
120	100.29–100.73	100.51	0.27

TABLE IV. Statistical parameters for the intermediate precision (*n* = 5) at mexiletine hydrochloride concentration of 222 µg mL⁻¹

Statistical parameter	Day 1	Day 2
Mean peak area, mAU	268.78	272.52
<i>SD</i>	0.71	0.88
<i>RSD</i> / %	0.12	0.15

Limits of detection and quantification. The limits of detection (*LOD*) and quantification (*LOQ*) were determined based on the standard deviation of the response (*y*-intercept) and the slope of the calibration plot for low concentrations, in accordance with ICH guidelines.²² The *LOD* and *LOQ* for mexiletine hydrochloride were 2.07 and 6.21 µg mL⁻¹, respectively.

Sample stability. The stability of mexiletine hydrochloride in aqueous solutions was tested during a 15-day test period. All the samples were kept in the dark at a temperature of +4 °C (in a refrigerator). All the samples were injected into the appropriate HPLC system after 48 h, 7 days and 15 days against fresh standard solutions. No changes in the chromatographic response of the stored samples were found and no additional peaks appeared when compared with chromatograms of the freshly prepared samples.

Robustness. The experimental results of the robustness study are summarized in Table V. Critical chemical and instrumental chromatographic parameters, such as the composition and flow rate of the mobile phase, the column temperature and the injection volume, were deliberately varied in the narrow range compared to their optimal values. The peak areas obtained using mexiletine hydrochloride standard solution of 222 µg mL⁻¹ confirmed the robustness of the HPLC assay, since the obtained values were within the acceptance limits (95.0–105.0 %) in all cases.

Analysis of marketed products. The validated method was used for the analysis of two mexiletine hydrochloride drug products. This included drug products from two different manufacturers, as capsules with a dose strength of 200 mg,

using the proposed method. The dissolution profiles of both products are presented in Fig. 4.

TABLE V. Robustness study of the HPLC assay

Chromatographic parameters	Percent recovery ^{a,b} ±SD
Optimal conditions ^c	99.32±0.7
Variation of the mobile phase flow rate, mL min ⁻¹	
1.0	98.51±0.6
1.4	98.32±1.9
Variation of the buffer : acetonitrile ratio, v/v	
58:44	99.65±0.2
62:40	99.54±1.1
Variation of the injection volume, µL	
18	98.99±1.2
22	100.20±0.4
Variation of column temperature, °C	
28	100.22±0.4
32	100.35±0.8

^aPercent recovery according to the calibration curve obtained under optimal conditions (mean of three injections ± standard deviation); ^beach sample contained 222 µg mL⁻¹ (100 % concentration level); ^cfor the experimental details, see chromatographic conditions in the Experimental part

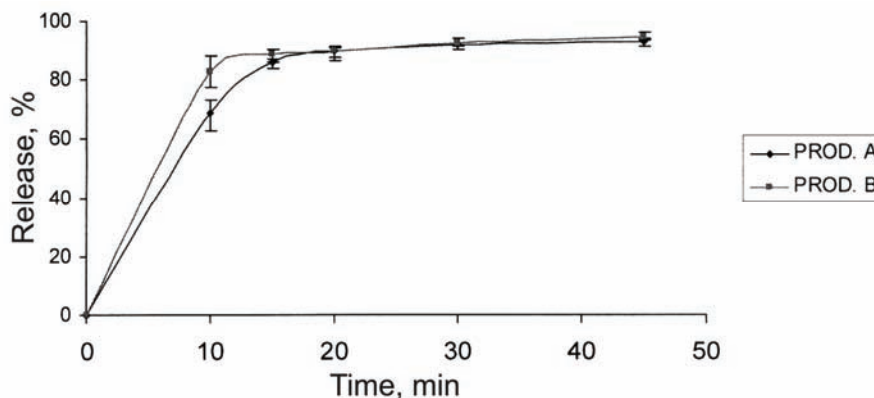


Fig. 4. Dissolution profile of capsule products A and B.

The two capsule products (products A and B) showed a similar dissolution profile with over 85 % dissolution within 15 min (similarity factor $f_2 = 85$). The dissolution profiles were compared by the calculated similarity factor (f_2) derived using the following equation:¹⁴

$$f_2 = 50 \times \log \left\{ 100 \left[1 + \left(\frac{1}{n} \right) \sum_{t=1}^n (R_t - T_t)^2 \right]^{-0.5} \right\} \quad (1)$$

where n is the number of time points, R_t the dissolution value of the reference batch at time t and T_t is the dissolution value of the test batch at time t . Generally, f_2 values greater than 50 (50–100) indicate similarity of the compared dissolution profiles. The USP acceptance limits for the dissolution of mexiletine capsules were not less than 80 % of the labeled amount in 30 min.

CONCLUSIONS

A simple and efficient HPLC method was developed and found to be accurate, precise and linear across the analytical range. The method was suitable for the determination of mexiletine hydrochloride in dissolution samples. The methods may be used to assess the quality of commercially available mexiletine hydrochloride drug products. In addition, a significant advantage of the method is that no additional pretreatment of the samples is required prior to the measuring step, thus accelerating the quality control process. An overall duration of the analysis of less than 11 min was achieved (including sample preparation). The method was used successfully to evaluate the dissolution profiles of two marketed drug products.

ИЗВОД

РАЗВОЈ И ПРИМЕНА ВАЛИДИРАНЕ HPLC МЕТОДЕ ЗА АНАЛИЗУ ДИСОЛУЦИОНИХ УЗОРАКА МЕКСИЛЕТИН-ХИДРОХЛОРИДА ИЗ КАПСУЛА

ДРАГАН М. МИЛЕНОВИЋ¹ и ЗОРАН Б. ТОДОРОВИЋ²

¹"Здравље-Actavis", Одељење аналитичког развоја, Центар за Истраживање и Развој, Влајкова 199, 16000 Лесковац и ²Технолошки факултет, Универзитет у Нишу, Булевар ослобођења 124, 16000 Лесковац

Циљ овог рада је био развити и валидирати једноставну, ефикасну, осетљиву и селективну методу за анализу узорака мексилетин-хидрохлорида добијених растварањем активне супстанце из капсула помоћу HPLC без претходне посебне припреме узорака (екстракције, разблаживања, упаравања, итд.). Сепарација је изведена са 5 μm LiChrospher 60, RP-Select В колоном (250 \times 4 mm, 5 μm), са мобилном фазом пуфер–ацетонитрил (60:42, в/в) изократским елуирањем за мање од 10 min са протоком од 1,2 mL min⁻¹. Узорци су детектовани на 262 nm. Линеарност је испитана у концентрационом подручју од 50–300 $\mu\text{g mL}^{-1}$ ($r^2 = 0,9998$). Валидационе карактеристике укључују тачност, прецизност, линеарност, специфичност, лимите детекције и квантификавања, стабилност и робустност. Валидациони критеријуми прихватљивости су постигнути у свим случајевима (реCOVERУ вредност се креће у опсегу од 100,01 до 101,68 %, RSD < 0,44 %). Метода се може користити за одређивање активне супстанце у узорцима након растварања мексилетин-хидрохлорида из капсула.

(Примљено 28. јула 2009, ревидирано 16. фебруара 2010)

REFERENCES

1. S. Kaushik, K. S. Alexander, *J. Liq. Chromatogr. Related Technol.* **26** (2003) 1287
2. *The Japanese Pharmacopoeia XIII*, Official Monographs for Part I, 1996, p. 515
3. Y. Liu, L. Sun, X. Di, Y. Sun, [C. A. 147/2007 249850]
4. H. Zhang, C. Yu, G. Liu, J. Jia, Y. Hong, X. Xu, [C. A. 141/2003 301594]

5. D. K. W. Kwok, L. Igwemezie, C. R. Kerr, K. M. McErlane, *J. Chromatogr. B* **661** (1994) 271
6. Z. Abolfathi, P. M. Belanger, M. Gilbert, J. R. Rouleau, J. Turgeon, *J. Chromatogr.* **579** (1992) 366
7. H. Liu, F. Feng, M. Ma, S. Cui, D. Xie, S. Xu, *J. Chromatogr. B* **858** (2007) 42
8. R. Pietras, D. Kowalczyk, H. Hopkala, *Chromatographia* **60** (2004) 17
9. *The United States Pharmacopoeia*, 31th ed., Official Monographs, USA, 2008, p. 2708
10. E. Lamparter, *J. Chromatogr. A* **635** (1993) 155
11. R. Pietras, D. Kowalczyk, H. Hopkala, *J. AOAC Int.* **90** (2007) 977
12. Z. Aydogmus, S. M. Cetin, S. Tosunoglu, *Turk. J. Chem.* **26** (2002) 839
13. A. M. El Walily, F. A. El Yazbi, S. F. Belal, O. Abdel Razak, *Anal. Lett.* **30** (1997) 2029
14. P. D. Tzanavaras, C. K. Zacharis, P. Rigas, *J. Pharm. Biomed. Anal.* **48** (2008) 1254
15. A. Gupta, A. B. Ciavarella, V. A. Sayeed, M. A. Khan, P. J. Faustino, *J. Pharm. Biomed. Anal.* **46** (2008) 181
16. C. V. Garcia, C. S. Paim, M. Steppe, E. E. S. Schapoval, *J. Pharm. Biomed. Anal.* **41** (2006) 833
17. E. Banoglu, Y. Özkan, O. Atay, *Il Farmaco* **55** (2000) 477
18. A. Savaser, S. Goral, A. Taso, B. Uslu, H. Lingeman, S. A. Özkan, *Chromatographia* **65** (2007) 259
19. P. D. Tzanavaras, A. Verdoukas, D. G. Themelis, *Anal. Sci.* **21** (2005) 1515
20. Y. Özkan, A. Savaser, S. A. Özkan, *J. Liq. Chromatogr. Related Technol.* **28** (2005) 423
21. C. M. B. Rolim, L. Brum, Jr., M. Fronza, M. D. Malesuik, L. Bajerski, S. L. Dalmora, *J. Liq. Chromatogr. Related Technol.* **28** (2005) 477
22. *International Conference on Harmonization Q2 (R1), Validation of Analytical Procedures, Text and Methodology*, <http://www.ich.org/LOB/media/MEDIA417.pdf> (accessed 20 April, 2009).



J. Serb. Chem. Soc. 75 (7) 987–996 (2010)
JSCS–4024

A study on the microstructure of a nitrate ester plasticized polyether propellant dissolved in HCl and KOH solutions

YONG LIU^{1,2*}, LUOXIN WANG³, XINLIN TUO², SONGNIAN LI^{1,2} and WEIMIN YANG¹

¹College of Mechanical and Electrical Engineering, Beijing University of Chemical Technology, Beijing 100029, ²Department of Chemical Engineering, Tsinghua University, Beijing 100084 and ³Wuhan University of Science and Engineering, Key Laboratory of Green Processing and Functional Textiles of New Textile Materials, Ministry of Education, Wuhan 430073, China

(Received 9 October 2009, revised 19 January 2010)

Abstract: Understanding of how the properties and performance of nitrate ester plasticized polyether (NEPE) propellants relate to microstructure is complicated by numerous components that have different characteristics. One approach to alleviating these complications is to observe a microstructure that has lost one or several components. This article examines the dissolution process, mass loss and change of the ion concentration of propellants in acid and alkali solutions. A scanning electron microscope was used to observe the dissolved residual of the propellants. The results revealed that the main constituents of NEPE propellant have different dissolving properties in solutions of HCl and KOH. By monitoring the dissolution process of NEPE propellant in HCl and KOH solutions, it was found that the microstructure of the propellant is generally compact and the polymer binder not only binds all the other components, but also protects the inner part of the propellant in solution.

Keywords: NEPE propellants; microstructure; interfaces; scanning electron microscope (SEM); swelling.

INTRODUCTION

Nitrate ester plasticized polyether (NEPE) propellants are high-energetic composite solid propellants that use a polyether, such as polyethylene glycol (PEG) or an ethylene oxide–tetrahydrofuran co-polyether, as a polymeric binder, and mixed nitrates (BG), usually 1,2,4-butanetriol trinitrate nitrate (BTTN) and nitroglycerin (NG), as plasticizer. Large amounts of solid particles, such as aluminum powder (Al), octogen or cyclotetramethylene-tetranitramine (HMX) and ammonium perchlorate (AP) are contained in the propellants.^{1,2} This type of propellant integrates the advantages of double-base propellants and composite pro-

* Corresponding author. E-mail: yongsd@iccas.ac.cn
doi: 10.2298/JSC091009073L

pellants, and adds excellent low temperature mechanical properties. Therefore, this type has been studied extensively and applied broadly in many countries since it was first developed in the USA in the 1970s.^{3,4} However, the microstructure of the propellant, which decisively affects its performance, has not been clearly studied.⁵⁻⁷ To obtain more energy or decrease the sensitivity of a NEPE propellant, it is necessary to obtain detailed characteristics of the microstructure of the propellant in advance. An NEPE propellant is a kind of composite containing many components. Through the study of solution processes and the specialty in different solvents, the state of different materials in the composite can be deduced. This is another way to obtain knowledge about the structural characters of a composite besides direct observation. Based on a former study concerning the microstructure and dissolution differences of a NEPE propellant in water and trichloromethane,⁸ the present article sequentially studies the dissolution differences of the propellant in HCl and KOH solutions and examines the dissolution peculiarities of different components of the propellant. Through these studies, it was expected that the microstructures of the propellant could be understood more thoroughly.

EXPERIMENTAL

The main constituents of the studied solid propellant, which was taken from a rocket, were PEG, BG, Al, HMX and AP in the approximate mass percentages 6–9, 15–21, 19, 43 and 8, respectively. The content of the other auxiliary agents, such as the crosslinking agent, was about 1–2 %.

The HCl and KOH employed in the dissolution experiments were analytically pure reagents. All the water used in the present study was distilled water.

The concentrations of NH_4^+ , Al^{3+} and AlO_2^- in the HCl and KOH solutions were measured using a Metrohm 761 Compact Ion Chromatograph (IC) (Switzerland) and Varion Vista-MPX inductively coupled plasma-atomic emission spectrometer (ICPES) (USA).

The microstructure of the NEPE was observed using a Hitachi S-4500 scanning electron microscope (SEM) (Japan). The samples were sprayed with gold for 5 min before observation.

RESULTS AND DISCUSSION

Solubility of the NEPE propellant in HCl

Concentrated HCl (36.5 %) (10 ml) was diluted with water (40 ml) in a beaker; five NEPE propellant samples, each about 2 mm×2 mm×1 mm, were put into the diluted HCl. Five days later, the samples had broken up into a powder. A translucent film had appeared on the bottoms of the beakers. Some small bubbles were observed in the film and small dust-like particles floated on the surface of the solutions. The powders were observed with the SEM; the morphology is shown in Fig. 1. For comparison, the SEM microphotograph of original NEPE propellant is presented in Fig. 2.⁸

Comparing Figs. 1 and 2, it is apparent that only solid particles were stacked in Fig. 1, while a film covered almost all the solid particles in Fig. 2. This phe-

nomenon can be attributed to the fact that the polymer binder in the NEPE propellants broke down into small molecules, such as ethylene glycol, in the HCl solution. After the polymer chains had decomposed into fragments, the solid particles, such as AP, HMX and Al, which had been bonded by the chains, fell to pieces and then became powder. The dust particles on the solution surface may be very small solid particles that had a relatively large specific surface area. These small particles collected together and floated on the liquid surface because they were subjected to strong surface tension. To confirm this deduction, some Al powder was put into dilute HCl. A little Al powder floated on the surface even after vigorous shaking, which validates the above supposition. The solid component HMX is a chemically stable material that generally does not react with dilute HCl or KOH at normal temperatures.⁹ The AP and Al particles can react with dilute HCl and dissolve into the solution:^{10,11}

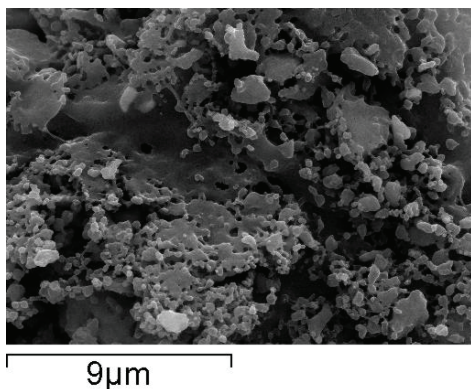
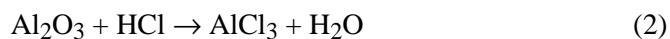
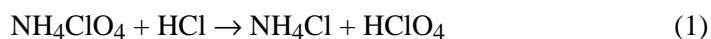


Fig. 1. SEM Image of the NEPE propellant powder treated with HCl solution.

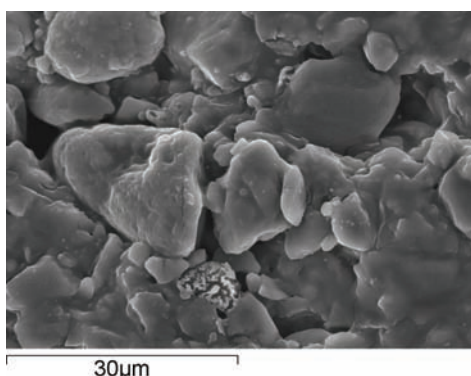


Fig. 2. SEM Image of the untreated NEPE propellant.

However, the quantity of these two reagents was large and the reactions are slow. As a result, at the end of the experiment, some of the AP and Al particles remained. For this reason, Fig. 1 shows small balls (Al), particles with a scraggy surface (AP) and numerous middle-size particles (HMX).⁸ The densities of the liquid plasticizers NG and BTTN are both greater than water. In addition, the plasticizers both are barely dissolved in water and HCl, hence they formed a translucent film at the bottom of the beakers. As some components react with HCl and produce gases such as H₂, some mini bubbles appeared in the film.

Information about the mass loss of a composite material in solution will reflect to some extent the microstructure of the composite, especially when the components have specific solubility in different solutions. The mass loss experiment with NEPE propellants in dilute HCl was performed as follows:

1. The propellant was cut into samples about 2 mm×1.5 mm×1 mm, weighed, and put into 5 weighing bottles.
2. Five ml 0.042 mol L⁻¹ HCl was put into each bottle.
3. The solution was poured out from each bottle after a certain interval.
4. The bottles with their remaining solution were dried at 30 °C for 24 h.
5. The residues were weighed and the mass losses were calculated and the results are shown in Fig. 3.

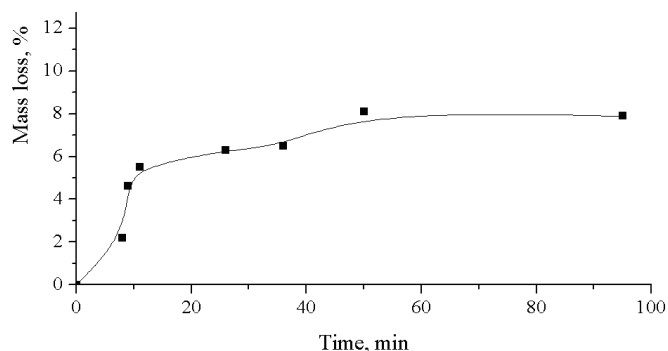


Fig. 3. Mass loss curve of the NEPE propellant soaked in dilute HCl.

From the mass loss curve in Fig. 3, it can be seen that at the initial stage (about 0–10 min) the propellant dissolved very quickly. During the second period (about 10–50 min), the dissolution slowed. Finally, after about 50 min, almost no components were dissolving. Considering the previous solubility of the components NEPE propellants in more concentrated HCl, the reason for the mass loss curve may be that when the small propellant particles are put into dilute HCl, the AP and Al on the surface dissolve quickly, but the polymer binder reacts with the HCl very slowly. About 10 minutes later, the inner AP and Al begin to dissolve, but the outer binder forms a protective covering that blocked the reaction of the

inner AP and Al with the HCl; hence the mass loss became slower and slower. By the end of the process, the dissolution reached a balance.

To examine the solubility of large NEPE propellant samples in dilute HCl, a 9.7 mm×10 mm×10.5 mm propellant cube was put into 500 ml 0.042 mol L⁻¹ HCl solution. The solution was stirred continuously and 1 ml aliquots were taken at intervals to measure, using the IC and ICPEs, the concentration of NH₄⁺ and Al³⁺ in the solution. The results are shown in Fig. 4.

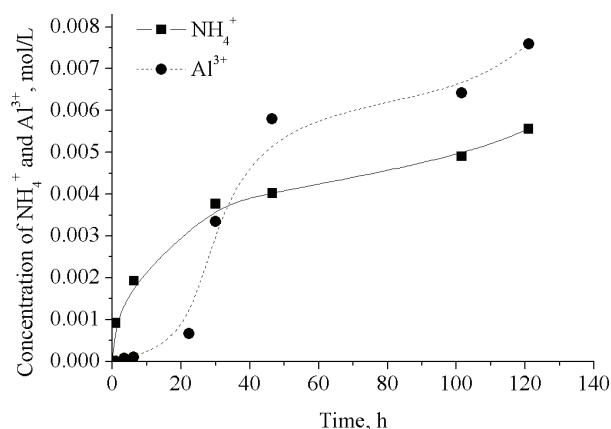


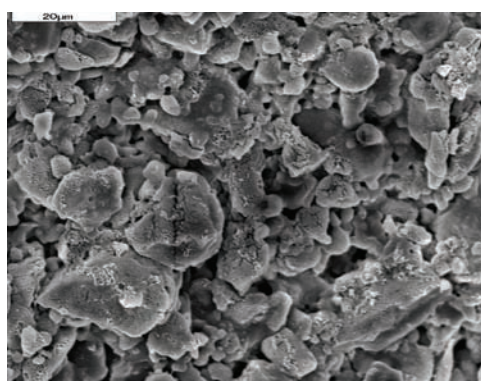
Fig. 4. Curves of the change in the concentrations of NH₄⁺ and Al³⁺ in dilute HCl with time.

From Fig. 4, it is apparent that the curve of NH₄⁺ concentration increased rapidly because the AP readily dissolved in the HCl solution. After the outer AP had dissolved, the rate of increase of the NH₄⁺ concentration slowed, illustrating that the polymer binder in the outer part blocked the HCl solution from entering the propellant. In contrast, the curve of the Al³⁺ concentration in Fig. 4 can be divided into three stages. During the first stage (about 0–20 h), the increase of the Al³⁺ concentration was slow. The reason may be that there was an oxide film on the Al surface, which reacted with HCl slowly and protected the inner Al. Thus, after the oxide film had been dissolved, the inner Al reacted rapidly with the HCl. As a result, the concentration of Al³⁺ increased very rapidly in the second stage (about 20–50 h). After the AP and Al in the surface layer of the propellants had dissolved, the polymer binder reacted with the dilute HCl very slowly and became a protective cover to the inner contents. The binder cover blocked the penetration of HCl into the propellant; for this reason, at the third stage (after about 50 h), the concentration of both Al³⁺ and NH₄⁺ increased slower and slower.

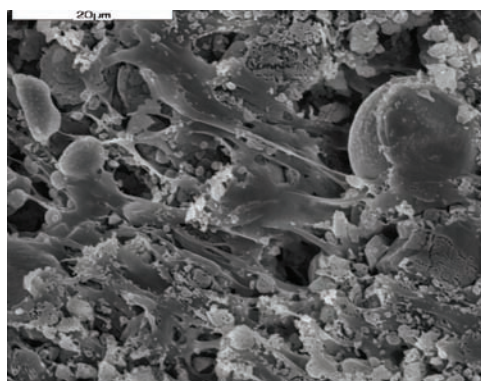
Solubility of the NEPE propellant in KOH solution

Similar to the experiment of NEPE propellants dissolved in HCl, a 2 mm×2 mm×1 mm NEPE propellant sample was put into 0.022 mol L⁻¹ KOH solution. The sample floated in the solution just under the surface of the liquid. About 24 h

later, a corner of the sample appeared to swell, and some mini blobs appeared on the sample. Four days later, the outer layer of the sample became translucent, like a gel. The color of the solution became yellowish. Six days later, the whole sample had swelled, and some mini pores could be observed on the surface of the sample. Some particles were suspended in the solution and the yellowish color deepened. After fourteen days, the sample was taken out, dried, and observed by SEM. The results are shown in Fig. 5.



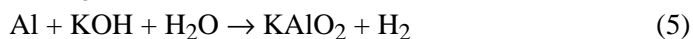
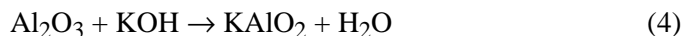
(a)



(b)

Fig. 5. SEM images of the NEPE propellant soaked in KOH solution, a) surface of the sample; b) interior of the sample.

The propellant sample may have a relatively strong surface tension in alkaline solutions, hence the sample floated in the solution near the surface. Initially, the polymer binder absorbed water and swelled, and then it reacted slowly with the KOH. This was the cause of the swell. A few polymer binders appeared on the surface, as shown in the SEM image (Fig. 5a). Both Al and its oxide film Al_2O_3 can react with KOH and then dissolve in the solution:



Finally, the reactions created a flock of $\text{Al}(\text{OH})_3$ sedimentation. These suspensions in solution caused the slight amount of ball-like Al that can be seen in Fig. 5a. HMX and AP are crystals and perhaps react with KOH very slowly; hence, after the grey Al had disappeared, the outer sample became translucent. It can be seen from Fig. 5a that many big scraggy particles (AP) and small, smooth particles (HMX) appeared on the image.⁸ Due to the swell and the dissolution of some components, mini pores became visible on the surface of the sample. The plasticizers BTTN and NG are yellow oil-like liquids. They hardly dissolve in a dilute alkali solution at normal temperature, hence the solution did not immediately become yellowish. However, over a long time period, the plasticizer dissolved a little and then the solution became yellow. Comparing Figs. 5a and 5b, the difference is apparent in that there are more polymer binders and ball-like Al in Fig. 5b, although the sample plumped. Thus, it can be concluded that the Al components reacted with difficulty with KOH under these conditions.

The mass loss experiment of the NEPE propellant in KOH was performed in exactly the same manner as that in HCl. The results are shown in Fig. 6.

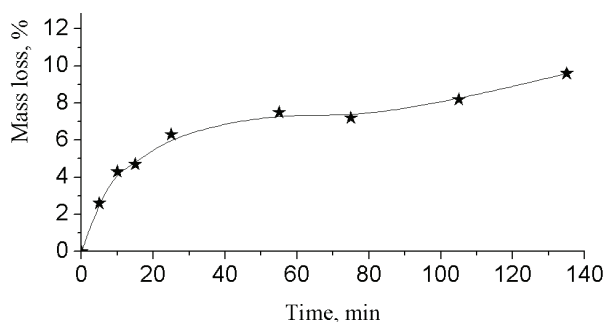


Fig. 6. Mass loss curve of the NEPE propellant soaked in KOH solution.

From the mass loss curve presented in Fig. 6, the dissolution process can be described as follows: when the small particles of propellants were soaked in KOH solution, the AP and Al on the surface layer of propellants promptly began to dissolve, hence the initial mass loss (about 0–20 min) was fast. Then during the following period (about 20–75 min) the dissolution proceeded more and more slowly. The possible reason was that the amount of AP and Al on the surface layer decreased on the one hand and the outer polymer binder blocked the KOH solution from entering the propellant on the other. However, because the propellant solution appeared to swell in KOH during the last period (after 75 min), the inner AP and Al began to dissolve again. The mass loss increased during the third stage.

The solubility of a cube of NEPE propellant (10 mm×10 mm×10 mm) in KOH solution was also examined in the same manner as in HCl. The change of the concentrations of NH_4^+ and AlO_2^- are shown in Fig. 7.

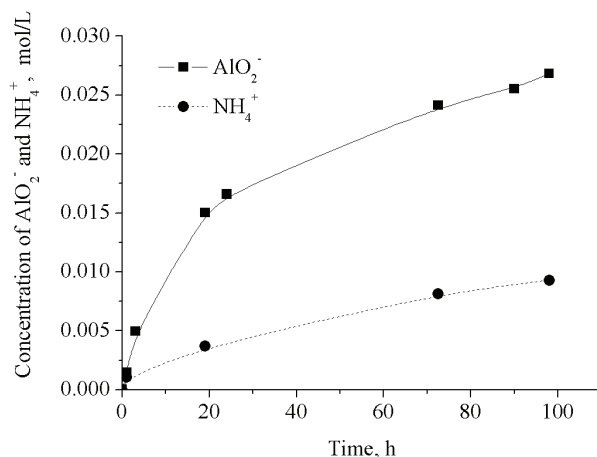


Fig. 7. Curve of the changes in the concentration of NH_4^+ and AlO_2^- in KOH solution with time.

Comparing Fig. 4 and Fig. 7, the change of the NH_4^+ concentration was different. The curve of the concentration of NH_4^+ in Fig. 7 is smooth and shows almost no major changes, while in Fig. 4, the curve changes abruptly during the initial stage, which illustrates that AP is a little difficult to dissolve in KOH. Another reason may be related to the swell of the sample, which allowed relatively greater contact between AP and the KOH solution. Thus, the amount of AP reacting with KOH changed little. The curve of AlO_2^- concentration in Fig. 7 is not like that of Al^{3+} in Fig. 4; it is rather like that of NH_4^+ in Fig. 4. This may be attributed to the fact that the oxide film on the surface of the Al particles reacted more easily than the inner Al with KOH. For this reason, the concentration of AlO_2^- increased faster during the initial 20 h than it did later.

CONCLUSIONS

From the results obtained in this study, the following conclusions can be drawn.

- i)* The NEPE propellant disaggregates in concentrated HCl. In contrast, it swells in a KOH environment, which leads to a loosening of the microstructure.
- ii)* The polymer binder does not react easily with HCl or KOH, and it forms a protective layer around the inner AP and Al particles. Hence the binder in the outer layer results in the interior of the propellant retaining an intact structure.
- iii)* The AP particles dissolve easily in dilute HCl or KOH solutions, while the Al powder has a better solubility in KOH solution than in HCl. The reason

may be that the oxide film on the Al surface is easier to remove in KOH solution than in HCl. The dissolution of the two materials would destroy the structure of the propellant.

iv) The dissolution mechanism of AP is different for big cubes of propellants in HCl and KOH. The swell of the propellant in KOH may be the main reason. More knowledge about the microstructure of the propellants may be obtained by comparing the solubilities of NEPE propellants in HCl and KOH.

Acknowledgements. This work was supported by the China Post-doctor Science Foundation (No. 20060390431).

ИЗВОД

АНАЛИЗА МИКРОСТРУКТУРЕ ЕКСПЛОЗИВА НА БАЗИ НИТРАТНИХ ЕСТАРА ПЛАСТИФИКОВАНИХ ПОЛИЕТРИМА И ТРЕТИРАНИХ РАСТВОРИМА HCl И KOH

YONG LIU^{1,2}, LUOXIN WANG³, XINLIN TUO², SONGNIAN LI^{1,2} и WEIMIN YANG¹

¹College of Mechanical and Electrical Engineering, Beijing University of Chemical Technology, Beijing 100029 ²Department of Chemical Engineering, Tsinghua University, Beijing 100084 и ³Wuhan University of Science and Engineering, Key Laboratory of Green Processing and Functional Textiles of New Textile Materials, Ministry of Education, Wuhan 430073, China

Разумевање утицаја микроструктуре на својства и примену композитних експлозива на бази нитратних естара пластификованих полиетрима (NEPE) је веома компликовано јер се састоје од великог броја компоненти различитих карактеристика. Један од начина да се поједностави поступак изучавања микроструктуре је да се уклони једна или више компоненти из композита. У овом раду је приказан поступак растварања NEPE композитних експлозива, праћен губитком масе као и променом концентрације јона у киселој и базној средини. Скенирајућа електронска микроскопија (SEM) је коришћена за анализу микроструктуре у раствору преосталог композита. Резултати су показали да се основне компоненте композитних експлозива различито растварају у киселој и базној средини. Анализом процеса растварања NEPE композитних експлозива у HCl и KOH растворима је показано да је структура композита углавном компактна и да улога полимерног везива није само да повезује компоненте композита већ и да штити унутрашње делове честица у раствору.

(Примљено 9. октобра 2009, ревидирано 19. јануара 2010)

REFERENCES

1. T. H. Zhang, Y. L. Bai, S. Y. Wang, P. D. Liu, *Propellants Explos. Pyrotech.* **28** (2003) 37
2. G. A. Butcher, AIAA 90-2524, AIAA/SAE/ASME/ASEE 26th Joint Propulsion Conference, Florida, CA, USA, 1990, p. 125
3. S. W. Beckwith, H. B. Carroll, *J. Spacecr. Rockets* **22** (1985) 156
4. F. T. Chen, Y. Q. Duo, S. G. Luo, Y. J. Luo, H. M. Tan, *Propellants Explos. Pyrotech.* **28** (2003) 7
5. F. Xu, N. Aravas, P. Sofronis, *J. Mech. Phys. Solids* **56** (2008) 2050
6. A. H. Lepie, A. Adicoff, *J. Appl. Polym. Sci.* **18** (1974) 2165
7. R. Manjari, L. P. Pandureng, U. I. Somasundaran, T. Sriram, *J. Appl. Polym. Sci.* **51** (1994) 435
8. Y. Liu, L. X. Wang, X. L. Tuo, S. N. Li, *J. Serb. Chem. Soc.* **75** (2010) 369

9. T. S. Ren, *Chemistry and industry technology of nitramines and nitric acid ester explosive*, Weapon Industry Press, Beijing, 1994, p. 1
10. L. Meda, G. Marra, L. Galfetti, S. Inchingalo, F. Severini, L. D. Luca, *Compos. Sci. Technol.* **65** (2005) 769
11. L. Meda, G. Marra, L. Galfetti, F. Severini, L. D. Luca, *Mater. Sci. Eng. C* **27** (2007) 1393.



J. Serb. Chem. Soc. 75 (7) 997–1003 (2010)
JSCS–4025

NOTE

Reliable prediction of heat of vaporization of *n*-alkanes at 298.15 K

JOVAN D. JOVANOVIĆ and DUŠAN K. GROZDANIĆ*

*Faculty of Technology and Metallurgy, University of Belgrade, Karnegijeva 4,
11000 Belgrade, Serbia*

(Received 23 November 2009, revised 3 March 2010)

Abstract: A reliable model for the prediction of the heat of vaporization for *n*-alkanes at 298.15 K with the number of carbon atoms and normal boiling point as the only input parameters is recommended. The new model is compared with other literature models and was found to give the best results with absolute mean percentage deviation of 0.81 % and maximum absolute percentage deviation of 2.93 %.

Keywords: heat of vaporization; *n*-alkanes; prediction; model.

INTRODUCTION

The heat of vaporization, or enthalpy of vaporization, is the difference between the enthalpy of a saturated vapor and that of a saturated liquid at the same pressure and temperature. Heats of vaporization at the temperature $T = 298.15$ K, $\Delta H_{v,298}$, are essential parameters in thermodynamic studies. In many calculations associated with process design and simulation, it is necessary to know the physical and thermodynamic properties of pure compounds, including their heat of vaporization. The accurate prediction of the heat of vaporization $\Delta H_{v,298}$ for hydrocarbon fluids is of particular interest in the petroleum industry.

The objective of this work was to develop a reliable predictive model for the estimation of the heat of vaporization $\Delta H_{v,298}$ of *n*-alkanes.

EXISTING MODELS

Many prediction models for the heat of vaporization have been proposed in the past. The majority of these models are applicable only at $T = 298.15$ K, or to a specific group of compounds. Most of the later ones are applicable only to *n*-alkanes. In these models, the critical temperature, T_c , critical pressure, p_c , triple point temperature, T_t , normal boiling point, T_b , and heat of vaporization at the

* Corresponding author. E-mail: dule@tmf.bg.ac.rs
doi: 10.2298/JSC091123067J

normal boiling point, ΔH_{vb} , as well as molar weight, M , and number of carbon atoms, n_c , are the input parameters.

NEW MODEL

Experimental values for many of the above-mentioned input parameters for higher n -alkanes are non-existent. However, experimental normal boiling point, T_b , is usually a known and a reliable parameter.

The experimental calorimetric heat of vaporization data for n -alkanes at 298.15 K and the experimental normal boiling points used are listed in Table I.

TABLE I. Experimental data

Compound	n_c	T_b / K	$\Delta H_{v,exp} / J mol^{-1}$	Ref.
Pentane	5	309.2	26423.1	1
			26427.0	2
			26217.7	3
			26870.0	4
			26628.0	5
Hexane	6	341.9	31550.0	6
			31568.5	7
			30993.6	8
			31545.5	1
Heptane	7	371.6	36580.0	6
			36542.4	1
			36547.0	9
			36610.0	4
Octane	8	398.8	41470.0	6
			41528.9	10
			41478.8	1
			41616.8	11
			40988.8	12
			41491.2	13
			41449.3	13
			41491.2	14
			41340.0	15
			41491.2	16
Nonane	9	424.0	46431.6	1
			46420.0	4
Decane	10	447.3	51380.4	10
			51358.8	1
			50241.6	12
			50116.0	12
			51288.3	13
			51037.1	13
			50702.1	13
			50576.5	13
50450.9	13			
			51380.0	17

TABLE I. Continued

Compound	n_c	T_b / K	$\Delta H_{v,exp} / J mol^{-1}$	Ref.
Decane			51390.0	18
			51360.0	19
Undecane	11	469.1	56471.6	10
			56312.5	13
			56019.4	13
			55935.6	13
			55475.1	13
			55768.2	13
			55517.0	13
			56440.0	17
Dodecane	12	489.1	56770.0	20
			61780.0	21
			61336.6	22
			59536.3	12
			60876.1	13
			60499.3	13
			60457.4	13
			60331.8	13
Tridecane	13	508.6	61270.0	18
			66402.6	22
Tetradecane	14	526.7	71133.7	22
			68998.5	12
			68789.9	12
			68705.4	12
			70463.8	13
			70338.2	13
			69668.3	13
			69584.6	13
Pentadecane	15	543.8	71008.1	23
			76241.6	22
			76800.0	24
Hexadecane	16	560.0	81433.3	22
			81400.0	24
			67993.6 ^a	12
			70673.2 ^a	12
			79716.7	13
			78711.8	13
			79591.1	13
			78586.2	13
80700.0	25			
Heptadecane	17	575.2	80600.0	20
			86080.6	22
			86500.0	24
Octadecane	18	589.9	91400.0	24
Nonadecane	19	603.0	96400.0	24
Eicosane	20	617.0	101800.0	24

TABLE I. Continued

Compound	n_c	T_b / K	$\Delta H_{v,\text{exp}} / \text{J mol}^{-1}$	Ref.
Heneicosane	21	629.7	109400.0 ^a	24
			106800.0	26
Docosane	22	641.8	115600.0 ^a	24
			111900.0	26
Tricosane	23	653.2	120500.0 ^a	24
			117000.0	26
Tetracosane	24	664.5	125600.0 ^a	24
			121900.0	26
Pentacosane	25	675.1	126900.0	24
			126800.0	26
Hexacosane	26	685.0	139100.0 ^a	24
			131700.0	26
Heptacosane	27	695.4	145100.0 ^a	24
			135600.0	26
Octacosane	28	704.8	151400.0 ^a	24
			141900.0	26
Nonacosane	29	714.0	147100.0	26
			162900.0 ^a	24
Triacontane	30	722.9	152300.0	26
			157300.0	27
Hentriacontane	31	732.2 ^b	157300.0	27
Dotriacontane	32	740.2	162500.0	27
Tritriacontane	33	748.5 ^b	167600.0	27
Tetratriacontane	34	756.0	172700.0	27
Pentatriacontane	35	763.2	178100.0	27
Hexatriacontane	36	771.0	182900.0	27
Heptatriacontane	37	778.0	187600.0	27
Octatriacontane	38	785.0	192700.0	27

^aNot used in the correlation; ^bestimated by the Kreglewski–Gamba–Soave–Pellegrini method²⁸

Data from Table I were used for the development of a reliable predictive model for the estimation of the heat of vaporization, $\Delta H_{v,298}$, of n -alkanes:

$$\Delta H_{v,298}[\text{J/mol}] = 5684.27 + 5295.41n_c - 17.2732T_b \quad (1)$$

RESULTS AND DISCUSSION

The estimation capability of the new model was compared with that of other models and the results are presented in Table II. The absolute mean percent deviation is defined as:

$$p_{\text{av}} = (100 / N) \sum_{i=1}^N |(\Delta H_{v,298,\text{exp}} - \Delta H_{v,298,\text{cal}}) / \Delta H_{v,298,\text{exp}}| \quad (2)$$

The maximum absolute percent deviations are listed in the last column of Table II. The results presented in Table II indicate that the new model is the best predictive model for heat of vaporization of n -alkanes at 298.15 K.

Table II. Comparison of the Models

Model	Input parameters	$p_{av} / \%$	$p_{max} / \%$
Dunkel ²⁹	GC^a	7.66	14.83
Laidler-Lovering-Nor-McCurdy ³⁰⁻³³	GC	1.25	3.09
Klages ³⁴	T_b	14.47	48.23
Klages-Wadsö ³⁵	T_b	10.99	43.54
Abramzon ³⁶	GC	2.57	6.91
Wall-Flynn-Straus ³⁷	n_c	7.43	27.38
Morawetz ²²	n_c	0.87	3.78
Månsson-Sellers-Stridh-Sunner ³⁸	n_c	0.92	3.68
Ducros-Gruson-Sannier ³⁹⁻⁴²	GC	0.95	3.47
Chickos-Hyman-Ladon-Liebman I ⁴³	n_c	3.83	7.03
Chickos-Hyman-Ladon-Liebman II ⁴³	nc	2.89	6.67
Guthrie-Taylor I ⁴⁴	GC	1.06	3.17
Guthrie-Taylor II ⁴⁴	GC	1.51	5.06
Constantinou-Gani ⁴⁵	GC	3.19	10.65
Chickos-Wilson ²⁴	n_c	3.55	10.43
Marano-Holder ⁴⁶	n_c	0.92	3.57
Phillips ⁴⁷	M	10.58	26.46
Marrero-Gani ⁴⁸	GC	1.12	3.47
Chickos-Hanshaw ²⁷	n_c	0.92	4.22
Kolská-Růžička-Gani ⁴⁹	GC	2.56	8.23
This model	n_c, T_b	0.81	2.93

^aGroup contributions

CONCLUSIONS

The experimental values of the heat of vaporization of *n*-alkanes at 298.15 K, together with appropriate literature predictive models are reviewed in this work. A new reliable predictive model with two input parameters was developed. The obtained results indicate that the model with only two input parameters, one structural (n_c) and one property (T_b) parameter, gave a more reliable prediction of the heat of vaporization than the model with only one input parameter.

Acknowledgement. The authors gratefully acknowledge the financial support received from the Research Fund of the Ministry of Science and Technological Development of the Republic of Serbia and the Faculty of Technology and Metallurgy, University of Belgrade (project No 142064).

NOMENCLATURE

n_c	Number of carbon atom
M	Molar weight, g mol ⁻¹
T_t	Triple point temperature, K
T_c	Critical temperature, K
p_c	Critical pressure, bar
ω	Acentric factor
ΔH_{vb}	Heat of vaporization at normal boiling point, J mol ⁻¹
$\Delta H_{v,298}$	Heat of vaporization at 298.15 K, J mol ⁻¹

N	Number of data points
p_{av}	Absolute mean percent deviation, %
p_{max}	Maximum absolute percent deviation, %

ИЗВОД

ПОУЗДАН МОДЕЛ ЗА ПРЕДСКАЗИВАЊЕ ТОПЛОТЕ
ИСПАРАВАЊА n -АЛКАНА НА 298,15 К

ЈОВАН Д. ЈОВАНОВИЋ и ДУШАН К. ГРОЗДАНИЋ

Технолошко–металурички факултет, Универзитет у Београду, Карнегијева 4, 11000 Београд

У овом раду предложен је поуздан модел за процену вредности топлоте испаравања n -алкана на температури 298,15 К са бројем угљеникових атома и нормалном температуром кључања, као јединим потребним вредностима. Предложени модел упоређен је са постојећим одговарајућим моделима и дао је најбоље, како средње процентуално одступање 0,81 %, тако и најмању вредност максималног процентуалног одступања 2,93 %.

(Примљено 23. новембра 2009, ревидирано 3. марта 2010)

REFERENCES

1. N. S. Osborne, D. C. Ginnings, *J. Res. NBS* **39** (1947) 453
2. A. Hossenlopp, D. W. Scott, *J. Chem. Thermodyn.* **13** (1981) 415
3. G. H. Messerly, R. M. Kennedy, *J. Am. Chem. Soc.* **62** (1940) 2988
4. R. Fuchs, L. A. Peacock, *Can. J. Chem.* **58** (1980) 2796
5. R. Fuchs, L. A. Peacock, W. K. Stephenson, *Can. J. Chem.* **60** (1982) 1953
6. V. Majer, V. Svoboda, S. Hála, J. Pick, *Coll. Czech. Chem. Comm.* **44** (1979) 637
7. G. Waddington, D. R. Douslin, *J. Am. Chem. Soc.* **69** (1947) 2275
8. J. F. Lemons, W. A. Felsing, *J. Am. Chem. Soc.* **65** (1943) 46
9. T. B. Douglas, G. T. Furukawa, R. E. McCoskey, A. F. Ball, *J. Res. NBS* **53** (1954) 139
10. I. Wadsö, *Acta Chem. Scand.* **20** (1966) 536
11. I. Wadsö, *Acta Chem. Scand.* **14** (1960) 566
12. E. Morawetz, S. Sunner, *Acta Chem. Scand.* **17** (1963) 473
13. E. Morawetz, *Acta Chem. Scand.* **22** (1968) 1509
14. R. M. Varushchenko, G. L. Gal'chenko, V. A. Medvedev, *Zh. fiz. khim.* **51** (1977) 992
15. J. O. Fenwick, D. Harrop, A. J. Head, *J. Chem. Thermodyn.* **7** (1975) 943
16. J. H. Hallman, W. K. Stephenson, R. Fuchs, *Can. J. Chem.* **61** (1983) 2044
17. R. J. Irving, *J. Chem. Thermodyn.* **4** (1972) 793
18. K. Kusano, *Thermochim. Acta* **88** (1985) 109
19. J. Furukawa, M. Sakiyama, S. Seki, Y. Saito, K. Kusano, *Bull. Chem. Soc. Jpn.* **55** (1982) 3329
20. M. A. V. Ribeiro da Silva, M. A. R. Matos, L. M. P. F. Amaral, *J. Chem. Thermodyn.* **27** (1995) 565
21. R. A. Melaugh, M. Mansson, F. D. Rossini, *J. Chem. Thermodyn.* **8** (1976) 623
22. E. Morawetz, *J. Chem. Thermodyn.* **4** (1972) 139
23. V. P. Lebedev, E. A. Miroshnichenko, Y. N. Matyushin, B. P. Larionov, V. S. Romanov, Y. E. Bukolov, G. M. Denisov, A. A. Balepin, Y. A. Lebedev, *Zh. fiz. khim.* **49** (1975) 1928
24. J. S. Chickos, J. A. Wilson, *J. Chem. Eng. Data* **42** (1997) 190

25. M. A. V. Ribeiro da Silva, M. L. C. C. H. Ferrao, F. Jiye, *J. Chem. Eng. Data* **40** (1995) 426
26. J. S. Chickos, W. Hanshaw, *J. Chem. Eng. Data* **49** (2004) 77
27. J. S. Chickos, W. Hanshaw, *J. Chem. Eng. Data* **49** (2004) 620
28. S. Gamba, G. S. Soave, L. A. Pellegrini, *Fluid Phase Equilibria* **276** (2009) 133
29. M. Dunkel, *Z. physik. Chem.* **A138** (1928) 42
30. K. J. Laidler, *Can. J. Chem.* **34** (1956) 626
31. E. G. Lovering, K. J. Laidler, *Can. J. Chem.* **38** (1960) 2367
32. E. G. Lovering, O. M. Nor, *Can. J. Chem.* **40** (1962) 199
33. K. G. McCurdy, K. J. Laidler, *Can. J. Chem.* **41** (1963) 1867
34. F. Klages, *Ber.* **82** (1949) 358
35. I. Wadsö, *Acta Chem. Scand.* **20** (1966) 544
36. A. A. Abramzon, *Zh. prikl. khim.* **40** (1967) 2598
37. L. A. Wall, J. H. Flynn, S. Straus, *J. Phys. Chem.* **74** (1970) 3237
38. M. Månsson, P. Sellers, G. Stridh, S. Sunner, *J. Chem. Thermodyn.* **9** (1977) 91
39. M. Ducros, J. F. Gruson, H. Sannier, *Thermochim. Acta* **36** (1980) 39
40. M. Ducros, J. F. Gruson, H. Sannier, *Thermochim. Acta* **44** (1981) 131
41. M. Ducros, H. Sannier, *Thermochim. Acta* **54** (1982) 153
42. M. Ducros, H. Sannier, *Thermochim. Acta* **75** (1984) 329
43. J. S. Chickos, A. S. Hyman, L. H. Ladon, J. F. Liebman, *J. Org. Chem.* **46** (1981) 4294
44. J. P. Guthrie, K. F. Taylor, *Can. J. Chem.* **61** (1983) 602
45. L. Constantinou, R. Gani, *AIChE J.* **40** (1994) 1697
46. J. J. Marano, G. D. Holder, *Ind. Eng. Chem. Res.* **36** (1997) 2399
47. J. C. Phillips, *J. Appl. Polym. Sci.* **70** (1998) 731
48. J. Marrero, R. Gani, *Fluid Phase Equilibria* **183–184** (2001) 183
49. Z. Kolská, V. Růžička, R. Gani, *Ind. Eng. Chem. Res.* **44** (2005) 8436.



J. Serb. Chem. Soc. 75 (7) 1005–1018 (2010)
JSCS–4026

A simulation experiment as a method for the investigation of the mobility of heavy metals from inundated land

DJOKICA PETROVIĆ^{1*#}, MARIJA TODOROVIĆ^{2#}, DRAGAN MANOJLOVIĆ^{2#}
and VOJIN D. KRSMANOVIC^{2#}

¹Vinča Institute, Laboratory for Radioisotopes, P.O. Box 522, 11001 Belgrade and ²Faculty of Chemistry, University of Belgrade, P.O. Box 51, 11158 Belgrade 118, PAK: 105305, Serbia

(Received 17 February 2009, revised 4 May 2010)

Abstract: A simulation experiment was used to study the interaction of river water with different soils (arable land, orchards, meadows, pastures and forestland). The results obtained by sequential extraction before and after the simulation experiment were compared in order to determine the substrates of the heavy metals in inundated land and to evaluate their mobility. Samples of various soils were collected from the region of the future accumulation Lake Bogovina (Serbia) and analysed for ten elements using AAS, GFAAS and ICP. Investigation of the nature of the association of heavy metals and the identification of their substrates were provided by a five-step sequential extraction. Correlation analysis was used as a method for the determination of the substrates for heavy metals. The good correlation among the microelements and certain macroelements indicated the substrates of the microelements. Manganese and iron had a good correlation with most of the microelements. Calcium had only a few correlations with some microelements. Some elements, such as nickel and cadmium, had one substrate before and another after the simulation experiment.

Keywords: zinc; heavy metals; accumulation lake; sequential extraction; inundated soil.

INTRODUCTION

Geochemistry of heavy metals is very important for the prediction of their behaviour in ecosystems, especially for their mobility and sorption processes.^{1–5} The mobility of microelements may be affected by different factors, such as: changes in pH and ionic strength.^{6–9} The action of microorganisms could contribute to a change in the environment and to an increased accessibility of metal ions.

* Corresponding author. E-mail: djpetrovic@vin.bg.ac.rs

Serbian Chemical Society member.

doi: 10.2298/JSC090217061P

The aim of this work was to define the mechanisms that control the geochemical and ecochemical behaviour of heavy metals in the future accumulation Lake Bogovina (Serbia). The future accumulation Bogovina is near RTB (Mining and Melting Corporation – Bor) which discharged large amounts of heavy metals and, therefore, it is important to study the distribution of heavy metals and other parameters in the inundated land that could be important for the quality of water. An investigation of the nature of the associations of heavy metals and the identification of their substrates could contribute to an evaluation of possible mobilizations^{10,11} of heavy metals from future inundated land. The combination of a simulation experiment with sequential extraction was used in order to determine the substrates of heavy metals and evaluate their mobility. The method is new and was recently used in a study of the accumulation Lake Rovni.¹² Special attention was given to zinc, which was relatively abundant and significant amounts were found in various phases of the applied sequential extraction.¹²

Water circulates through different type of soils such as sediments, water deposits, arable lands, forestlands, meadows, *etc.* In such environments, microelements could be attached in several ways: non-specific (adsorbed), attached to carbonates by co-precipitation and sorbed on iron and manganese oxides.¹³ Microelements could be incorporated in the silica matrix, bonded to clay or bonded to organics (especially in arable land).^{14,15}

Substrates could be sources of microelements (heavy metals) and therefore contribute to environmental pollution. They could associate and release microelements depending of the conditions. Microelements can change or degrade substrates, which can result in the release of microelements in inundate water. The mobility of microelements is influenced by different factors, such as change of pH, redox potential and the effect of microorganisms that can change the environment and the mobility of elements.⁶⁻⁹

At the end of 80's, many authors used a combination of different extraction media to study soil samples. Very soon thereafter, they adopted a division of phases connected with the applied extraction means using extractants with suitable chemical properties that fulfilled the criteria of efficiency and selectivity.^{16,17} Since then, the method was adopted and changed by different authors.¹⁸⁻²³

Sequential extraction was chosen as a suitable method. By successive extraction of soil samples with different mediums, the extraction of a specific fraction of heavy metals was possible. Special attention was dedicated to mobile fractions of heavy metals, as they were the most interesting and the most important from ecochemical aspects.

One of the most common divisions of phases for sequential extraction is the following:

Sorptive (adsorptive and ion exchange) phase. This phase is used in order to estimate the maximal quantity of sorbed ions that a geological material can re-

lease without the visible decomposition of any mineral phase. Neutral solutions of salts (NH_4OAc , MgCl_2 , CaCl_2 , BaCl_2 , KNO_3 , *etc.*) are usually used for this extraction phase. Their concentrations (and ionic strengths) must be sufficiently high to initiate complete ion exchange and desorption from all substrates.

“Easily reducible” phase. Weak reduction means, for example, hydroxylamine is used for the selective reduction (solvent) of manganese oxy-hydrates and the most mobile fraction of amorphous iron oxides. All the microelements co-precipitated with these oxides will be detected in the solution.

“Moderate reducible” phase. For amorphous iron oxides, some stronger reduction agents are used, *i.e.*, oxalic acid, sodium dithionite and similar.

Organic-sulphide phase. The distinguishing of the organic and sulphide metal fraction in a geological material is one of the disadvantages of sequential extraction. This problem is still not resolved. Pure nitric acid, or its combination with other acids, is a very effective means but it leads to a noticeable decomposition of silicate material. The usage of the hydrogen peroxide is acceptable at higher temperatures and low pH (about 2).

Residual phase. This is the least interesting phase from the ecochemical viewpoint as it includes silicate and oxide materials as well as incorporated metal ions, *i.e.*, in natural conditions, this fraction cannot be mobilized from the geological material. Concentrated mineral acids and their mixtures are usually used for the decomposition of this crystal matrix.

EXPERIMENTAL

Soil samples

The future accumulation Bogovina will inundate 5.32 km^2 of land and the volume of the lake will be 77 millions m^3 ; the River Crni Timok will fill the accumulation. The sampling locations are shown in Fig. 1.

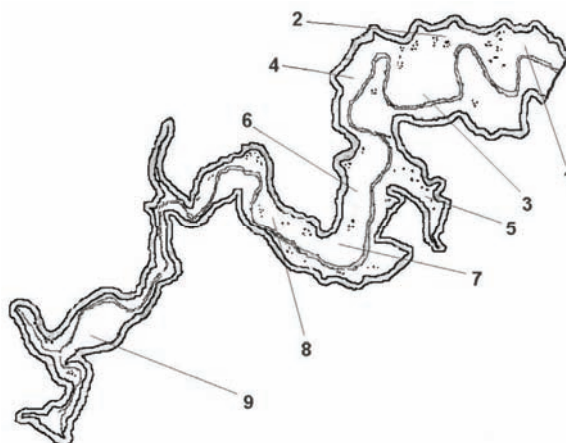


Fig. 1. Shape of the future Lake “Bogovina” with the sampling locations marked.

The soil of the future accumulation Bogovina differs considerably due to land exploitation¹² (Table I). During the sampling, special care was given to the percent distribution and additionally to the area pattern. Hence, the samples were taken from three locations of arable land, three locations of forestland and one location each of pastures, meadows and orchard. Furthermore, one sample was taken from suspended detritus.

TABLE I. The percent of different soils types of the future accumulation "Bogovina"

Land use	Percent	Number of samples	Label of samples
Arable land	30.1	3	1, 3, 8
Orchards	2.7	1	4
Meadows	16.8	1	7
Pastures	15.5	1	6
Forestland	24.6	3	2, 5, 9

Due to the dangerous atmospheric accumulation of heavy metals emitted by the large smelting corporation RTB Bor and their possible deposition on the land, it was decided to remove the surface layer of the basin (30 cm in depth). Therefore, samples were taken from the depths: 30–40, 40–50 and 50–60 cm. All samples were denoted by Arabic numbers from 1 to 9, while the samples from a depth of 30–40 cm were marked as A, from 40–50 cm as B and from 50–60 cm as C. Thus, the complete set of samples was: 1A, 1B, 1C, 2A, 2B,...,9A, 9B and 9C. The studied suspended detritus layer was denoted as M.

One portion of each soil sample was subjected to sequential extraction in five phases. Another portion of each sample was left in contact with river water (simulation experiment) and then another sequential extraction was performed.

Simulation experiment

The simulation experiment was realised according to a previously described procedure.¹² Each sample was transferred into a 10-L cylindrical plastic vessel and left in contact with 8 L of river water. The experiment was performed at 5–8 °C. The height of the soil was 10 cm and the height of the water column was 30 cm in all vessels. Small aliquots (100 cm³) were pipetted from the middle of water column each week. The experiment lasted eight weeks and the dependence of emission, pH, O₂, P, Mn, Ntotal, NH₄⁺, NO₂⁻ and NO₃⁻ on contact time were monitored.²⁴ For all experiments, the microelements were determined as well as their possible substrates.

Procedure for sequential extraction

The five-step procedure developed by Tessier¹⁷ and Polić¹⁶ was used to define the fractions of trace metals. Sequential extraction could provide information about the association of microelements with appropriate substrates. In addition, this analysis was complemented by experiments in which the processes at the bottom of the future lake were simulated. Furthermore, the sequential extraction performed after the simulation experiment could provide important data about the activity of microorganisms, re-absorption processes and co-precipitation of microelements on the available substrates. The solid/solution ratios were 1:45. The summarized procedure is shown in Table II.

Instrumental methods of analyses

All filtrates obtained in the simulation experiment and in the sequential extraction were analyzed by the appropriate technique. Flame AAS was used for the determination of Cu, Ni,

Fe, Pb, Mn, Co, Mg, Ca, K, Na, Cd and Cr (Perkin Elmer – A100). ICP was used for the determination Si and Al (ICP-ARL3410). Flow injection (cold vapour) was used for the determination of Hg (quartz tube, SnCl₂ as the reductant, Ar as carrier gas) (Perkin Elmer – FIMS100).

TABLE II. The sequential extraction procedure

No.	Phase	Reagents, conditions, time
1	Exchangeable	1M CH ₃ COONH ₄ , pH 7, 2 h
2	Bound to carbonates and easily reducible	0.6 M HCl, pH 4, 0.1 M NH ₂ OH and HCl, pH 2, 12 h
3	Moderately reducible	0.2 M (NH ₄) ₂ C ₂ O ₄ and 0.2 M H ₂ C ₂ O ₄ , pH 3, 7 h
4	Organic-sulphide	HNO ₃ , pH 2, 30 % H ₂ O ₂ , 85 °C, 3h, 3.2 M CH ₃ COONH ₄ , 30 min
5	Residual	6M HCl, 85 °C, 9 h

RESULTS AND DISCUSSION

The results obtained by the sequential extractions were grouped by phases for each element. The content of each element was determined before and after the simulation experiment and then the results were compared.

The most common elements are shown in Table III, and these elements represent substrates that associate many microelements.

TABLE III. The most common elements (in ppm)

Element	Phase				
	I	II	III	IV	V
Ca	500–1300	75–1400	–	–	–
Mg	5–20	4–14	–	2.4–30	15–150
Fe	–	15–45	110–340	1–6.1	25–330
Mn	–	5–15	–	4.2–20.6	–
Al	–	8–34	31–204	–	203–1830
Si	–	3–19	25–91	–	–
K	–	–	–	–	31–226

The results obtained in this study could be interpreted in two ways. The first is a comparison of the results before and after the simulation experiments and the other is to correlate the microelements with possible substrates or microelements with other microelements (Table III).

The changes of the concentrations of zinc before and after the simulation experiment are shown in Fig. 2.

Zinc was associated with manganese and iron oxy-hydroxides (high concentration of zinc in the third phase). The concentrations before and after the simulation experiment were similar. The only exception was in the fourth phase, where the amount of zinc after the simulation experiments was several times higher than before. Similar results were obtained by other authors.^{25,26}

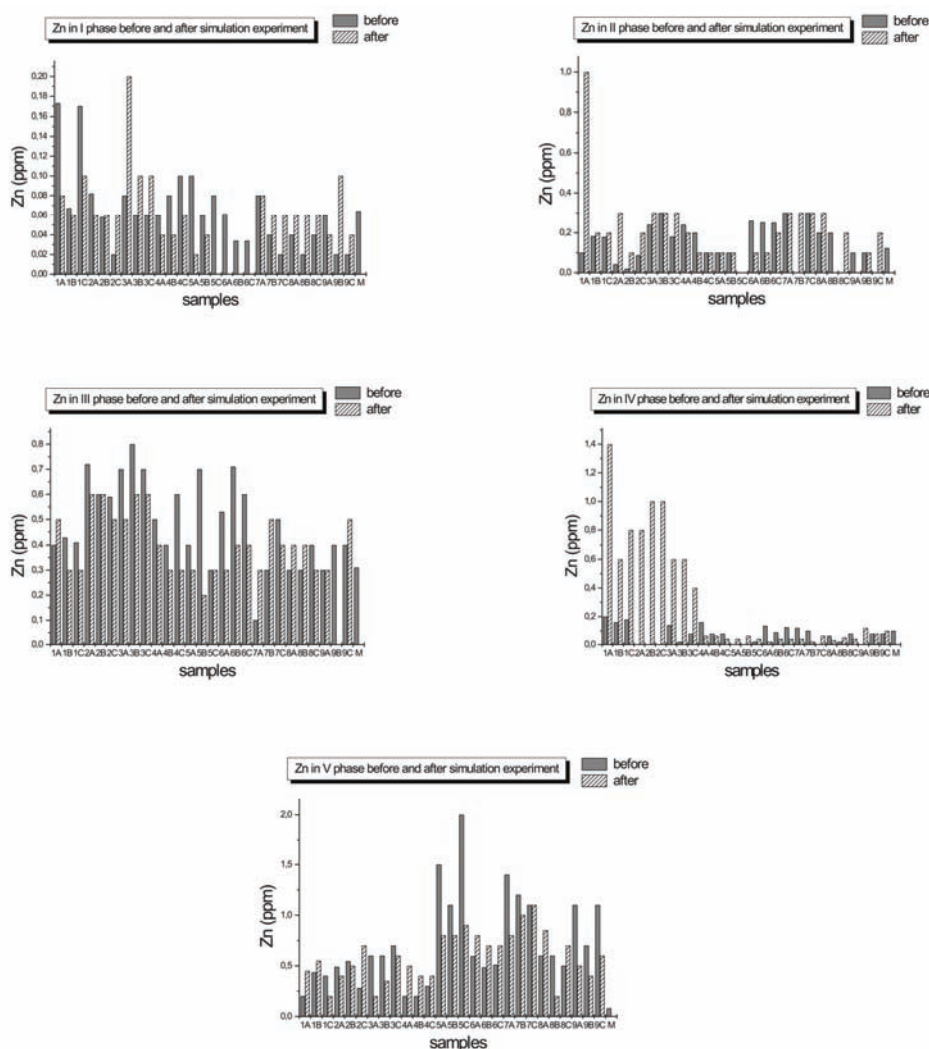


Fig. 2. Concentrations of zinc in all phases (I–V) before and after the simulation experiment.

A huge amount of nickel was incorporated in the mineral matrix. Similar quantities were associated in the first three phases (sorpitive, easily reducible and moderate reducible). There was no nickel in the organic phase. In addition, after simulation experiment, increased concentrations were found in the sorpitive and carbonate phase. These results indicate the contribution of biological processes in the release of nickel.

The results of the first and second phase of the extraction implied that cadmium was partially sorbed on carbonates. The higher concentration found in the second phase samples after the simulation experiment in could be attributed to

the change in pH. These results were compatible with the results obtained for the inundation area of the accumulation Lake Rovni near Valjevo (Serbia).⁶ In addition, the results in the third phase were outside the detection limit.

There was no lead extracted in first phase and there was only a small amount extracted in the second phase (only in the pastureland). Small amounts of lead were also found in the fourth and fifth phase of the extraction, mostly in the forest samples. High amount of lead in the third phase implied that this metal was associated with manganese/iron oxy-hydroxides.²⁷ There was good compatibility with the results obtained for the accumulation Lake Rovni, except that after the simulation experiment, there were no increases of lead in the second phase. The same conclusion was reached that manganese oxides were the main substrate for lead.⁶

Cobalt was found in all extraction phases with the exception of the organic phase. Biological processes were noticed in the second phase, as the release of cobalt was several times higher after the simulation experiment.

Small amounts of mercury were found in some samples. They were closed to the limit of detection by the employed method (0.8 ppb).

Based on a comparison of the results obtained before and after the simulation experiments, some conclusions could be drawn: the action of microorganisms could significantly influence the release of microelements; the changes in pH could also be the result of the release of microelements; the release of manganese and iron as substrates could affect the release of microelements associated with them and organic substances and sulphides could play an important role in the binding of microelements.

Hydroxylamine hydrochloride and hydrochloric acid were used in the second phase of the sequential extraction. Silica matrices are often attacked in this extraction procedure and low concentrations of aluminium and silicon could be extracted in this phase.

Due to the existence of several oxides of some microelements, it is sometimes difficult to dissolve them and destroy the mineral matrices. Furthermore, these oxides often have different solubility. This was the case with two types of manganese oxides. Hydrated and amorphous oxides of manganese are readily soluble. On the other hand, the dissolution of crystalline manganese(IV) oxide is slow and depends of the period of the action of the reducing agent.²⁸

Based on the results of the sequential analysis, it was not always possible to differentiate microelements bound to iron oxides and manganese oxides. However, the use of correlation analysis could increase the reliability of the conclusions. Correlation analysis could provide information on whether the microelements in the third phase were associated with iron or manganese oxide. It could also be helpful in distinguishing the microelements associated with carbonates of calcium and magnesium. In the fifth phase correlation analysis, it could help in

the differentiation of the associations of microelements with clay and silica matrices.

The concentration of each microelement was correlated with the concentration of corresponding elements in possible substrates. Calcium and magnesium represent carbonates as substrates. Iron and manganese represent their oxides. Aluminium and silica represent clay and mineral matrices.

Nickel had a positive correlation with Ca (NiICaII, $r = 0.81900$; $p = 0.000$) and negative one with Mn (NiIMnII, $r = -0.6429$; $p = 0.013$). After the simulation experiment, it was apparent that it had positive correlations with Ca (NiII/2CaI/2, $r = 0.64467$; $p = 0.024$), Al (NiII/2AlI/2, $r = 0.68182$; $p = 0.015$; NiIII/2AlI/2, $r = 0.73490$; $p = 0.010$) and Mg (NiIII/2MgIV/2, $r = 0.65074$; $p = 0.030$), while the correlations with Mn were negative (NiI/2MnV/2, $r = -0.7429$; $p = 0.006$).

The concentrations of cadmium in the samples were very low and correlations were found only in the second phase. Positive correlations were found with Ca and Mg (CdIICaII, $r = 0.98424$; $p = 0.18$; CdIIMgII, $r = 0.97055$; $p = 0.000$; CdIIMgIV, $r = 0.83649$; $p = 0.005$) and negative ones with Fe (CdIIFeI, $r = -0.7785$; $p = 0.005$) and Mn (CdIIMnII, $r = -0.7209$).

Positive correlations of cobalt with Mn (CoIMnII, $r = 0.99988$; $p = 0.000$; CoIIMnII, $r = 0.77840$; $p = 0.001$; CoIIMnIII, $r = 0.82430$; $p = 0.000$; CoIVMnIV, $r = 0.78722$; $p = 0.0012$), Si (CoISiIV, $r = 0.86515$; $p = 0.000$; CoIIISiIII, $r = 0.67939$; $p = 0.021$) and Al (CoIIAlIV, $r = 0.78278$; $p = 0.001$; CoIIIAlIV, $r = 0.67642$; $p = 0.022$) were registered, as well as negative ones with Mg (CoIMgI, $r = -0.8831$; $p = 0.020$; CoIMgII, $r = -0.8815$; $p = 0.020$; CoIMgIII, $r = -0.8425$; $p = 0.035$).

Correlation analysis for lead was not performed, as the concentrations found in sediments were too low.

Correlations of zinc with other elements are shown in Fig. 3. There are two types of correlation diagrams: before and after the simulation experiments. These diagrams differ slightly, which could be the consequence of the activities of microorganisms at the bottom of the lake.

Positive correlations of zinc with Si (ZnIISiII, $r = 0.67490$; $p = 0.001$; ZnIIISiIII, $r = 0.66781$; $p = 0.000$), Al (ZnIIAlIII, $r = 0.69583$; $p = 0.000$; ZnVAlI, $r = 0.64197$; $p = 0.000$), Mn (ZnIIIMnIII, $r = 0.63930$; $p = 0.000$; ZnIVMnIV, $r = 0.73287$; $p = 0.000$) and Fe (ZnVFeV, $r = 0.64472$; $p = 0.000$) were found. A negative correlation of zinc with Ca (ZnIICaII, $r = -0.6503$; $p = 0.001$) was found. It could be concluded that zinc was bound to or sorbed on manganese and iron oxy-hydroxides but that it was also built in the silicate matrix. The negative correlation with Ca could imply that only a small amount of zinc was associated with carbonates.

Correlation diagrams obtained after the simulation experiment are shown in Fig. 4.

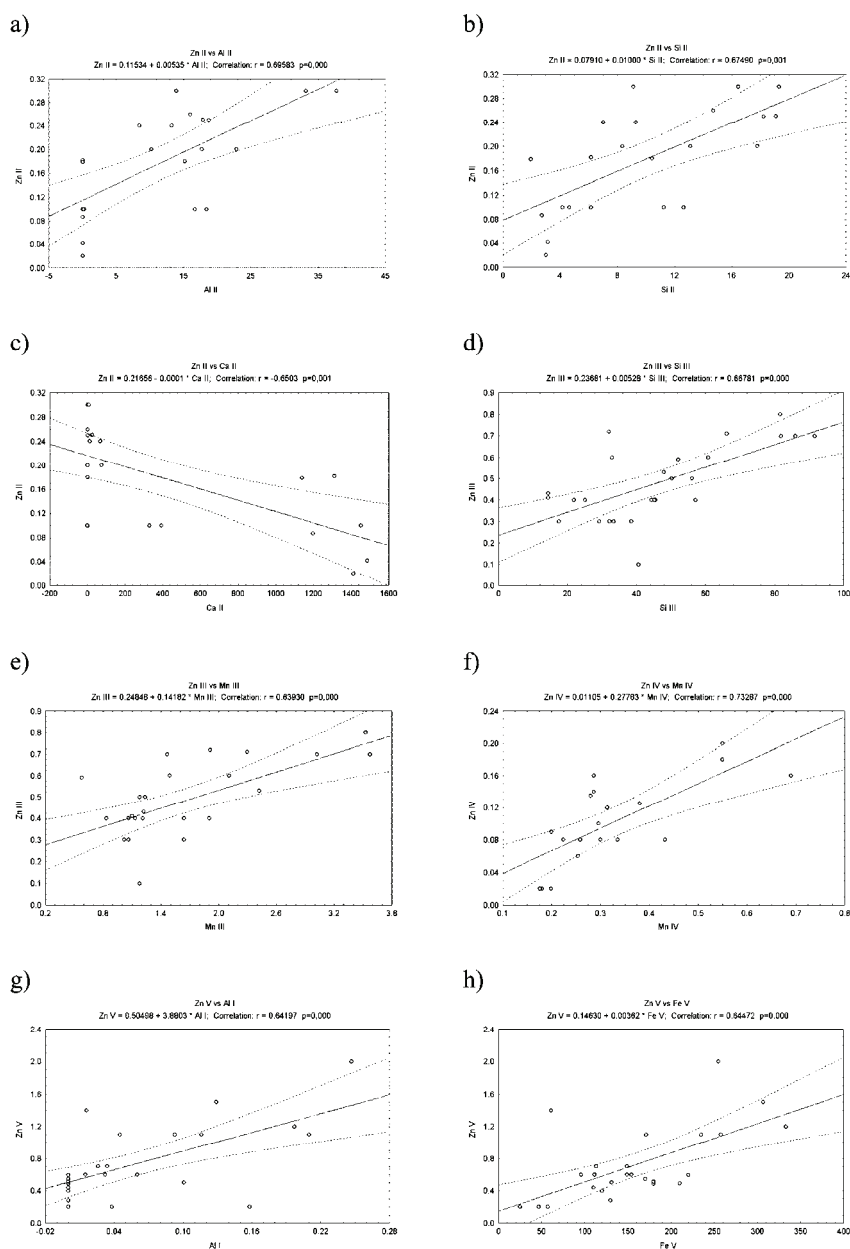


Fig. 3. Correlation diagrams before the simulation experiment: a) Zn in the second phase vs. Al in the second phase; b) Zn in the second phase vs. Si in the second phase; c) Zn in the second phase vs. Ca in the second phase; d) Zn in the third phase vs. Si in the third phase; e) Zn in the third phase vs. Mn in the third phase; f) Zn in the fourth phase vs. Mn in the fourth phase; g) Zn in the fifth phase vs. Al in the first phase and h) Zn in the fifth phase vs. iron in the fifth phase).

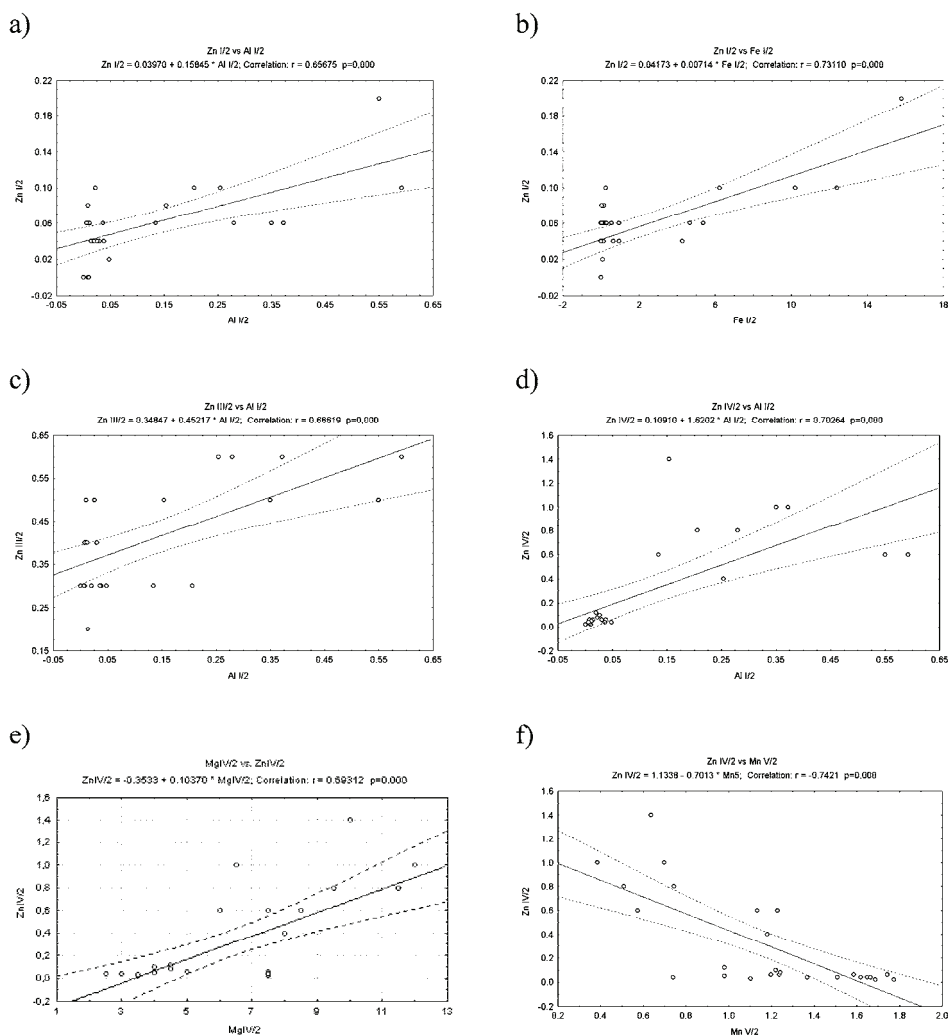


Fig. 4. Correlation diagrams after the simulation experiment: a) Zn in the first phase vs. Al in the first phase; b) Zn in the first phase vs. Fe in the first phase; c) Zn in the third phase vs. Al in the first phase; d) Zn in the fourth phase vs. Al in the first phase; e) Zn in the fourth phase vs. Mg in the fourth phase and f) Zn in the fourth phase vs. Mn in the fifth phase.

After the simulation experiment, there were some positive correlations between Zn and Al ($ZnI/2AlI/2$, $r = 0.65675$; $p = 0.000$; $ZnIII/2AlI/2$, $r = 0.66619$; $p = 0.000$; $ZnIV/2AlI/2$, $r = 0.70264$; $p = 0.000$), Fe ($ZnI/2FeI/2$, $r = 0.73110$; $p = 0.000$) and Mg ($ZnIV/2MgIV/2$, $r = 0.69312$; $p = 0.000$), and a negative correlation with Mn ($ZnIV/2MnV/2$, $r = -0.7421$; $p = 0.000$).

Based on results presented in Figs. 3 and 4, it could be concluded that after the simulation experiment, zinc was associated only in the silica and clay matri-

ces (Figs. 4a–4d). The negative correlation with manganese (Fig. 4f) implied that microorganisms acted on the redox cycles of manganese.

Low concentrations of lead were found in the extracts. This is in accordance with the theory that lead can be efficiently removed from water.^{28,29} Lead was not correlated with any of the examined elements.

Nickel was extracted in the first, second and third phase of the sequential extraction before the simulation experiment and in the first and second phase after the simulation experiments. Similar results were obtained for the correlation analysis before and after the simulation experiments. Before the simulation experiments, most of the nickel was associated with calcium, but after it was associated with calcium and magnesium. The correlations of nickel with manganese were negative. There were better correlations after the simulation experiments than before it. The results of correlation analysis were in accordance with results obtained by sequential extraction. The main conclusion is that sequential extractions have good selectivity for nickel. These results also indicated that the main substrates for nickel are carbonates and that there were no associations with iron and manganese oxides.

Small amounts of cadmium were extracted in second phase and only in a few samples. These results showed that cadmium was associated with carbonates before the simulation experiments. After the simulation experiments, the amounts associated with carbonates were smaller. Obviously, the action of microorganisms resulted in the release of cadmium. Cadmium had positive correlations with calcium and magnesium but negative with iron and manganese. After the simulation experiments, there were no significant correlations. There was good agreement of the results obtained by sequential extraction with the correlation analysis. It could be concluded that cadmium was associated with carbonates, with no associations existing with iron and manganese.

Cobalt was found in the first, third and fifth phase of the sequential extractions. These results indicated that cobalt was associated with iron or manganese oxides but that it was also incorporated in the silicate matrices and clays. The results of the correlation analysis also indicated that cobalt was non-specifically sorbed on different substrates. Good correlation was found for cobalt with manganese and aluminium. Moreover, after the simulation experiments, good correlations were found for cobalt with calcium, magnesium, iron, silicon and aluminium. Analysis of these results indicated that cobalt was an easily removable element that could be reabsorbed after the primary dissolution. Manganese oxides and clay were the substrates of cobalt before the simulation experiment and they were replaced with carbonates and mineral matrices afterwards. The explanation for such behaviour could be very complicated and it might involve different adsorptivity of the substrates and the activity of microorganisms.

Zinc, the element to which special attention was paid in this study, was extracted in the third and fifth phases before the simulation experiments. After the simulation experiments, zinc was extracted in the fourth and fifth phases. These results show that zinc was associated with iron oxides and possibly with manganese(IV) oxide. It was also incorporated in silicate and clay matrices. Correlation analysis resolved the doubt about the association of zinc in the second and third phase because there were only positive correlation of zinc with silicon, aluminium and iron before the simulation experiments. In addition, there was a negative correlation between zinc and calcium. After the simulation experiments, there was a positive correlation of zinc with magnesium, iron and aluminium. The correlation with manganese was negative. These results confirmed that carbonates were not a substrate for zinc. The doubt about the oxides in third phase of the extraction was clarified by the negative correlation of zinc with manganese. Therefore, iron oxide was a substrate for zinc.

CONCLUSIONS

A combination of double sequential extraction with correlation analysis was found to be useful for the prediction of substrates of heavy metals.

Most of the heavy metals were sorbed on the most abundant substrates. Some of them migrated easily from the solid phase to water. The results of the presented study indicated that changes in pH intensified the dissolution of most microelements, such as nickel, cadmium and lead. The increase in the concentrations of cobalt and zinc was not affected by changes of pH, as they were not associated with carbonates.

Changes in redox potential affected higher concentrations of nickel and zinc, as they were associated with manganese and iron oxy-hydrates.

Only small quantities of some elements (Ni, Co) were non-specifically bound and they could be released by changing the ionic strength.

The major processes in inundated land could be dissolution as a result of changes in ionic strength, redox potential or pH. The activity of microorganisms could also play an important role in the dissolution processes. Co-precipitation from water to another substrate could also occur. From the comparison of results for zinc before and after the simulation experiment, it could be concluded that before the simulation experiments the main substrates were iron and manganese oxides and after the organic substances because of the activity microorganisms.

These results are important for the provision of good quality water in the future accumulation Lake Bogovina (Serbia).

ИЗВОД

СИМУЛАЦИОНИ ЕКСПЕРИМЕНТ КАО МЕТОДА ЗА ПРОУЧАВАЊЕ МОБИЛНОСТИ
ТЕШКИХ МЕТАЛА ИЗ ПОТОПЉЕНОГ ЗЕМЉИШТАЂОКИЦА ПЕТРОВИЋ¹, МАРИЈА ТОДОРОВИЋ², ДРАГАН МАНОЈЛОВИЋ² и ВОЛИН Д. КРСМАНОВИЋ²¹"Винча" Институт за нуклеарне науке, Лабораторија за радиоизотопе, б. бр. 522, 11 001 Београд и²Хемијски факултет, Универзитет у Београду, б. бр. 51, 11158 Београд 118, ПАК: 105305

Симулациони оглед је употребљен за проучавање интеракције речне воде са различитим земљиштем (оранице, воћњаци, ливаде, пашњаци и шумско земљиште). Резултати добијени секвенцијалном екстракцијом пре и после симулационог експеримента упоређивани су како би се одредили супстрати тешких метала у потопљеном земљишту и проценила њихова мобилност. Узорци различитих екохемијских типова земљишта, који су узети у региону будућег акумулационог језера Боговина (Србија), испитивани су на десет елемената помоћу ААС, GFAAS и ICP. Секвенцијална екстракција у пет фаза примењена је за испитивање природе асоцијације тешких метала и идентификацију њихових супстрата. Корелациона анализа је употребљена за одређивање супстрата тешких метала. Добра корелација између микроелемената и одређених макроелемената указује на њихове супстрате. Већина микроелемената је показивала добру корелацију са манганом и гвожђем. Само неки од микроелемената су имали добру корелацију са калцијумом. Цинк и кадмијум су имали један супстрат пре, а други после симулационог огледа.

(Примљено 17. фебруара 2009, ревидирано 4. маја 2010)

REFERENCES

1. J. Kumpiene, A. Lagerkvist, C. Maurice, *Waste Manage.* **28** (2008) 215
2. G. J. Lair, M. Graf, F. Zehetner, M. H. Gerzabek, *Environ. Poll.* **156** (2008) 207
3. Y. Xu, L. Axe, T. Boonfueng, T. A. Tyson, P. Trivedi, K. Pandya, *J. Colloid Interface Sci.* **314** (2007) 10
4. T. Boonfueng, L. Axea, Y. Xua, T. A. Tysonb, *J. Colloid Interface Sci.* **303** (2006) 687
5. J. Kyziol, I. Twardowska, P. Schmitt-Kopplin, *Chemosphere* **63** (2006) 1974
6. D. Manojlovic, M. Todorovic, P. A. Pfendt, V. D. Krsmanovic, in *Proceedings of Fifth International Symposium and Exhibition on Environmental Contamination in Central and Eastern Europe*, Prague, Czech Republic, (2000), CD ROM, Prague University, Prague, 2000, Paper No. 507
7. D. Relić, D. Djordjević, A. Popović, T. Blagojević, *Env. Inter.* **31** (2005) 661
8. W. F. Pickering, *Ore Geol. Rev.* **1** (1986) 83
9. J. J. McAlister, B. J. Smith, *Microchem. J.* **63** (1999) 415
10. T. Prechthai, P. Parkpian, C. Visvanathan, *J. Hazard. Mater.* **156** (2008) 86
11. L. Horckmans, R. Swennen, J. Deckers, *Sci. Total Environ.* **376** (2007) 86
12. D. Manojlovic, *Ph.D. Thesis*, University of Belgrade, Faculty of Chemistry, Belgrade, 2004 (in Serbian)
13. P. Polić, P. Pfendt, *J. Serb. Chem. Soc.* **61** (1996) 1001
14. D. C. Adriano, *Trace Elements in the Terrestrial Environment*, Springer, Berlin, 1986, p. 623
15. M. B. Aceves, C. Grace, J. Ansorena, L. Dendooven, P. C. Brookes, *Soil Biol. Biochem.* **31** (1999) 867
16. P. S. Polić, *Ph.D. Thesis*, University of Belgrade, Faculty of Chemistry, Belgrade, 1991
17. A. Tessier, P. G. C. Campbell, M. Bisson, *Anal. Chem.* **51** (1979) 844

18. J. T. Sims, J. Sklin, *J. Environ. Qual.* **20** (1991) 387
19. G. Petruzzelli, L. Lubrano, E. Veschetti, *Agrochimica* **38** (1994) 277
20. J. Pichtel, M. Anderson, *Bioresour. Technol.* **60** (1997) 223
21. A. J. Fernandez, M. Ternero, F. Fernandez, J. C. Jimenez, F. J. Barragan, *Toxicol. Environ. Chem.* **82** (2001) 59
22. S. Amir, M. Hafidi, G. Merlina, J. C. Revel, *Chemosphere* **59** (2005) 801
23. A. J. Fernandez, M. Ternero, F. Fernandez, A. Gutierrez, D. Trigo, *Intern. J. Environ. Anal. Chem.* **86** (2006) 641
24. D. Manojlovic, T. Damjanovic, R. Golubovic, M. Todorovic, *J. Env. Prot. Ecol.* **2** (2001) 174
25. R. Carignan, J. O. Nriagu, *Geochim. Cosmochim. Acta* **49** (1985) 1753
26. R. Carignan, A. Tessier, *Science* **228** (1985) 1524
27. M. Fan, T. Boonfueng, Y. Xua, L. Axe, T. A. Tyson, *J. Colloid Interf. Sci.* **281** (2005) 39
28. T. T. Chao, *Soil Sci. Soc. Am.* **36** (1972) 764
29. G. Benoit, H. F. Hemond, *Environ. Sci. Technol.* **24** (1990) 1224.